

NBSIR 73-403

Development and Analysis of Techniques for Calibration of Kerr Cell Pulse-Voltage Measuring Systems VII

Esther Christmas Cassidy, Robert E. Hebner,
Richard J. Sojka, and Markus Zahn

High Voltage Measurements Section
Institute for Basic Standards
National Bureau of Standards
Washington, D. C. 20234

November 1, 1973

Final Report on

Sandia Corporation Order No. FAO-28-0734

Sandia Requester and Technical Consultant: S. R. Booker, 7452

Sandia Contracting Representative: John G. Boyes, Org. 4361

Prepared for

Sandia Corporation

Bldg. 894, Kirtland AFB

East Albuquerque, New Mexico 87115

NBSIR 73-403

**DEVELOPMENT AND ANALYSIS OF
TECHNIQUES FOR CALIBRATION OF
KERR CELL PULSE-VOLTAGE MEASURING
SYSTEMS VII**

Esther Christmas Cassidy, Robert E. Hebner,
Richard J. Sójka, and Markus Zahn

High Voltage Measurements Section
Institute for Basic Standards
National Bureau of Standards
Washington, D. C. 20234

November 1, 1973

Final Report on

Sandia Corporation Order No. FAO-28-0734
Sandia Requester and Technical Consultant: S. R. Booker, 7452
Sandia Contracting Representative: John G. Boyes, Org. 4361

Prepared for
Sandia Corporation
Bldg. 894, Kirtland AFB
East Albuquerque, New Mexico 87115



U. S. DEPARTMENT OF COMMERCE, Frederick B. Dent, Secretary
NATIONAL BUREAU OF STANDARDS, Richard W. Roberts, Director

TABLE OF CONTENTS

INTRODUCTION.....	1
I. KERR SYSTEM DESIGN AND CONSTRUCTION.....	4
A. New Cell Construction.....	4
II. ELECTRIC FIELD AND SPACE CHARGE BEHAVIOR IN NITROBENZENE.....	8
A. Introduction.....	8
B. Experimental Apparatus and Techniques.....	11
C. Theory.....	17
D. Experimental Results.....	23
E. Summary and Conclusions.....	51
III. MEASUREMENT OF THE KERR CONSTANT OF NITROBENZENE.....	54
A. Introduction.....	54
B. Experimental Techniques.....	55
C. Results.....	64
IV. KERR SYSTEM PEAK-READING VOLTMETER WITH AUTOMATIC DIGITAL DISPLAY.....	73
A. Instrumentation and Procedure.....	74
B. Kerr System Measurement Principles.....	82
C. Results and Conclusions.....	85
V. MEASUREMENT OF HIGH MEDICAL X-RAY MACHINE VOLTAGES.....	89
A. Introduction.....	89
B. Field Trip Report.....	90
C. Conclusions.....	90
D. Recommendations.....	92
E. Results and Benefits.....	93
VI. FUTURE PLANS.....	95
APPENDIX A: MEASUREMENT OF 60 HZ VOLTAGES USING THE KERR EFFECT.....	98
APPENDIX B: RECENT REFINEMENTS AND DEVELOPMENTS IN KERR SYSTEM ELECTRICAL MEASUREMENT TECHNIQUES.....	102
APPENDIX C: EXPERIMENTAL STUDY OF THE BEHAVIOR OF NITROBENZENE UNDER VARIED HIGH VOLTAGE CONDITIONS.....	110
REFERENCES.....	119

INTRODUCTION

Previous NBS High Voltage Measurements Section research adapting use of the Kerr electro-optical effect for purposes of electrical measurement has been presented in detail in references [1] through [6]. In addition, several accounts covering the more important phases of this continuing project have also been published in the open literature. Included in these have been three papers [7-9] concerned with development, calibration, and refinement of conventional Wunsch-type [10] pulse-measuring Kerr systems. Utilization of the techniques and correction methods described has enabled measurement of pulses peaking as high as 320 kV. Pulse durations have ranged from 5 to 15 μ s, with rise times of 1-2 μ s. Accuracy within $\pm 1\%$ is estimated for measurements of the peak magnitudes of the nearly rectangular pulses, which were in almost all cases measured simultaneously by a calibrated Kerr cell and a calibrated NBS pulse voltage divider.

Also included in the publications prepared under the NBS program have been papers reporting development of Kerr electro-optical fringe-pattern techniques for mapping and measurement of both steady-state dc [11] and transient [12] electric fields between and around the Kerr cell electrodes, and two papers reporting results from use of these methods for studies of electric field and space-charge behavior in nitrobenzene during high voltage operation [13,14]. A third paper, presenting for the first time results from electro-optical field mapping and space-charge studies under low frequency alternating high voltage conditions, is now nearing completion. The details of this work, which required analysis and evaluation of results from hundreds of fringe-pattern observations, are included in Section II of this report.

A paper reporting use of a Kerr system for optically coupled measurements of high 60 Hz alternating voltages [15] was also completed during this year. In keeping with our earlier practice, its reprint and reprints of references [9] and [14], also completed in FY 1973, are given in Appendices A-C.

The main body of this report, which covers FY 1973 progress on this program in some detail, is divided into sections. As in previous years, the first section reports on new Kerr cell construction. Section II compares results from studies of electric field and space charge behavior in nitrobenzene under varied high voltage conditions. Because of their novelty and promise for ultimate attainment of an ac procedure allowing accurate (to $\pm 0.5\%$ or better) high voltage calibrations of pulse measuring Kerr systems, the ac studies are emphasized.

Results from extensive experimental measurements of the Kerr electro-optical coefficient of nitrobenzene, over a range of selected operating temperatures and wavelengths, are given in Section III. Section IV reports on development of a Kerr system peak-reading voltmeter which utilizes commercially available equipment for digital display of the Kerr cell count at the peak of a high voltage pulse, thereby yielding an immediate semi-automatic measure of the peak magnitude of μs duration high voltage pulses. Section V describes experiments performed on a field trip to the Bureau of Radiological Health in Rockville, Maryland. During this trip a Kerr system was employed for measurement of medical X-ray machine voltages. As in the short (μs) pulse work, results are evaluated and compared with simultaneous divider measurements.

Finally, this year's report concludes with a brief statement of plans for work to be completed in FY 1974. As during past years, the program will continue to receive partial financial support from the Atomic Energy Commission through the Sandia Corporation of Albuquerque, New Mexico.

I. KERR SYSTEM DESIGN AND CONSTRUCTION

A. New Cell Construction

For the most part new cell construction during FY 73 involved attempts at fabrication of a cell virtually free of effects from the fringing electric fields at the electrode ends. Such a cell is desirable for two reasons: (1) its half-wave retardation voltage or cell constant, V_m , would be easily calculable from the cell dimensions and the Kerr electro-optical coefficient of the liquid, and (2) its use would allow measurement of the Kerr coefficient without need for evaluation and correction of difficult-to-predict errors introduced by the fringing end fields.

During this year, two cells* were constructed which confined the birefringent Kerr-cell liquid within a central interior volume well removed from the electrode ends. This would appear to offer an obvious, simple solution to the fringing end-field problem. End- and side-view photographs of one of the cells constructed this year, that with interior liquid volume dimensions 1 cm wide x 1 cm thick x 4 cm long, are shown in Figs. 1 and 2. The construction of the other cell is essentially the same, except that the length of the Kerr cell liquid path is 10 cm. In both cases the electrodes are stainless steel with dimensions 5 cm wide x 14 cm long x 0.75 cm thick. The surfaces of the glass cells and electrodes are ground optically flat so as to allow glass-to-metal sealing without use of sealing gaskets or compounds.

*The special grinding and sealing processes involved in fabrication of these cells was performed in the NBS Glassblowing Shop. The authors are especially grateful to Edward Muth whose skill in these techniques made construction of these cells possible.

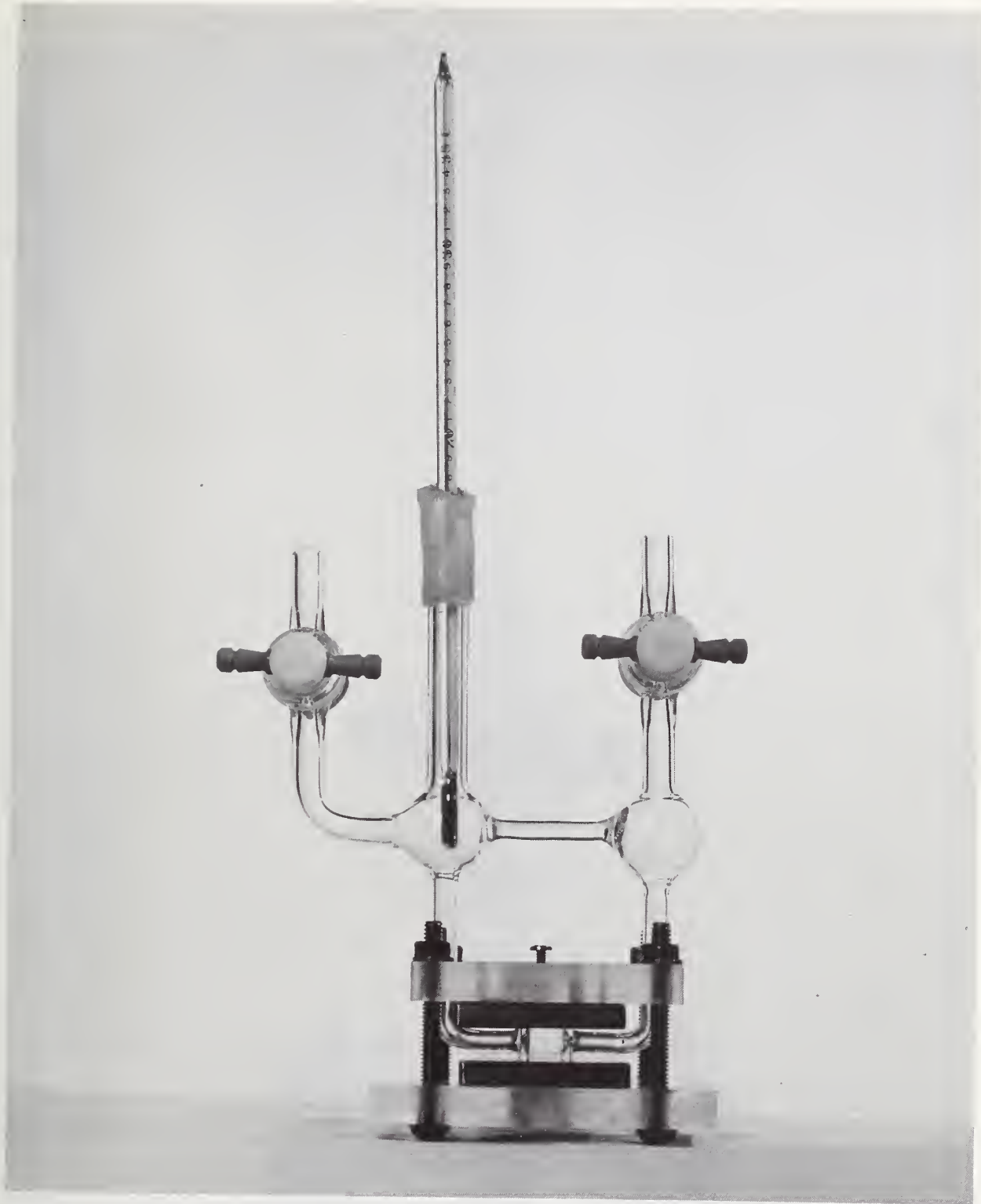


Figure 1. End view of "end-field-free" cell. Liquid volume is $1 \times 1 \times 4$ cm.

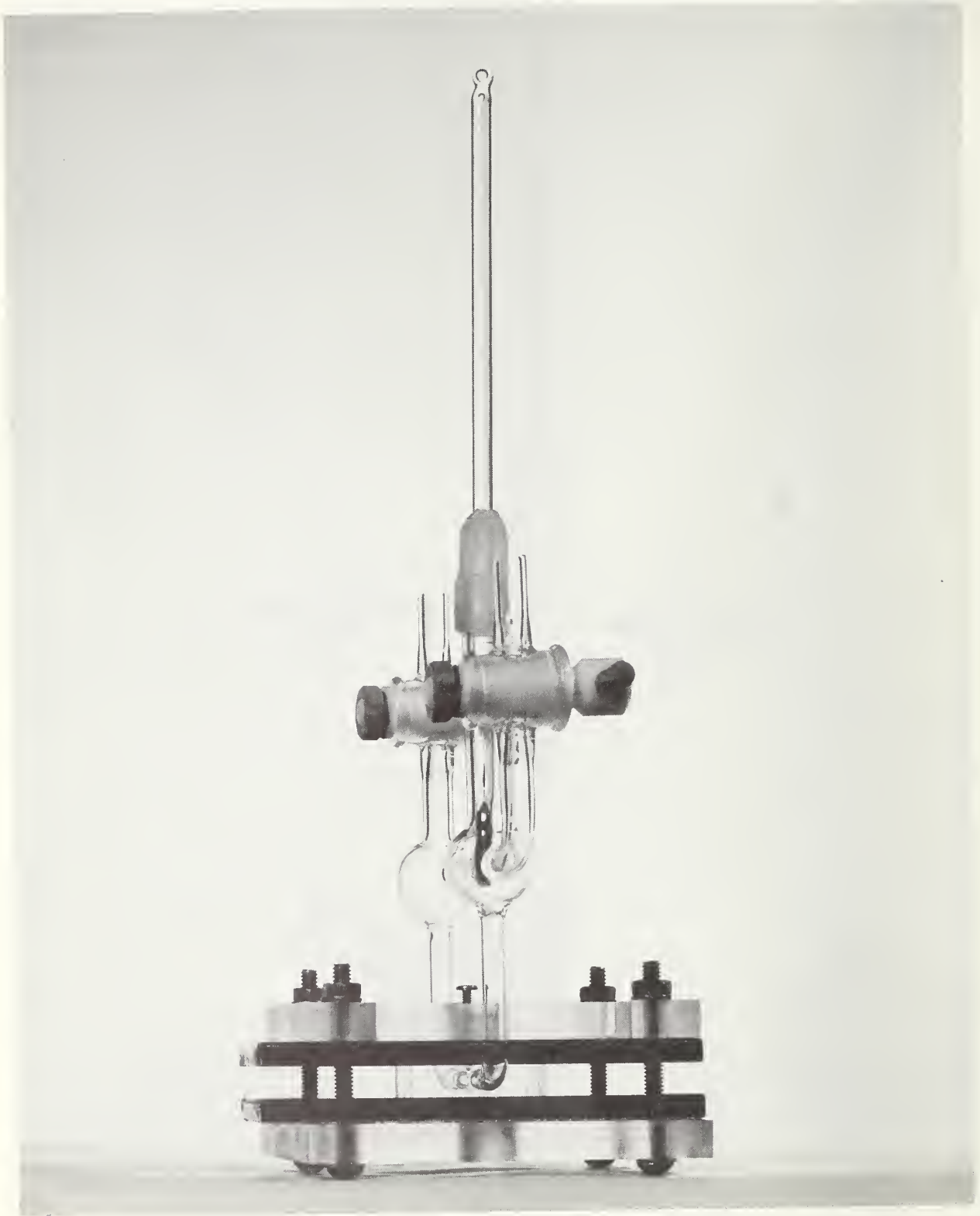


Figure 2. Side view of "end-field-free" cell.

The junctions at the corners of the rectangular glass vessel are also ground and then welded by a glass-to-glass sealing process. The entire vessel, including its expansion and thermometer volumes, is then annealed to relieve residual strain, especially in the end windows where the laser beam passes during system operation. Polariscope inspection of these windows after annealing showed that they are free of residual strain in these areas.

After completion and cleaning of both the glass cell and the electrodes, the glass volume was placed in a centrally located region between the electrodes and held "finger tight" as assembled in Figs. 1 and 2 while a vacuum was pumped through one of the outlets, the other outlet being sealed. The cell assembly was thus drawn evenly and tightly together, effecting a dry seal between the flat glass and steel surfaces. The bolts passing through the external clamping assembly were then tightened lightly to maintain the seal during later handling of the cell. Unfortunately, it was soon found that the force exerted on the glass cell by the clamps introduced strain in the cell windows, thereby producing an effect comparable to that resulting from the fringing end fields. Because of this difficulty, our attempts to fabricate a Kerr cell free of fringing end-field and strain effects were again frustrated. The cells were, however, useful in allowing measurement of the Kerr coefficient; a method involving use of measurements at two different voltage levels was devised to enable experimental correction of the errors. This method is discussed in detail in Section III.

II. ELECTRIC FIELD AND SPACE CHARGE BEHAVIOR IN NITROBENZENE

A. Introduction

Recent experimental work has demonstrated the usefulness of the electro-optic Kerr effect for the determinations of various electrical parameters under the influence of high voltage. Among these are the measurement of pulsed high voltage [7,8,10,16], the determination of space charge effects in nitrobenzene [17-18] and chlorinated biphenyls [19], the measurement of the electric field distortion caused by the insertion of a solid dielectric in a liquid insulant [20], the measurement of 60 Hz alternating voltages [15], and the observation of the spatial and temporal variation of the electric field distribution caused by pulsed and direct voltage [11,12,21]. In addition, theoretical advances in the understanding of space charge phenomena in insulating liquids have been made in such areas as the prediction and description of bulk space charge [22] and polarization waves [23] in charged liquid systems and the role of particulate charge carriers in electrical conductance [24].

Realizing that further advances are predicted on a knowledge of electric field and space charge behavior in liquid dielectrics, we have used refined Kerr electro-optical fringe pattern techniques [11,12] to measure and compare electric field and charge distributions in nitrobenzene-filled parallel plate capacitors during pulsed, direct and low frequency alternating high voltage operation. The purpose of this work, which supplements the substantial quantity of data published from earlier nitrobenzene studies, is the determination of, and ultimately control of, the complex mechanisms that lead to electrical breakdown in insulating liquids. The present work was also undertaken partly to increase the precision of 60 Hz voltage measurements. The results demonstrate both the feasibility and the effectiveness of using electro-optical fringe-pattern techniques to visualize electric field distributions and space charge

behavior under steady-state alternating high voltages. Field strengths as high as 85 kV/cm are applied. The effects of voltage level and frequency on space charge density and distribution are investigated between 0 and ± 50 kV; frequencies range from 40 to 200 Hz.

Nitrobenzene is the liquid investigated, primarily because of its high electro-optical coefficient (of order 10^{-12} m/V²) and relatively high electrical breakdown strength (>100 kV/cm). Though its powerful solvent, hygroscopic, and toxic properties make this liquid impractical for many insulating applications, nitrobenzene is uniquely suited to serve in this capacity for a multiplicity of diverse specialized applications, ranging from its use as the dielectric in prototype "high-energy" electrostatic generators [25] to its widespread use in high-speed photographic shutters [26] and laser "Q-switching" devices [27], to its use for precision measurements of pulsed high voltages. In connection with the latter application, extensive studies, now underway for more than five years, of the performance of nitrobenzene-filled Kerr cells immersed in oil under both transient (μ s pulses) and steady-state dc and ac operation have demonstrated that the physical behavior of nitrobenzene under high field conditions is essentially the same as that of most insulating liquids. Its conductivity and breakdown strength are, for example, affected by space charge effects [28], whether they result simply from moisture, impurities, and particulate contaminants in the liquid, or from more complex mechanisms such as charge formation by electrochemical reaction or field emission at the electrodes. Its performance is also affected by other widely reported high-field phenomena [29] such as electrohydrodynamic motion, bubble formation, electrophoretic and dielectrophoretic forces, the Sumoto effect, etc. All of these phenomena are known to be more or less pronounced depending upon the condition of the liquid, the electrode design, the nature and level of applied voltage, etc. Yet, our

understanding of electric field and charge behavior, and thus of breakdown, in the bulk of insulating liquids remains admittedly poor.

It has been our philosophy in preparation of this paper that much is to be gained from careful analysis of electrical stress and space charge behavior which can be so easily observed experimentally in nitrobenzene by use of Kerr effect fringe pattern techniques. Although the chemical composition of nitrobenzene differs significantly from that of more commonly used insulating fluids, it is reasonable to expect that behavior attributable to physical phenomena, such as conduction by particulate impurities or electrohydrodynamic motion of the liquid, is similar in both cases. Accordingly, more than 600 individual experiments investigating such behavior were performed with sealed nitrobenzene-filled cells under a variety of carefully monitored high voltage conditions. The results demonstrate significant differences between the pulsed and steady-state ac or dc field and charge behavior in the bulk of the liquid. Whereas expected conditions were observed during short pulse operation, several significant unforeseen trends were observed in the steady-state experiments, thereby pointing up the fact that extreme care should be exercised in inferring behavior at power-line frequency from characteristics observed under dc or pulsed voltage operation. If, for example, it is suspected that the degradation of an insulating liquid is due to the presence of space charge, whether formed chemically or carried by particulate impurities, the data presented here suggest questioning of the common practice of inferring the liquid's performance at power frequency from accelerated aging (for shorter times at frequencies much higher than 60 Hz) testing or dc testing results.

The experimental techniques and methods of data analysis employed in the present work are described in Sections II and III, respectively. The fourth

section presents and discusses the data obtained under direct voltage and under alternating voltages. The final section, Section V, presents the summary and conclusions.

B. Experimental Apparatus and Techniques

A schematic diagram of the experimental apparatus is given in Fig. 3. The system consists of a nitrobenzene-filled parallel-plate capacitor within a glass vessel (Kerr cell), a triggerable pulsed argon laser, crossed polarizers oriented at + and -45° to the interelectrode field direction, retardation plates oriented as indicated for elimination of field-directional fringes^[30] not pertinent in the present work, and appropriate photographic equipment for recording of the transmitted fringe patterns observed when the laser is flashed during high voltage operation. The laser beam diameter is expanded and collimated as indicated to illuminate the area between and around the test cell electrodes. The beam is focussed and passed through the circular aperture to exclude extraneous reflections and, on occasion, to allow Schlieren observations of the liquid motion invariably produced by steady-state high voltage operation. For purposes of illustration, the diagram includes a typical fringe pattern photographed by flashing the laser with -20 kV dc applied to the test cell. During such direct voltage studies, the high voltage (0-±50 kV) was connected to the parallel combination of the test cell and a calibrated 100-M Ω resistive divider^[31] as shown. The divider was used to measure the high voltage across the cell. For current measurements a microammeter was placed in series with the Kerr cell, between the cell and ground.

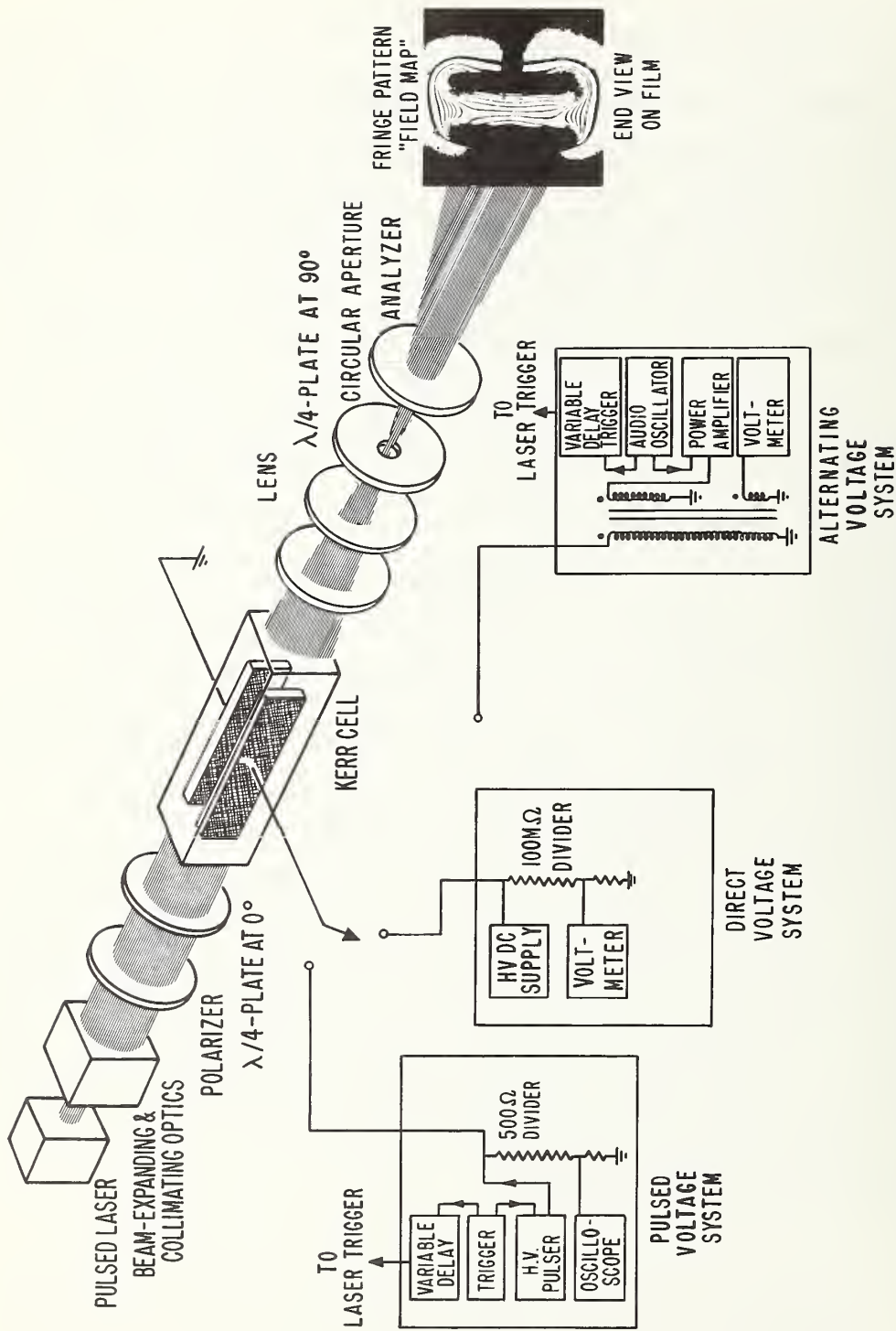


Figure 3. Schematic diagram of the apparatus used to measure the electric field distributions in nitrobenzene. Typical Kerr effect fringe pattern is shown on the right of the drawing. The systems used to supply and measure the applied voltage are also shown.

For the ac studies, alternating high voltage was obtained by amplifying the output of an audio oscillator. This power-amplified signal supplied a step-up transformer, and the latter's output voltage, as high as 40 kV rms with frequencies over the range from 40 to 200 Hz, was applied to one electrode of the cell, the other electrode being grounded. The rms value of the applied voltage was measured using a 1000:1 metering tap on the transformer.

In order to control the timing (during a cycle) of the ac fringe pattern observations, triggering of the laser pulse (flash duration $\approx 6 \mu\text{s}$) was synchronized with the high alternating voltage applied to the cell. This was accomplished by using the audio-oscillator output signal to trigger an oscilloscope equipped with a manually adjustable delayed output voltage pulse for triggering of the laser pulse. The delay and synchronization of this delayed trigger signal were adjusted, Fig. 4, so that the laser flashed in a strobe-like manner to allow discrete observations of the fringe pattern at a selected time(s) during a cycle. The time interval, Δt , between the triggering of the oscilloscope and the triggering of the laser was monitored using a conventional counter which counted its internal clock pulses during Δt . Two methods were used to correlate a value for the interval Δt with a specific point during a cycle of the applied voltage. The first was to detect a portion of the laser light pulse with a photomultiplier and display the time relationship between the laser light pulse and the applied voltage on the oscilloscope screen. The time interval Δt was then adjusted until the light pulse coincided with the peak of the positive half-cycle. The second and somewhat more accurate method was to adjust Δt until the fringe pattern resulting from the electro-optic Kerr effect indicated that the laser was pulsed at the peak

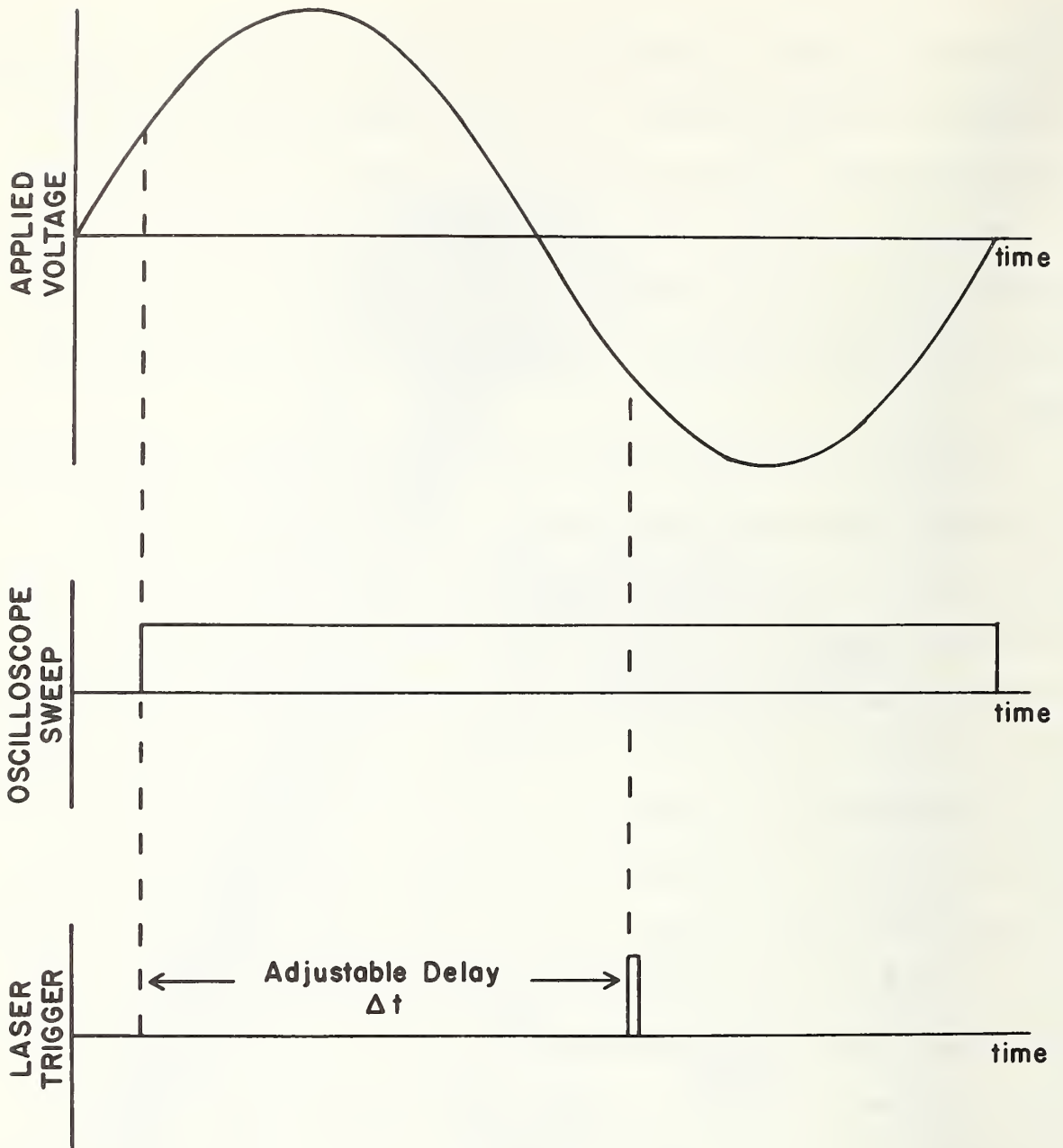


Figure 4. Timing diagram of system used to observe the electric field distribution at various instants of time during a cycle of alternating voltage. The upper trace shows one cycle of the applied voltage. The center trace represents the time for one sweep of the horizontal time base of the oscilloscope. The oscilloscope is externally triggered by the applied voltage waveform. The bottom trace shows the laser trigger pulse. The delay between the start of the oscilloscope sweep and the laser trigger pulse is manually adjustable and the duration of the laser light pulse is of order $6 \mu\text{s}$.

of the positive half-cycle, i.e., until the number of fringes produced was maximum. All attempts to correlate a specific point on the applied voltage waveform with a value of Δt were reproducible to within $\pm 20 \mu s$, i.e., to within $\pm 0.8\%$ of the shortest half-cycle used.

The present work was conducted using two specially prepared cells (see Table 1), one with electro-polished stainless steel electrodes of dimensions 4 cm wide by 12 cm long, and the other with glass-blasted nickel electrodes of dimensions 2 cm wide by 12 cm long. The electro-polishing and glass-blasting procedures were adopted to minimize the effects of electrode surface contamination. The electrode edges and corners were rounded to avoid premature electrical breakdown. The nominal electrode spacing in both cases is 0.5 cm. Glass-to-metal seals are used for inserting tungsten rods which provide electrical connection and support for the electrodes. An expansion volume is included to prevent failure of the glass vessel when the test liquid expands due to heating. A thermometer is sealed into the nitrobenzene for monitoring of its temperature. (Temperature increases as large as $20^\circ C$ were encountered during prolonged high voltage ac operation). External surface and air flashovers were avoided by immersing the test vessel in transformer oil. More complete details of our cell construction technique were presented elsewhere^[12].

With regard to the test cell insulant, nitrobenzene was, as mentioned above, selected primarily because of its high electro-optical coefficient and relatively high electrical breakdown strength. Though the electrical resistivity of commercially pure grades was inadequate (of order $10^3 \Omega \cdot m$) for steady-state high voltage operation, increased resistivity is readily obtained by passing reagent grade liquid through a chromatographic adsorption column of activated alumina. In the present work, this procedure, which has

CELL	ELECTRODE MATERIAL	ELECTRODE STRUCTURE & PREPARATION	CELL CONSTANT ($\bar{E}_m d$)
A	Nickel	Parallel-plate Glass-blasted	4900 V
B	Stainless Steel	Parallel-plate Electro-polished	4600 V

TABLE 1. Parameters for the test vessels described in text. The cell constants listed are valid for 514.5nm argon laser radiation at a liquid temperature of approximately 298 K.

long been used to remove moisture and other impurities from insulating oils^[32], increases the nitrobenzene's resistivity to the order of $10^8 - 10^9 \Omega \cdot m$. At this level, prolonged steady-state high voltage dc and ac operation could be maintained without excessive liquid heating or turbulence due to current leakage. Gas chromatographic analysis of the liquid before and after processing showed that, as is often the case with insulating oils, water was the principal contaminant. Thus, because of the hygroscopic and toxic properties of nitrobenzene, our entire cell-filling and sealing procedure is performed under vacuum.

C. Theory

Comprehensive theoretical discussions of the electro-optic Kerr effect, including derivations of the Kerr constant^[33-35], the application of the Kerr effect to high voltage measurement, and methods for eliminating the effects of fringing fields^[9], are available in the literature. The purpose of this section is to make explicit the assumptions used in the analysis of the data presented. The governing equation for the Kerr effect is

$$n_{11} - n_{\perp} = \lambda B E^2, \quad (1)$$

where $n_{11(\perp)}$ is the index of refraction for light polarized parallel (perpendicular) to the direction of the applied field, E . The Kerr constant of the liquid is B and λ is the wavelength of the monochromatic light traversing the Kerr cell. Eq. (1) can be solved for the phase shift, ϕ , between the components of the light beam polarized parallel to and perpendicular to the direction of the applied field:

$$\phi = 2\pi \int_0^L E^2 B d\ell. \quad (2)$$

In Eq. (2), L is the geometrical length of the optical path through the applied field. To reduce Eq. (2) to a more convenient form it is necessary to make a

number of observations concerning the electric field distributions in the cells used. To clarify this discussion, define a set of coordinate axes so that the z-direction is the direction of propagation of the light beam, the x-direction is perpendicular to and the y-direction is parallel to the surface of the electrodes. In this notation Eq. (2) can be rewritten

$$\phi(x,y,t) = 2\pi \int_0^L B E^2(x,y,z,t) dz, \quad (2a)$$

which also explicitly includes time dependence. The first assumption is that B is a constant, so that

$$\phi(x,y,t) = 2\pi B \int_0^L E^2(x,y,z,t) dz. \quad (2b)$$

In the present work, all field mapping is done in the x-direction. We have therefore analyzed data only at a specific value of y, the geometric center of the electrodes. It is shown in our data and has been shown in previous studies in cells with similar geometry that $\phi(y)$ varies only slightly near the center of the plates so that errors in locating the exact center of the plates are negligible in comparison to other errors in the analysis.

We can therefore rewrite Eq. (2b) as

$$\phi(x,t) = 2\pi B \int_0^L E^2(x,z,t) dz. \quad (2c)$$

Because the experimental set-up is such that light polarized at an angle of 45° to the direction of the applied field passes through the Kerr cell and

then impinges upon an analyzer oriented perpendicular to the direction of polarization, the light transmitted by the analyzer obeys the relation:

$$\frac{I(x,t)}{I_m} = \sin^2 [1/2 \phi(x,t)]. \quad (3)$$

In this equation we have again suppressed the y dependence and $I(x,t)/I_m$ is the relative irradiance of the transmitted light at a position x at any given time t, I_m being the maximum transmitted irradiance. We have assumed that temporal and spatial variations in I_m , which are dependent solely on the light source and the attenuation in the media through which the light beam propagates, are negligible; especially so in the present work as we measured only the values of x for which $I(x,t)/I_m = 0$, i.e. the positions of the dark fringes.

It has been shown [9] that Eq. (3) can be rewritten

$$\left(\frac{I(t)}{I_m}\right)_x = \sin^2 \left[\frac{\pi}{2} \left(\frac{\bar{E}(t)}{\bar{E}_m}\right)_x^2 \right], \quad (4)$$

where the overbar (e.g. in \bar{A}) denotes the following:

$$\bar{A} = \left[\frac{1}{L} \int_0^L A^2 dz \right]^{1/2},$$

and

$$\left(\frac{I(t)}{I_m}\right)_x \text{ denotes } \frac{I(x,t)}{I_m}$$

at a specific value of x.

In Eq. (4), \bar{E}_m is the smallest effective field strength that produces a maximum I_m in the amount of transmitted light. Methods have been developed to correct the observed values of $(I(t)/I_m)_x$ for variations in the x direction due to the fringing fields at the electrode ends [9]. However, these corrections were not applied to the present data because it has been shown previously that they modify values of $(\bar{E}(t)/\bar{E}_m)_x$ measured with parallel-plate electrodes greater than 10 cm in length and spaced less than 1 cm apart by less than 1%.

In this study information was obtained concerning $[\bar{E}(t)]_x$, and thus the space charge density, at certain times during the cycle of an applied steady-state alternating high voltage operation. These data were obtained by illuminating the cell with a light pulse which was short compared to the observed temporal variation of the field. (Details were given in Section II-B). To make explicit this situation Eq. (4) can be written

$$\left(\frac{I}{I_m}\right)_{x,t} = \sin^2 \left[\frac{\pi}{2} \left(\frac{\bar{E}}{\bar{E}_m}\right)_{x,t}^2 \right], \quad (5)$$

where t denotes the instant at which the observation is made.

Electric field and space charge distribution information were obtained from photographs of the transmitted fringe pattern at time t (see, for example, Figs. 3 and 4). The relative positions (x/d) of the centers of the dark bands along a centrally located path (of total length d) between and perpendicular to the inner electrode surfaces were measured and recorded.

The center of each dark band or fringe was assumed to indicate a relative intensity of $(I/I_m)_{x,t} = 0$, and thus, from Eq. (5), a point where the relative electric field intensity $(\bar{E}/\bar{E}_m)_{x,t}$ was equal to the square root of an even integer. In keeping with the convention established earlier^[10,11], numerical values n were assigned to each dark fringe by counting ($n = 0, 2, 4, 6, \dots$) successively from the outermost dark region where $n = 0$ inward to the desired fringe located on the scanning path (from $x/d = 0$ to 1) between the electrodes (see Figs. 3 and 4). The experimental values of (x/d) and $(\bar{E}/\bar{E}_m)_{x,t}$ obtained from each photograph were fitted to a first degree polynomial:

$$\left(\frac{\bar{E}}{\bar{E}_m}\right)_t = a + b (x/d), \quad (6)$$

or to a second degree polynomial:

$$\left(\frac{\bar{E}}{\bar{E}_m}\right)_t = A + B (x/d) + C (x/d)^2 \quad (7)$$

where a , b , A , B , and C were coefficients determined by a least-squares best fit method^[36]. The appropriate polynomial was judged to be sufficiently accurate whenever

$$\left(\frac{\bar{E}}{\bar{E}_m}\right)_{\text{fitted}} = \left(\frac{\bar{E}}{\bar{E}_m}\right)_{\text{exp}} \pm 0.05 \left(\frac{\bar{E}}{\bar{E}_m}\right)_{\text{exp}}. \quad (8)$$

In order to obtain the space charge density ρ from the electric field distribution, the differential form of Gauss' Law was used, i.e.,

$$\frac{\partial E}{\partial x} = \frac{\rho}{\epsilon}, \quad (9)$$

where ϵ is the dielectric constant of the liquid medium. For the purposes of this paper numerical values of ρ were not needed, and, neglecting the effects of fringing end fields, Eq. (9) was reduced to:

$$\frac{\partial(\bar{E}/\bar{E}_m)_t}{\partial(x/d)} = \frac{\rho d}{E_m \epsilon} \quad (10)$$

Computations of the coefficients in Eqs. 6 and 7 were used to plot the electric field distribution, i.e., $(\bar{E}/\bar{E}_m)_t$ as a function of (x/d) and to allow convenient examination of space charge effects in terms of the reduced space charge density ρ_r :

$$\rho_r = \frac{\partial(\bar{E}/\bar{E}_m)_t}{\partial(x/d)}. \quad (11)$$

Whenever a linear electric field distribution, of which the dc pattern in Fig. 6 is typical, was observed, Eq. (6) was fitted to the data and the reduced space charge density was given simply by

$$\rho_r = b \quad (12)$$

Whenever a parabolic field distribution was computed (see, for example, the ac pattern in Fig. 6), the reduced space charge distribution was determined as follows

$$\rho_r = B + 2C(x/d). \quad (13)$$

D. Experimental Results

It was reported earlier^[9,12] that electric fields produced by applying short (5 to 20 μ s duration) pulses as high as 300 kV show no evidence of space-charge distortion. A typical Kerr effect fringe pattern demonstrating this conclusion is given in Fig. 5. This photograph, which is a 0.3 μ s exposure taken at the peak of a 10 μ s long 65.4 kV nearly rectangular pulse, shows the irradiance transmitted through a parallel-plate cell similar to those used in the present work. With this geometry, the field between the electrodes should be uniform. The pulsed field's compliance with this condition is verified experimentally by the uniformity in the irradiance (the absence of fringes) transmitted between the electrodes.

In contrast, Fig. 6 shows typical records taken during steady-state dc and 60 Hz ac experiments with the cell having parallel-plate glass-blasted nickel electrodes. The presence of space charge and its distortion of the interelectrode field is evident from the fringes recorded between the electrodes. Further, plotting (see Fig. 7) of the distorted field distributions from the fringe numbers and positions, as described in Section III, shows a profound difference between the dc and 60 Hz field and charge distributions. Observations and discussions of these and other anomalies in steady-state dc and ac field distributions are discussed separately in the following sections.

Discussions of the reproducibility of the electrical and electro-optical measurements are included, and several alternative explanations are presented and discussed. Because the data presented typify results from over 600 individual photographs, the majority of the data are presented in graphical form. A number of photographs of raw data are included to indicate



Figure 5. Fringe pattern photographed (exposure time $0.3 \mu\text{s}$) at the peak of a 65.4 kV , total duration $10 \mu\text{s}$, pulse. The fact that the field is uniform between the plates is demonstrated by the absence of interelectrode fringes. The side fringes are due to the fringing field along the length of the electrodes.

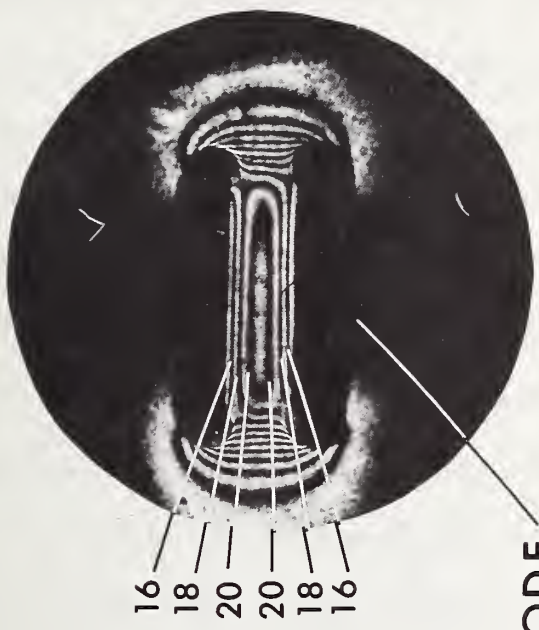
STEADY-STATE VOLTAGES APPLIED

dc



-18.00 kV

60 HZ ac



-22.62 kV PEAK

Figure 6. Typical observations of the fringe patterns resulting from the application of direct and 60 Hz alternating voltages. The interelectrode fringes show that the interelectrode field is not uniform under these conditions. The fringe numbering procedure is described in Section III.

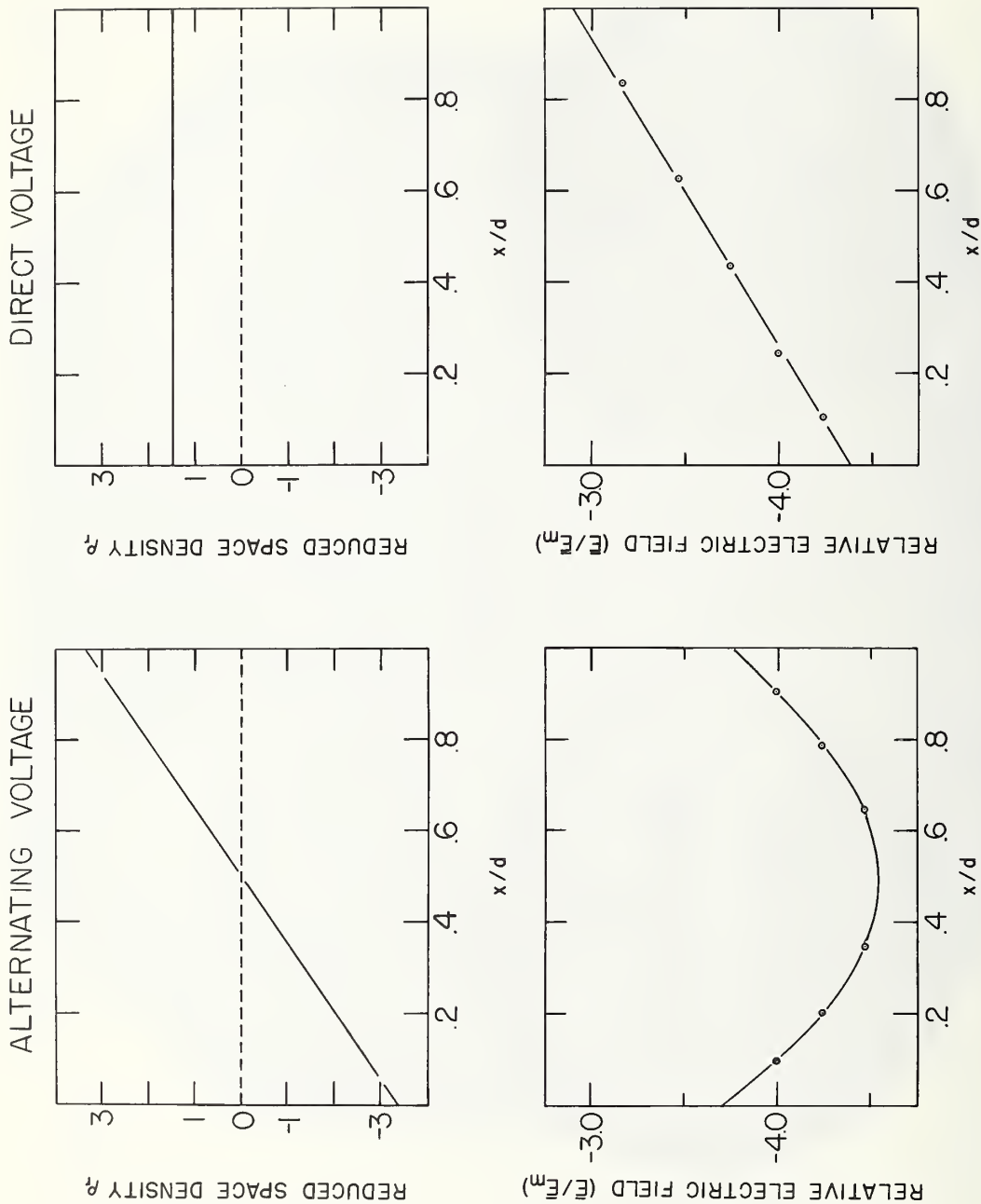


Figure 7. The relative electric field strength and the associated space charge density as a function of relative position between the plates (x/d). This data was obtained from the two photographs in Fig. 4. Although the average field strengths are approximately the same in the two cases, the electric field distribution, and consequently the space charge densities, are radically different.

to readers unfamiliar with this technique the types of observations that can be made.

1) Measurements of Current under Direct Voltage

When the test cell is first filled with the purified nitrobenzene the current passed by the cell upon application of steady-state high voltage (alternating or direct) is very high, being as much as a thousand times greater than the steady-state current. For several minutes, the conduction and electric field properties of the cell are not stable and measurements, either electrical or optical, made during this period are non-reproducible. After high voltage has been applied for about half an hour, the current through the cell approaches a steady-state value, and further electrical and electro-optical measurements are reproducible. However, when there is a significant time interval between voltage applications (e.g., overnight), or when the type of voltage excitation is changed (e.g., from direct to alternating or even if the polarity of direct voltage is changed), the current initially increases above the steady-state value but within a few minutes returns to the same steady-state value. During this period the electro-optic fringe pattern also changes slowly indicating changes in electric field and space charge distribution. Thus, whenever changes in voltage excitation are made, reproducible measurements reoccur only after several minutes of high voltage conditioning. The cells in this study were used over a three-month period with the reproducibility of all measurements occurring after the brief conditioning periods. Other sealed cells have been in use for over three years with similar results. (Because

nitrobenzene is hygroscopic, unsealed cells do not maintain this reproducibility).

Other authors^[37,38] have noted both the decrease in current with time during application of a constant high voltage and the dramatic increase in current with the decay back to a steady-state when the polarity is reversed. In their work, however, the electrodes were coated with an electrolytic varnish. In that case, the following explanation for current behavior was postulated^[38]:

"... the oncoming residual ions are trapped within the polymer matrix while electrical neutrality is preserved thanks to the stationary counterions; charge displacement in the reverse direction cannot occur unless the matrix has sufficient electronic conductivity. Of course, if voltage is reversed, the mobile ions are injected into the liquid and the arrangement works as a very efficient injector."

However, as noted above, the same time and polarity dependent behavior of the current was observed in our cells in which the electrodes were not varnished. A different, equally qualitative explanation for this behavior has been postulated^[39]. This hypothesis, which seems a plausible and perhaps a more accurate explanation for our observations, contends that electrical conduction is primarily the result of the motion of micrometre-size particles carrying charges between the electrodes. If this is the case, two processes involving trapping of particles on the electrodes can account for the current behavior:

1. Conducting micrometre and sub-micrometre sized particles become trapped on insulating areas of the metallic electrodes because the insulating areas prevent them from readily giving up their charge to

the metal electrode. This explanation accounts for both the decrease of current with time (the trapping sites slowly fill, thereby reducing the density of charge carriers and thus the current) and for the increase of current with polarity reversal^[39] (Coulombic repulsion on reversal may be expected to restore the density of charge carriers temporarily to its original high value).

2. Fluid motion can bring small insulating particles in contact with one of the electrodes^[24]. The particles eventually accept enough charge from the electrode to be repelled to the other electrode^[40], where the charging and repulsive action are repeated. Under a constant applied voltage this process continues until the charge distribution in the liquid bulk eventually reaches a condition of steady-state current leakage and charge-induced distortion in the interelectrode field. Again, polarity reversal, whether under dc or periodic ac conditions, interferes with these slower processes, causing increased repulsion and/or attraction of the particles from (or to) the electrode to which they are attached and accordingly an increase in current.

It should perhaps be noted that in addition to the work presented and referenced here concerning the effects of particles on the space charge distribution in liquid insulators, there is a substantial body of literature concerned with the fact that the insulation strength of compressed gases is greatly reduced by free particles^[41].

2) Electric Field Measurements and Charge Behavior with High Direct Voltage

Typical field distribution data under direct voltage are shown in Fig. 8. This figure contains information obtained from fringe-pattern measurements by applying 0 ± 30 kV direct voltage to one electrode of Cell A (see Table 1). Several minutes of conditioning were allowed at each voltage level to insure steady-state operation. Schlieren observations during these experiments indicated that the dielectric fluid was in motion. The fringe patterns were, however, stable and reproducible after the conditioning period. This indicates that the equilibrium space charge distribution in the liquid was stable in the presence of and in spite of steady-state fluid motion.

Fig. 9 shows explicitly the effects of high voltage conditioning described earlier. The dashed lines show the electric field distribution immediately after polarity reversal (the power supply polarity was reversed so that the nongrounded electrode was changed from positive to negative). During one half hour of negative high voltage operation, with sequence as shown in the figure, the field distribution shifted to those shown by the solid lines. These results are in agreement with those reported by previous workers^[29,42], in so far as all observations show that the field distribution shifts with time when high voltage is first applied to the plates. It is noted, however, that the shape of the field distributions reported by earlier workers differs from those shown in Figs. 8 and 9. This difference is probably attributable to differences in our electrodes; they used varnished brass electrodes, while the present results were obtained using a cell equipped with bare nickel electrodes. Further evidence suggesting that the field shape is

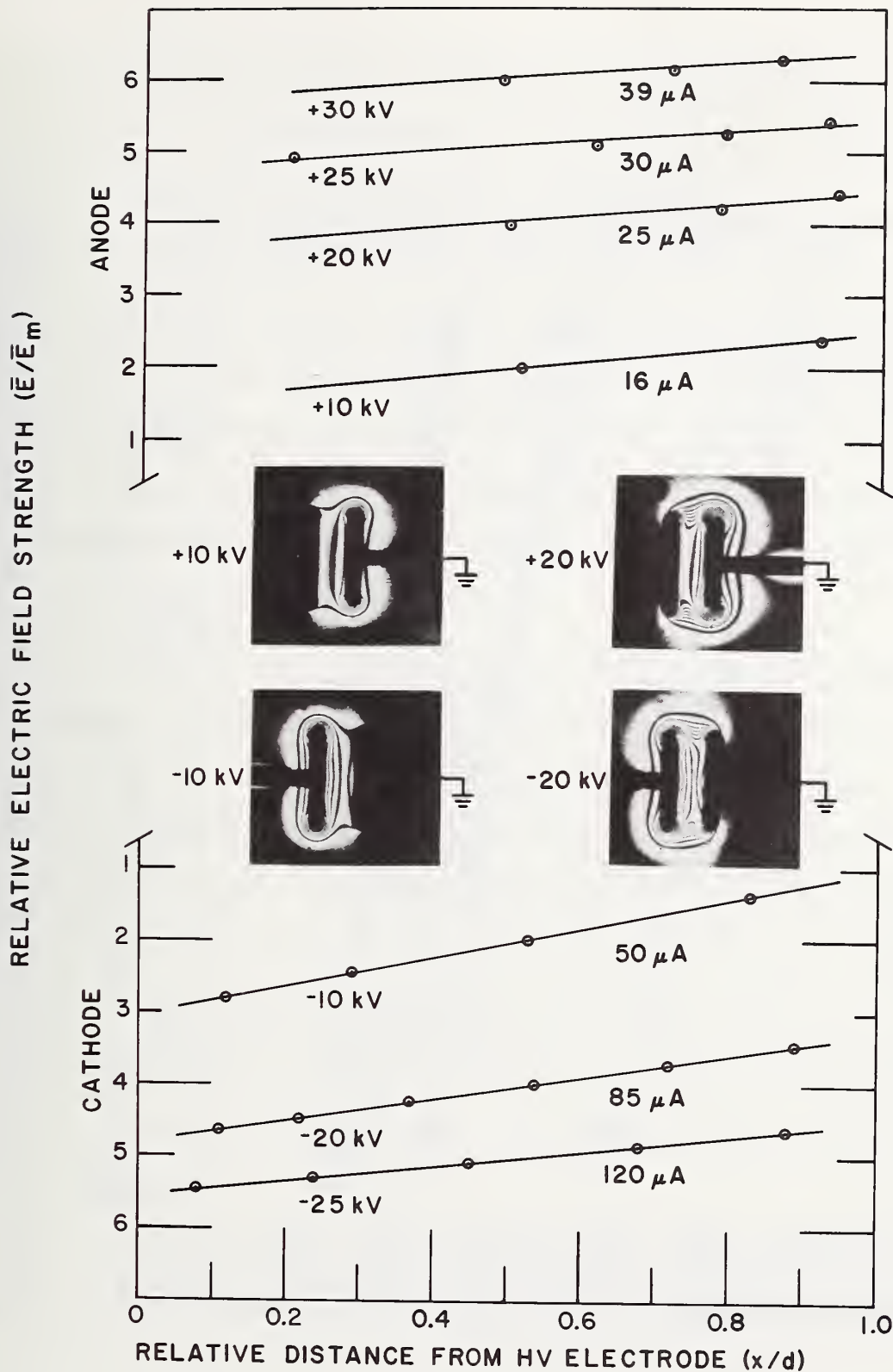


Figure 8. Typical field distribution data under direct voltage. Photographs from which some of the data were taken are presented in the center of the figure. The presence of fringes behind the negative electrode is discussed in the text.

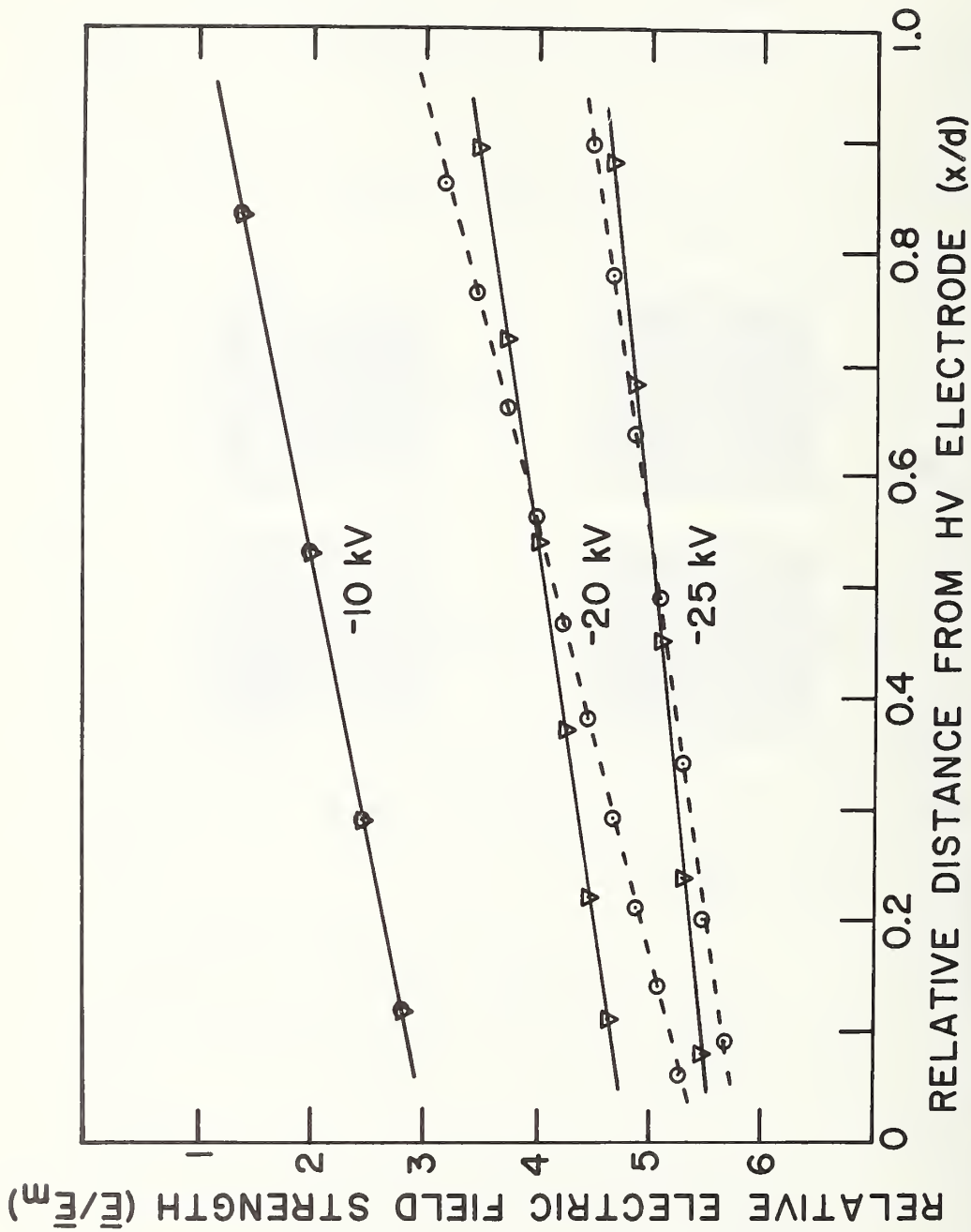


Figure 9. This demonstrates the effects of high voltage conditioning on the data presented in Fig. 6. The dashed lines represent the electric field distribution immediately after the application of negative high voltage while the distribution obtained after high voltage was applied for about a half hour is shown by the solid line.

affected by the electrode material is presented in discussion of Figs. 11 and 14 which show the difference between ac field distribution results when using stainless steel and nickel electrodes, respectively.

Calculations of the interelectrode field distribution, i.e., of $(\bar{E}/\bar{E}_m)_{x,t}$ as a function of relative position (x/d) between the electrodes, and of the reduced space charge density ρ_r were performed as described in Section III. In the dc cases the field distributions were computed and plotted by fitting the data to a first degree polynomial (Eq. 6). In this case ρ_r was independent of the relative position (x/d) between the electrodes and its value was determined from Eq. (12).

Results calculated from the measurements of Figs. 6 and 7 with Cell A and from similar typical experiments with Cell B are listed in Table 2.

Inspection of the results shows several trends over the range studied:

- (1) the net charge in the liquid was always positive and uniformly distributed in the bulk;
- (2) the space charge density in the bulk decreased as the applied voltage (average field) increased;
- (3) the net charge in the liquid bulk was slightly greater when negative high voltages were applied;
- (4) the net charge in the liquid was reduced by extended high voltage operation (conditioning);
- and (5) the net density of space charge was greater in the cell with nickel electrodes (Cell A).

These trends lend evidence to the postulate that leakage conduction is dominated by the motion of small particles between the plates. Previous

TABLE 2. Reduced space charge density in bulk of liquid during high direct voltage operation.

CELL A		
Applied Voltage	Reduced Charge Density	
	Before Conditioning	After Conditioning
(kV)	ρ_r	ρ_r
+10	-	0.87
+20	-	0.88
+25	-	0.77
+30	-	0.62
-10	2.35	2.35
-20	2.64	1.54
-25	1.43	0.90
CELL B		
+15	0.64	-
+30	0.56	0.47
+35	-	0.39
-30	-	0.21

work^[37] has shown that if the particles were metallic with work function smaller than the work function of the electrodes, the particles would receive a greater positive charge at the positive electrode than negative charge at the negative electrode. Because nickel has a very large work function it is likely that in our case such conducting particles would have a smaller work function and therefore that the net space charge density would indeed be positive.

Similarly, the above trends are also compatible with the postulate that the current conduction is governed by the action of insulating particles, in this case perhaps of sub-micrometre size alumina particles which were imperceptibly carried with the liquid in passing from the chromatographic column during the process described in section B. If this be the case, the insulating particles may expect to be attracted to and form a resistive layer or dielectric coating on the electrode surface. This layer would be expected to increase in thickness with voltage and time, thereby slowly reducing the net charge circulating in the bulk and thus the leakage current through the liquid. On removal of the voltage, the attached particles would detach from the electrode and drift slowly back into the bulk. Upon reapplication of voltage they would repeat the same procedure, except that the initial current and rate of decay may be expected to be smaller due to the fact that some particles will undoubtedly remain attached to the electrodes. On polarity reversal, similar behavior would be expected except that the electrode of attraction would change with the polarity.

Schlieren observations of the liquid behavior on removal of the applied high voltage also tend to substantiate the particle postulate. Schlieren movies

beginning immediately before and continuing after sudden removal of high direct voltages show development of localized changes in the index of refraction of the liquid near the electrodes, with gradual development (over a period of several minutes) of differing refractive indices in the upper and lower regions of the test cell in a manner suggestive of gradual settling of the particles under gravity to the lower regions of the cell.

One additional discussion of the dc data is in order. The typical photographs in Fig. 6 show significant light transmission behind the negative electrode. Some light transmission is, of course, expected due to fringing fields behind the electrodes, but these fringing fields would be symmetric about both electrodes and hardly evident at lower voltages. Yet, Fig. 6 indicates that a field of significant intensity exists behind the negative electrode. The fringes behind the cathode in the +20 kV pattern, for example, indicate that $\sqrt{4} < (\bar{E}/\bar{E}_m) < \sqrt{6}$ in the region adjacent to the back of the cathode surface. In this cell, for which $\bar{E}_m = 9.8$ kV/cm, this indicates that $\bar{E} \approx 22$ kV/cm immediately adjacent to the back surface, that $\bar{E} = 0$ at a point located about 0.5 cm from the back surface of the negative electrode. This enhancement of the field behind the negative electrode probably results from the presence of positively charged particles in the liquid bulk. Under the influence of the imposed electrostatic forces the particles would move to and collect about the cathode, including its backside, and cause the observed field enhancement. The irradiance around the cathode support rod in Fig. 6 supports the postulate that charged particles also collect around this portion of the electrode. The fact that \bar{E} goes to zero at a point on the electrode support could indicate that the accumulation of charged particles in this region of the liquid is limited by the shielding

of charged particles already attached to the electrode or by fluid motions which cause the particles to be concentrated in certain regions of the liquid.

Such observations, indicating the existence of space charge in the bulk of the liquid behind an electrode, have not, to the authors' knowledge, been previously reported. Accordingly, this unforeseen behavior and its contribution to electrical stress in liquids are areas for further theoretical and experimental work. In the meantime, several trends are noted from the present work as characteristic of this effect: (1) The field enhancement behind the electrode always appears behind the cathode, whether or not it is grounded, thereby ruling out the possibility that it may result simply from stray capacitance between the high-voltage electrode and ground. (2) The field enhancement is most pronounced under steady-state direct voltage operation; it is barely noticeable under steady-state ac conditions (see Figs. 6 and 10). Under ac conditions the rapid variation of the electric field will not allow charged particles to collect behind an electrode; the particle does not have enough time to travel to the back surface of an electrode before the electrode polarity is reversed. Furthermore, Schlieren observations of the liquid during ac steady state operation show that the fluid motion is much more turbulent than under dc conditions. This greater turbulence would also tend to disperse any particles tending to collect near a given electrode. (3) The magnitude of the enhancement is affected both by the level of applied voltage and by the duration of exposure to high voltage operation: In a continuous experiment the enhancement was observed to increase with voltage

level, as is evident from the +10 and +20 kV fringe patterns in Fig. 6 (one fringe behind the electrode at 10 kV and nearly three at 20 kV) which were taken after days of intermittent exposure to voltage of positive polarity. In widely spaced experiments and those performed without extensive conditioning, the behavior of this enhancement is as yet less predictable. For example, the -20 and -10 kV patterns were taken in that order after about 50 minutes of exposure to voltage of negative polarity; the patterns show greater enhancement at -10 kV (after longer conditioning) than at -20 kV. Another fringe pattern, that recording the data for the -10 kV curve in Fig. 6 (immediately after reversal of the voltage polarity), shows greater enhancement (3 to 4 fringes) behind the electrode before conditioning. The cells were oriented with the plates horizontal and it was consistently observed that there was greater enhancement when the negative electrode was the lower rather than the upper electrode. It is therefore conceivable that the gravitational force might not be negligible in this case. It is evident, however, that further, specific, experimental observations are needed for a detailed and accurate explanation of the causes of field distortion and current leakage in the liquid bulk.

3) Measurements with Alternating High Voltages

Fringe-pattern data concerning the electric field distribution, and hence the space charge density and distribution were taken under a variety of alternating high voltage conditions: (1) Observations were made at the

Frequency

Hz	40	45	50	55	60	65	70	75	80	85	90	95	100	105	110	115	120	125	130	135
Fringe No. n																				
46									.06	.02	.02									
48					.02	.01	.06	.07	.11	.08	.08	.05	.02							
50			.02	.10	.09	.12	.13	.15	.13	.13	.09	.08								
52			.10	.18	.16	.17	.18	.20	.18	.17	.13	.12								
54		.08	.13	.11	.20	.25	.22	.23	.23	.26	.22	.22	.18	.17	.02					
56	.35	.31	.29	.25	.30	.32	.29	.29	.28	.32	.28	.28	.23	.22	.07	.05				
58	.59	.47	.43	.39	.40	.40	.38	.35	.34	.38	.34	.34	.30	.29	.13	.11	.08	.04	.03	
60	.77	.62	.58	.54	.50	.49	.45	.43	.41	.45	.41	.40	.37	.35	.21	.18	.15	.09	.08	.05
62	.91	.75	.72	.71	.62	.58	.55	.51	.49	.52	.47	.47	.44	.42	.29	.27	.23	.16	.16	.11
64		.88	.85	.88	.75	.68	.65	.59	.56	.59	.54	.54	.51	.50	.37	.36	.32	.25	.25	.19
66		.97	.96	.98	.88	.79	.75	.67	.64	.65	.61	.60	.58	.57	.47	.46	.41	.34	.38	.30
68					.98	.88	.85	.75	.71	.72	.68	.68	.64	.63	.56	.55	.52	.47	.52	.45
70						.97	.91	.84	.79	.79	.74	.74	.71	.68	.63	.64	.60	.57	.62	.59
72							.91	.86	.85	.81	.81	.78	.75	.75	.70	.72	.68	.67	.72	.72
74							.98	.93	.91	.87	.87	.85	.81	.81	.77	.79	.75	.75	.80	.80
76							.98	.97	.93	.93	.93	.91	.87	.87	.83	.86	.81	.83	.87	.88
78									.98	.98	.96	.92	.92	.92	.90	.92	.97	.89	.93	.94
80											.97	.97	.97	.97	.97	.98	.93	.95		

x/d
25 kV rms

TABLE 3 Fringe position x/d as a function of frequency with 25 kV rms applied to Cell B.

positive peak of sinusoidal voltages of various levels (to 30 kV rms) and frequencies (between 40 and 200 Hz); (2) Observations were made at $(1/16) T$ intervals over the course of an entire cycle of such operation; (3) As in the dc studies, these observations were conducted using both cell A and B so as to bring out behavioral differences which might be attributable to the electrode materials. Typical results from these studies are presented and discussed in the following paragraphs.

Fig. 10 shows the fringe patterns photographed at the positive maximum of a 22 kV rms sinusoidal voltage at various frequencies between 40-105 Hz using Cell B. The significant observation from these photographs is that the number of interelectrode fringes is frequency dependent, with a maximum at approximately 80 Hz. Typical data from frequency studies at 25 kV rms, obtained from twenty different fringe pattern photographs, are compiled in Table 3. In this table the relative position x/d of each transmission minimum, $(\bar{E}/\bar{E}_m)_{x,t}^2 = n$, is tabulated with the frequency of the applied voltage as a parameter. It is immediately obvious that the number of interelectrode fringes is frequency dependent, with a broad maximum in the vicinity of 80-105 Hz. From these data, the space charge density as a function of the frequency of the applied voltage can be calculated (Eqs. 11 and 12). Graphs showing the reduced space charge density ρ_r as a function of the frequency of the applied voltage at two different voltage levels are shown in Figs. 11 and 12. These data, like those in Fig. 10 and in Table 3, are the results of observations taken at the positive maximum of the applied voltage. Two conclusions can be seen from the plotted ρ_r vs. frequency curves: as the magnitude of the alternating voltage is increased, the frequency at which the maximum space charge occurs shifts toward higher frequencies and the magnitude of the maximum space charge increases.

22 kV rms, Positive Maximum

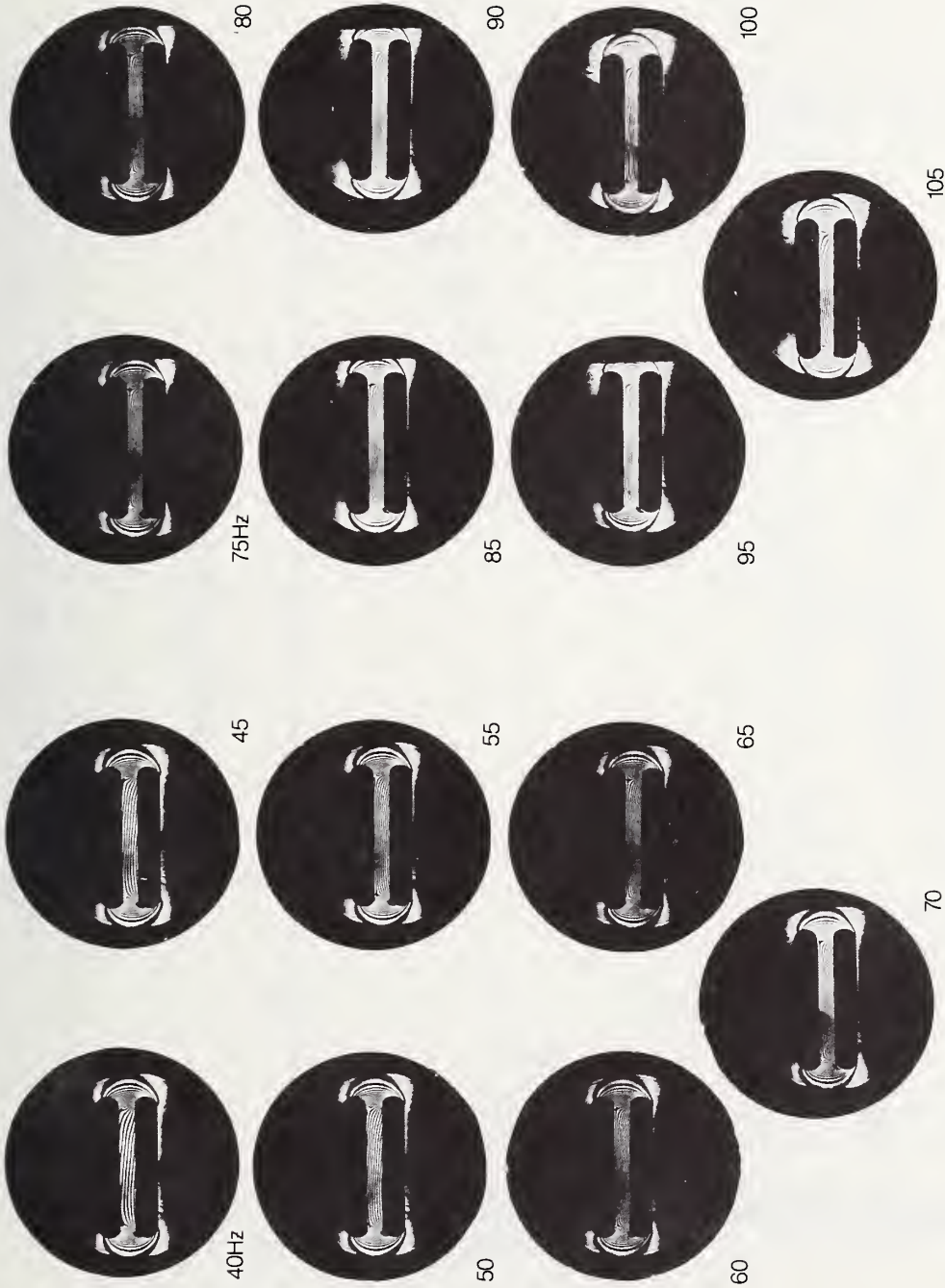


Figure 10. Photographs showing the fringe patterns taken at the positive peak of a 22 kV rms sinusoidal voltage at various frequencies between 40-105. It can be seen that the number of interelectrode fringes is frequency dependent with a maximum at approximately 80 Hz.

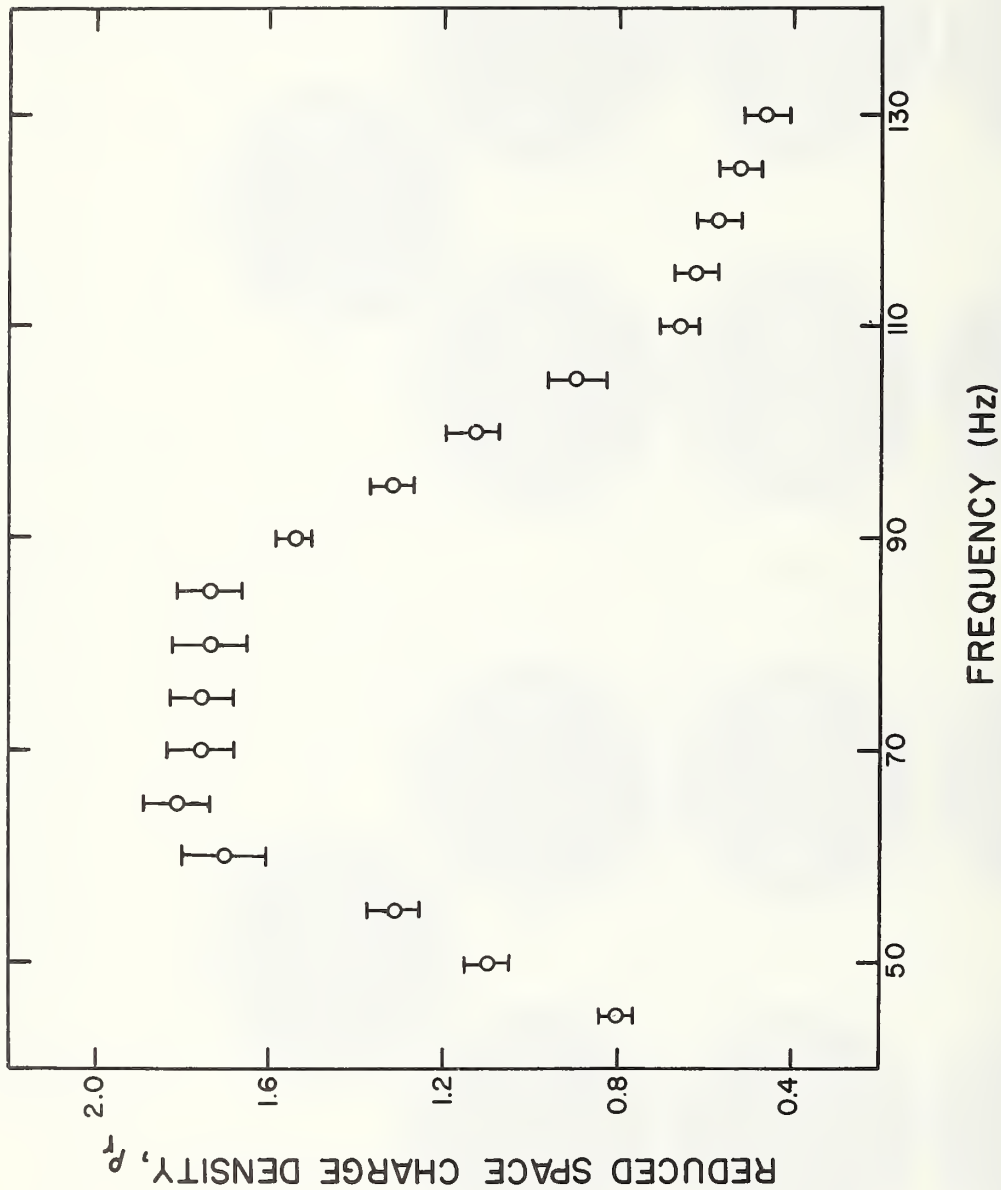


Figure 11. The reduced space charge density, ρ_r in Cell B as a function of the frequency of an applied 15 kV rms voltage. Each data point was determined from the electric field distribution observed at the positive peak of the applied sinusoidal voltage. The error bars indicate the standard deviation of the coefficient of the applied ρ_r as determined from a linear least squares fit of the electric field between the electrodes. Note that the reduced space charge density has a maximum at a frequency of approximately 60 Hz.

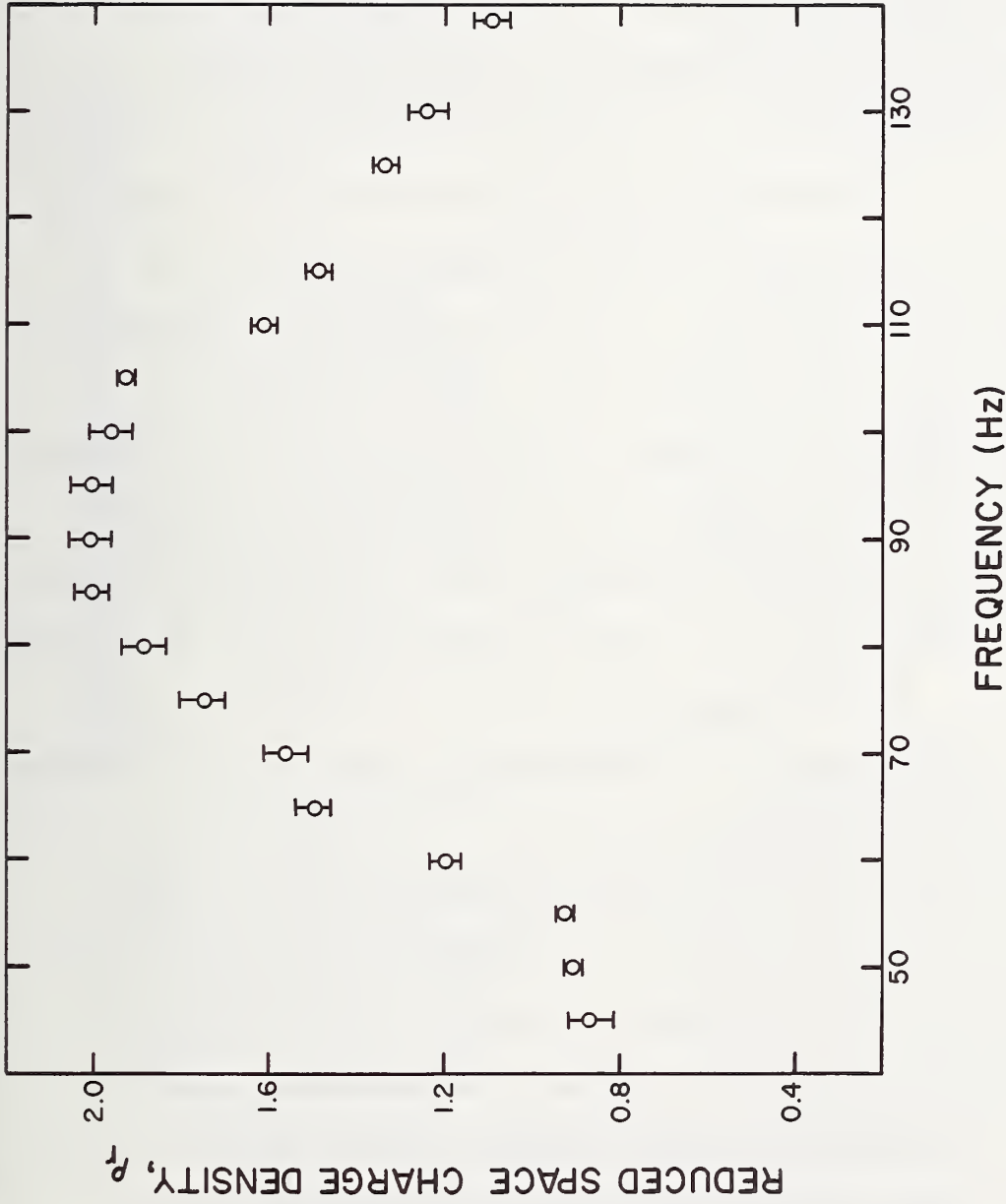


Figure 12. The reduced space charge density as a function of the frequency of an applied 25 kV rms voltage. The meaning of each data point is the same as in Fig. 9. In comparison with Fig. 9 the maximum reduced space charge density has shifted to a higher frequency of approximately 90 Hz.

During the course of this study, data were taken not only at the positive maximum of the applied voltage but also at selected points during the cycle of the applied voltage. Field distributions plotted from typical observations at various times during a cycle of 15 kV rms, 60 Hz operation using Cell B are shown in Fig. 13. We note that the electric field distribution is linear with positive slope throughout the whole cycle. If we extrapolate to zero, $1/2 T$, or T , the field distribution is linear, being equally positive and negative about the center ($x/d = .5$). Fig. 14 shows some of the fringe patterns from which these plots were obtained. Note that at time $1/2 T$, the applied voltage is instantaneously zero, yet light appears near the electrodes. When the voltage is instantaneously zero, the total surface charges on each electrode are negative and equal in magnitude, while the total volume bulk charge is double in magnitude and positive, keeping the system neutral. (The surface charge per unit area on the electrodes can be computed by the discontinuity of the normal component of $\epsilon\vec{E}$). At other times in the cycle, the volume charge density remains constant (independent of voltage polarity), while the surface charge on the electrodes varies sinusoidally with time.

It is also interesting to note from Fig. 14 that again some light, although over a much smaller area than was found with dc voltages, is also transmitted behind the cathode during ac operation. Further measurements over the complete cycle show this anomalous field enhancement follows the sinusoidal cycle, alternating between electrodes, as the field enhancement always appears behind that electrode which is instantaneously negative.

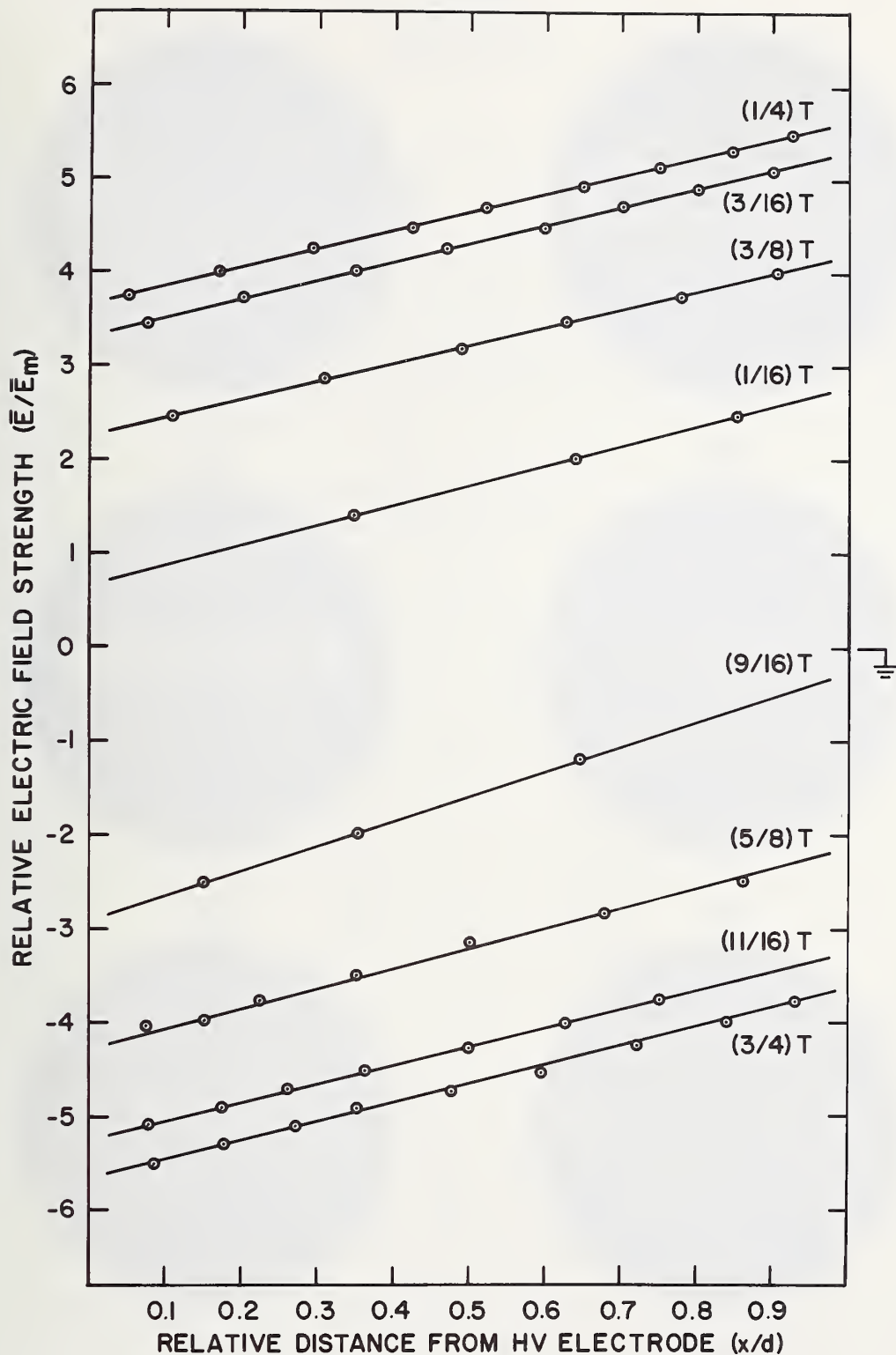
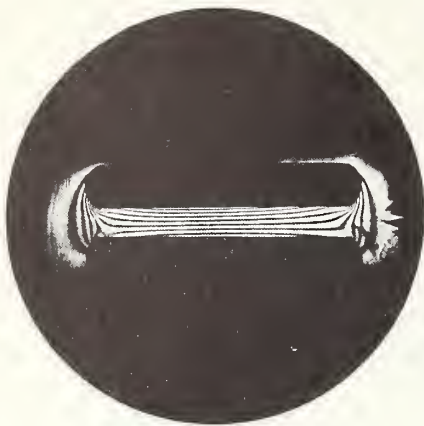


Figure 13. The electric field distribution in Cell B at various times during the cycle of 60 Hz, 15 kV rms applied voltage. The period of the applied waveform is denoted T, so, for example, the data designated as $1/4T$ were taken at the positive maximum of the applied voltage.

60Hz
15 kVrms



$\frac{3}{8}T$



$\frac{7}{16}T$



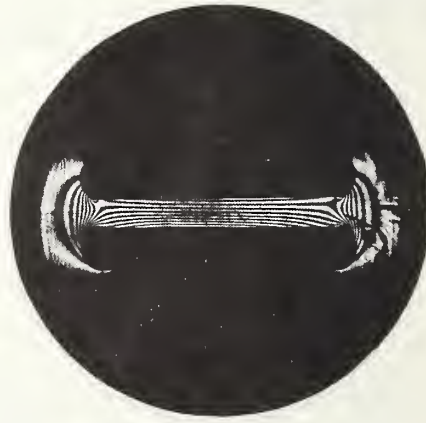
$\frac{1}{2}T$



$\frac{9}{16}T$



$\frac{5}{8}T$



$\frac{11}{16}T$

Figure 14. Photographs from which some of the data in Fig. 11 were taken. Note that there is some light transmitted at $1/2T$, i.e., when the voltage is instantaneously zero. As explained in the text, this indicates that the bulk space charge density is constant throughout the cycle.

Measurements of the electric field as a function of position at the positive maximum of the applied voltage at various voltage levels and selected frequencies are plotted in Fig. 15. From this type of observation, the following results, showing relationship between the frequency, f_{\max} , at which the net space charge density was maximum and the applied voltage level, were obtained:

TABLE 4 Measurements of f_{\max} At
Various Voltage Levels Using Cell B

Voltage (kV rms)	f_{\max} (Hz)
10	45-65
12	55-65
15	60-85
20	80-95
22	80-95
25	90-105

Similar measurements with Cell A showed many of the same features. The dc field was observed to be a linear function of position between the electrodes (see Fig. 7), again indicating a uniformly distributed net positive charge in the liquid bulk. In addition, observations at the peak voltages during ac operation at various frequencies indicated that the distortion in the ac field, and thus the density of charge in the liquid, was again frequency dependent. Measurements with 20 kV rms

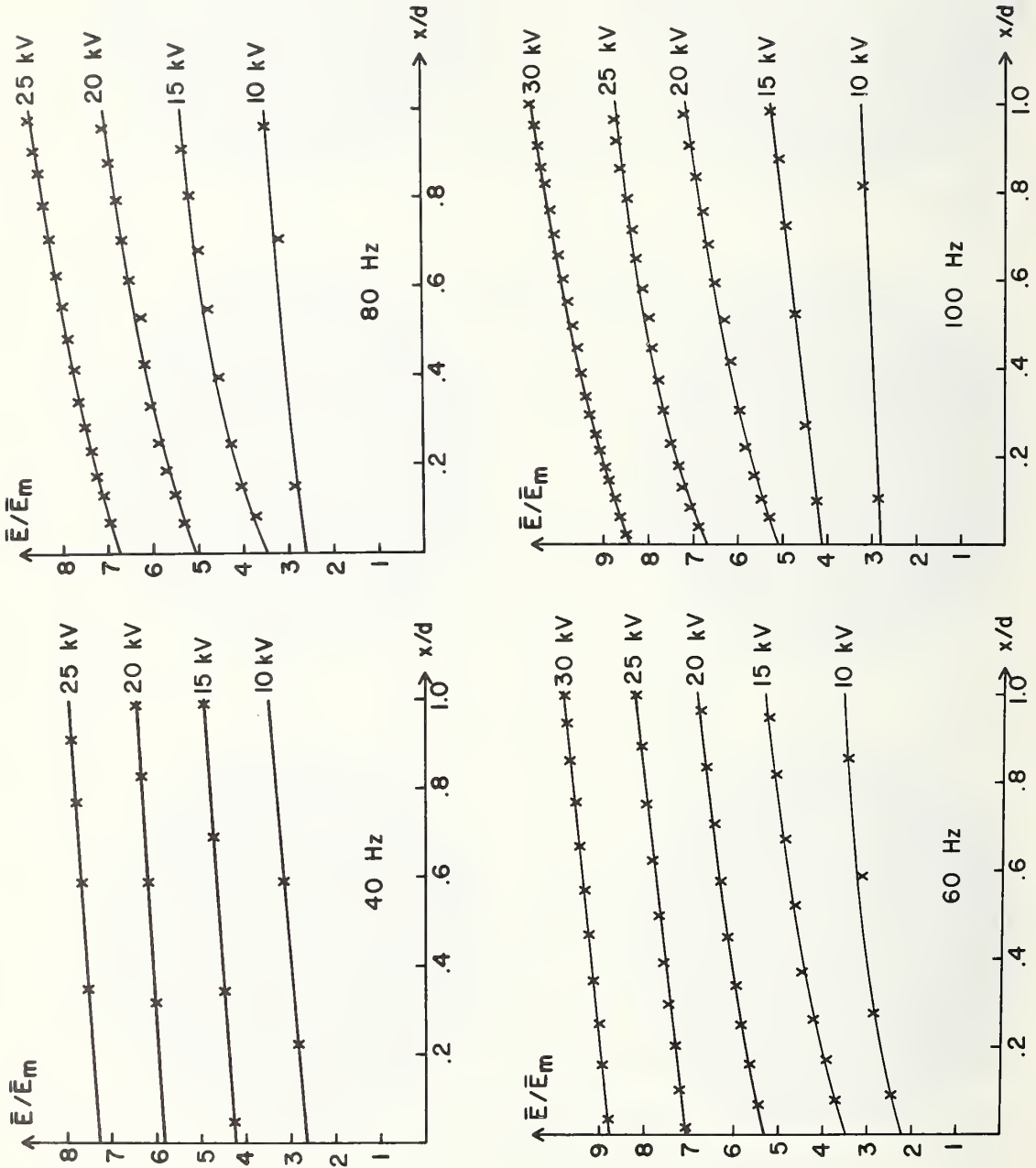


Figure 15. The electric field distribution at selected frequencies and voltage levels in Cell B. All of the data in this figure were taken at the positive maximum of the applied voltage.

applied showed, for example, that the field distortion and charge density were maximum at approximately 100 Hz, thereby demonstrating good agreement with the B-cell measurements which showed $f_{\max} = 80-95$ Hz at 20 kV rms (see Table IV).

There were, however, also significant differences between the A and B observations. The A-cell fringe-pattern measurements consistently showed that the A-cell ac electric field is not a linear function of position, and that the field distribution varies periodically with time during each cycle of ac operation, being periodically uniform and nonuniform as may be seen from the field measurement data plotted in Fig. 16. The curves show that maximum distortion occurs near the positive and negative peaks of the alternating voltage waveform. Moreover, observations at these times showed that the interelectrode field in this cell has an inverted "U-shaped" distribution (see the ac results in Figs. 7 and 16). Whereas a linear field distribution was found typical in Cell B, this inverted "U-shaped" distribution, which implies the presence of positive space charge near the anode and negative charge near the cathode (a situation noted by Croitoru [28] as being indicative of charge injection at the electrodes), was found typical of Cell A at the voltage peaks during ac operation.

Finally, since the field distributions characteristic of each cell were found to be reproducible for substantial periods of time in spite of repeated refillings of the cells with nitrobenzene, we have felt it reasonable to attribute the differences between their ac field distributions to the differences in their electrode materials and/or surface preparations.

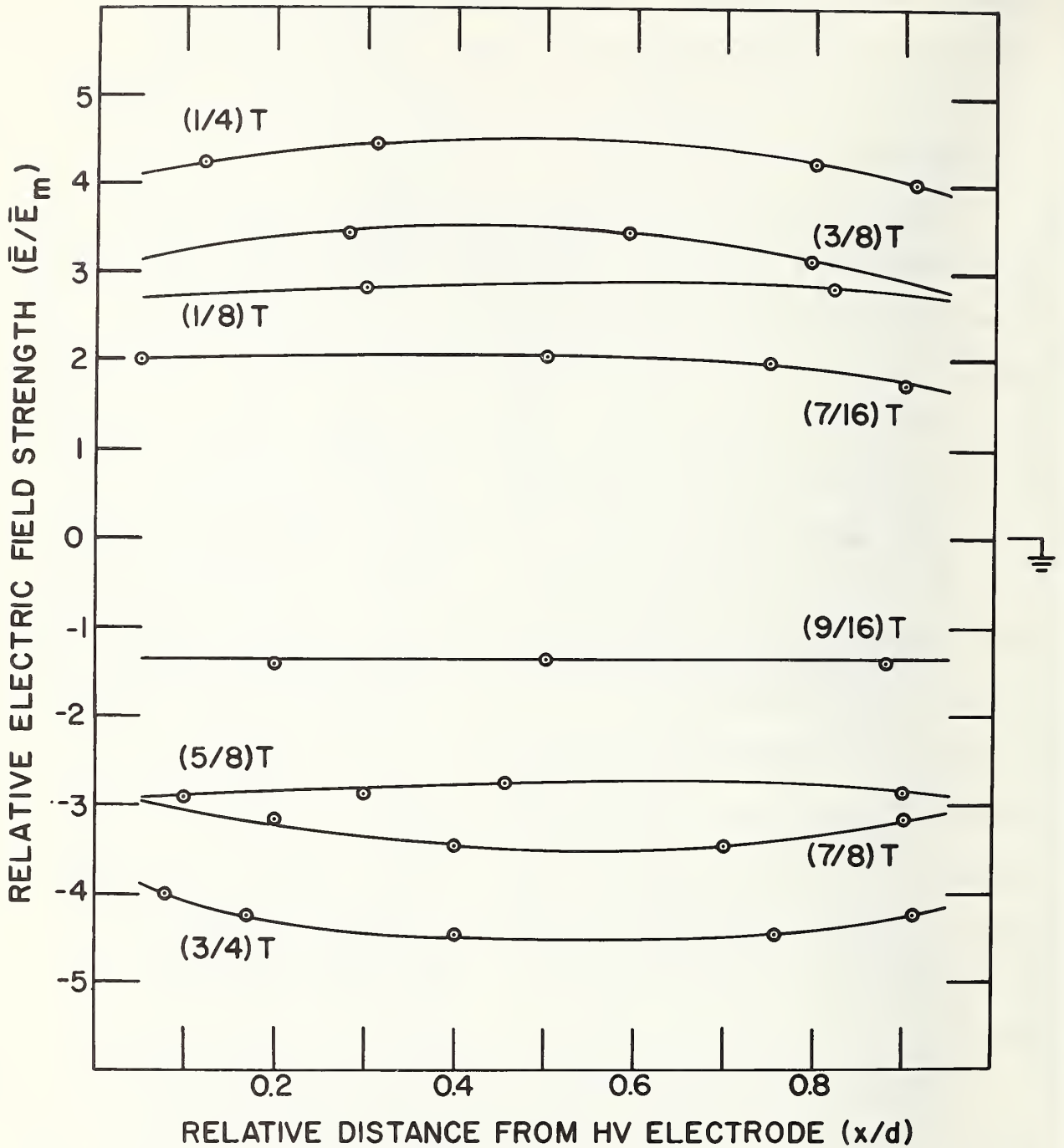


Figure 16. The electric field distribution in Cell A as a function of time with a 60 Hz, 15 kV rms applied voltage. Note that in this cell the field distribution is no longer linear but varies periodically during a cycle.

Verification of this conclusion and distinction of the relative contributions of the material from those of the surface conditions will, however, require further study.

E. Summary and Conclusions

Our purpose has been to document, from examination of results from extensive Kerr effect fringe-pattern observations in nitrobenzene, several space-charge-induced trends in the behavior of an insulating liquid under the stress of high voltage operation. We have demonstrated experimentally that electric field distributions in the bulk of the liquid are predictable only during operation under short (μs) pulse conditions. Results from observations during dc and low frequency ac operation have shown that the interelectrode electric field and space charge distributions are dependent upon the level and frequency of the applied voltage, the electrode material and their surface condition, and the immediate previous history of the system.

In a cell with electro-polished stainless steel electrodes, the interelectrode field distribution was approximately linear and the net space charge density was positive during operation under high dc and low frequency voltages. Further, the net charge measured during operation at a given ac voltage (i.e., at a constant rms level) was found to be independent of the instantaneous voltage. The net charge in the liquid bulk between the electrodes remained constant throughout the entire course of the ac cycle, even when the instantaneous voltage was zero, thereby suggesting that the field and charge distributions in this cell are governed primarily by a steady-state arrangement of charged particles uniformly distributed and suspended in the bulk by the steady streaming motion of the liquid

between and around the electrodes.

Observations with a cell having glass blasted nickel electrodes showed different results. The interelectrode field distribution was linear under direct voltage, but parabolic under alternating voltages. The observed ac fields were weaker near the electrodes and stronger in the region midway between them, thereby implying the formation of positive space charge near the anode and negative charge near the cathode. As might be expected in a charge injection process, the electric field distribution and charge density in the bulk also varied as a function of time (and thus voltage) during each cycle of ac operation. The difference between the field and charge behavior in the two cells is attributed to their differences in electrode materials and surface conditions.

Except for these features, essentially the same behavior was observed in both cells. Their dc fields were both linear functions of position between the electrodes, and both showed space charge enhancement of the field behind the negative electrode. This latter effect is maximum for direct voltages and decreases with excitation voltage frequency, whereas electrohydrodynamic motion of the liquid (always observed during steady-state high voltage operation), distortion of the interelectrode field, and charge density in the liquid are much more pronounced during low frequency ac operation.

With regard to the distortions in the ac fields, the distributions observed were found to be frequency dependent; as the frequency of the exciting voltage was increased the charge measured in the liquid bulk between the electrodes increased. The plot of space charge density vs. frequency exhibited a maximum, with this maximum shifting toward higher frequencies as the voltage

level is increased. As the frequency of excitation was further increased, the field distribution became uniform and the space charge density in the liquid approached zero, as would be expected when the time between polarity reversals was too short for charge collection in the liquid near and around the electrodes.

Finally, though these observations still offer no conclusive rules for reliable prediction of steady-state field and charge behavior (and thus of the onset of breakdown) in an insulating liquid, they do demonstrate several important, as yet undocumented trends to be expected in the bulk of the liquid when under the stress of high voltage operation. It is hoped that the experimental evidence presented will stimulate the further research and theoretical investigation needed for a more thorough understanding of the mechanisms of breakdown in liquid-insulated high voltage equipment.

III. MEASUREMENT OF THE KERR CONSTANT OF NITROBENZENE

A. Introduction

The electro-optic Kerr effect was identified by John Kerr in 1875. Since that time it has been used for a variety of purposes including high voltage measurement, electro-optic field mapping, high speed shutter applications, etc. Historically, the electro-optic Kerr coefficient has been measured in an attempt to obtain information concerning either molecular structure or molecular interactions in the liquid state. Because the molecular systems that exhibit a large Kerr coefficient were not amenable to convenient, accurate theoretical analysis, the accuracy requirements were not stringent. The development of high voltage measurement systems based on the electro-optic Kerr effect have however necessitated the accurate determination of the Kerr coefficient to insure proper design. In addition, it is necessary to know the temperature dependence of the Kerr coefficient so that measurements performed at different temperatures can be compared without loss of accuracy.

An additional significance of the present work is that most previous determinations of Kerr constants were made before lasers became commonplace. Most earlier determinations were not, therefore, performed at wavelengths of interest today. Although it is recognized that a general characterization of the Kerr constant as a function of wavelength is needed, the present study was designed to supplement existing information at specific laser wavelengths.

The Kerr constant was defined by Eq. 2 (Sec. II-C). Making the same assumptions that were previously discussed, we can rewrite Eq. 2c as

$$B = \phi(x, t) \left[2\pi \int_0^L E^2(x, z, t) dz \right]^{-1} \quad (14)$$

The work described here was confined to centrally located paths and the measurements of ϕ and E were performed simultaneously at the peak of a high voltage pulse of approximately 10 μ s duration. We therefore suppress the x and t dependence and rewrite Eq. 14

$$B = \phi \left[2\pi \int_0^L E^2 dz \right]^{-1} \quad (15)$$

At this point we depart from the notation developed earlier and write

$$B = \phi \left[2\pi \left(\frac{V}{d} \right)^2 L' \right]^{-1} \quad (16)$$

where V is the applied voltage, d is the plate spacing and L' is the effective length of the plates. This assumes that the actual field distribution can be represented as a uniform field of strength $\frac{V}{d}$ and extending over a length L' . Determination of the Kerr constant, therefore, requires that the phase shift ϕ , the applied voltage V , and the plate spacing d be measured and that the effective length L' be determined.

B. Experimental Technique

1) Introduction

This section describes two independent pulsed voltage techniques that were used to measure the Kerr electro-optic coefficient of liquid nitrobenzene at various temperatures and at selected wavelengths. In each technique, voltage pulses of 15-85 kV peak magnitude and approximately

10 μ s in duration are used. The following discussions include a brief description of the Kerr cell construction and the basic theory needed in determining the Kerr electro-optic coefficient of nitrobenzene using each technique.

2) "End-Field Free" Cell Technique

The "end-field free" cell, Fig. 1, used to make Kerr coefficient measurements is designed specifically so that the applied electric field is uniform over the nitrobenzene-filled segment of the light path, i.e., so that the fringing end field distortions are exterior to the nitrobenzene portion of the light path. The cell was constructed with two parallel plate electrodes overlapping a four-sided, rectangular, glass chamber used to confine the nitrobenzene. The interior dimensions of the glass chamber were given in Section I.

For a light path centrally located in the glass chamber and parallel to the length of the electrodes the total phase retardation ϕ is given by

$$\phi = \frac{2\pi BLV^2}{d^2} + \phi_{\text{mech}} \quad (17)$$

where L is the interior length of the glass chamber (the length of the nitrobenzene portion of the light path) and ϕ_{mech} is the phase retardation resulting from mechanical strain present in the glass windows at the ends of the chamber. Under the assumption that ϕ_{mech} is a constant, the electro-optic coefficient can be determined from two separate experiments which measure the phase retardations ϕ_1 and ϕ_2 at two different applied voltages V_1 and V_2 , respectively. Using this information, both B and ϕ_{mech} can be

calculated from Eq. 17:

$$B = \frac{(\phi_1 - \phi_2)d^2}{2\pi L (V_1^2 - V_2^2)} \quad (18)$$

and

$$\phi_{\text{mech}} = \frac{V_1^2 \phi_2 - V_2^2 \phi_1}{V_1^2 - V_2^2} \quad (19)$$

3) Two Cell Technique

This technique utilizes the two Kerr cells of conventional design shown in Fig. 17. For a centrally located light path between the electrodes in each cell the applied electric field will vary along the length of the light path due to the fringing fields at the ends of the electrodes. Each cell is identical except in the length of the electrodes where the respective lengths for cell A and cell B are 24 cm and 12 cm. From Eq. 16, the phase retardation for each cell can be written

$$\phi_A = 2\pi B \left(\frac{V}{d_A}\right)^2 L'_A \quad (20)$$

$$\phi_B = 2\pi B \left(\frac{V}{d_B}\right)^2 L'_B \quad (21)$$

The cells are constructed so that $d_A = d_B$ and so that

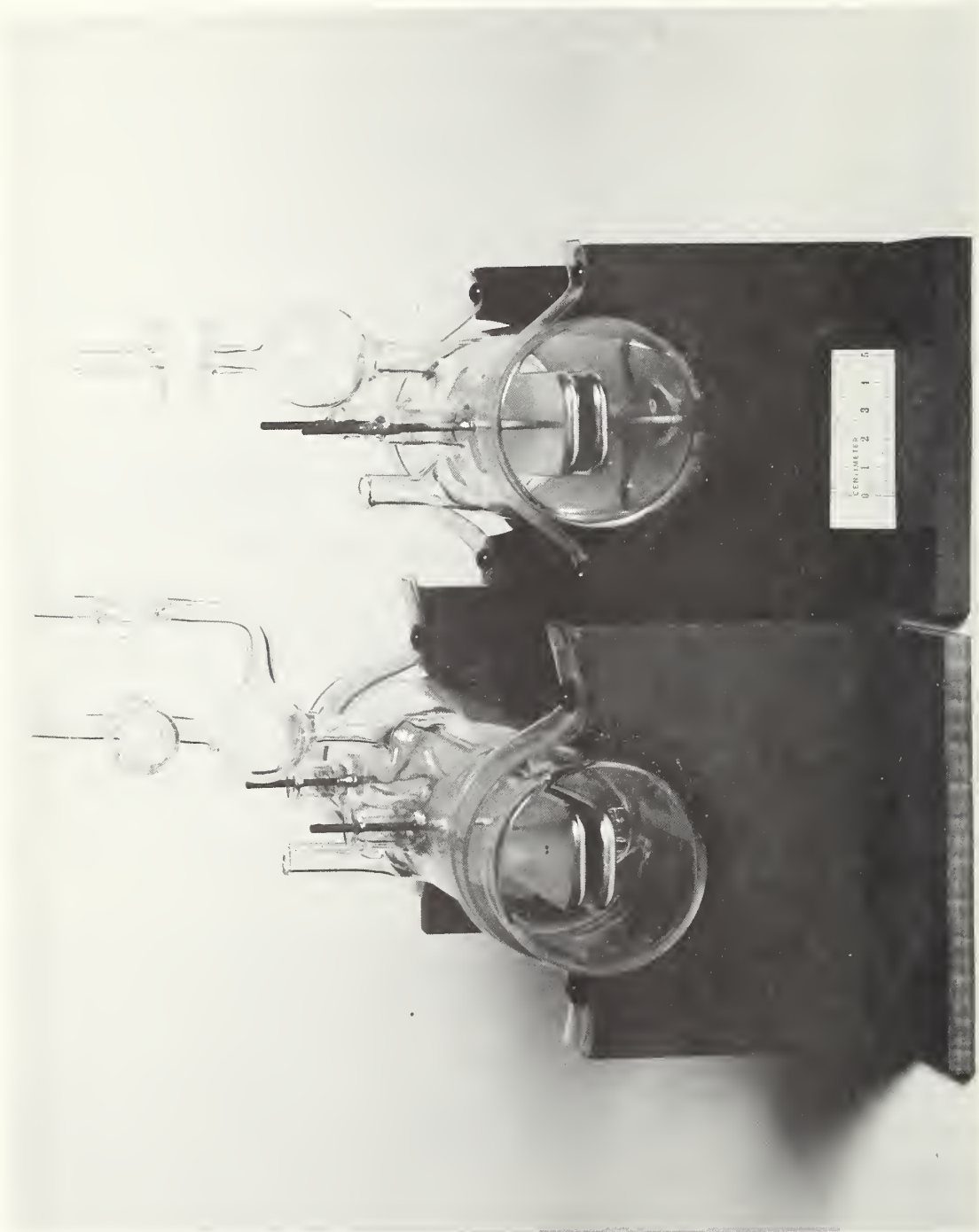


Figure 17. End view of cells used to determine the Kerr coefficient of nitrobenzene by the "two-cell method." The cells were designed so that all relevant geometric parameters, except the length of the electrodes, are identical.

$$L'_A = \ell_A + \Delta\ell \quad (22)$$

$$L'_B = \ell_B + \Delta\ell \quad (23)$$

where $\Delta\ell$ is the correction that must be added to the geometric length of the plates to obtain the effective length. The basis for the assumption that $\Delta\ell$ is independent of the length of the plate is the solution to the electrostatic boundary value problem first solved by Lemoine^[43],

$$L' = \ell + \frac{d}{\pi} \left[1 - \frac{d}{\ell} \log \frac{\pi\ell}{d} \right], \quad (24)$$

and later generalized by Chaumont^[44],

$$L' = \ell + \frac{d}{\pi} \left[1 + \frac{t}{d} \log \left(1 + \frac{d}{t} \right) \right]. \quad (25)$$

In these expressions ℓ is the electrode length, d is the spacing, and t is the thickness of the electrodes. Eq. 25 indicates that if one constructs two cells differing only in the length of their electrodes, the difference between the effective lengths would be equal to the difference between the geometrical lengths of their electrodes.

Using Eqs. 22 and 23, Eqs. 20 and 21 can be solved to yield

$$B = \frac{d^2}{2\pi V^2} \frac{\phi_A - \phi_B}{\ell_A - \ell_B} \quad (26)$$

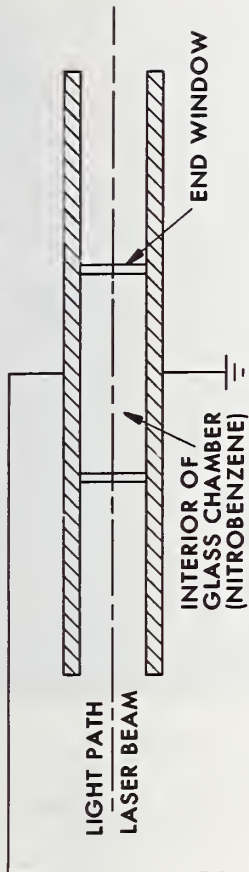
4) Experimental Procedure

The experimental arrangement of Kerr cells used in making Kerr coefficient measurements by the "end-field-free" cell and by the two-cell method is shown in Fig. 18. A schematic diagram of the pulse voltage generating and measurement system is also included. The basic apparatus used in each technique is conventional in high voltage pulse measuring Kerr systems, the details of which have been described previously [1-6]. Additions to this apparatus and procedural changes have been included to permit measurement of the electro-optic coefficient at selected wavelengths and over the temperature range from 290 K to 315 K.

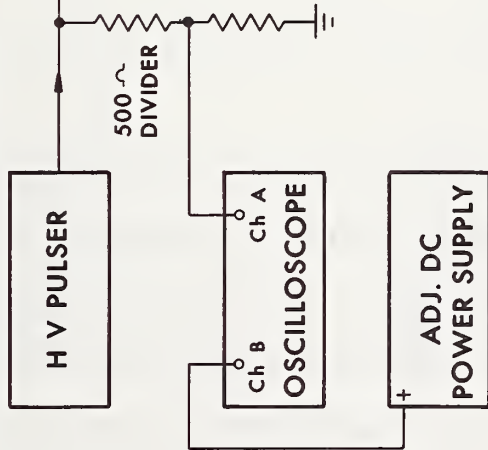
Electro-optic measurements are made at different wavelengths using either a cw HeNe laser (632.8 nm) or a pulsed argon laser. A wavelength selector at the output of the argon laser is used to obtain Kerr coefficient measurements at a number of laser wavelengths of argon gas, specifically 514.5, 496.5, 488.0, and 476.5 nm.

The temperature of the nitrobenzene is varied using a commercially available heater to stir and warm the oil bath in which the Kerr cell is placed. Measurements of the Kerr electro-optic coefficient are initially carried out at room temperature. The oil bath is then heated until the mercury thermometer sealed inside the Kerr cell indicates a temperature of approximately 310 K. The heater is then removed but measurements are not

END FIELD FREE CELL TECHNIQUE



PULSED VOLTAGE AND DIVIDER MEASUREMENT SYSTEM



TWO CELL TECHNIQUE

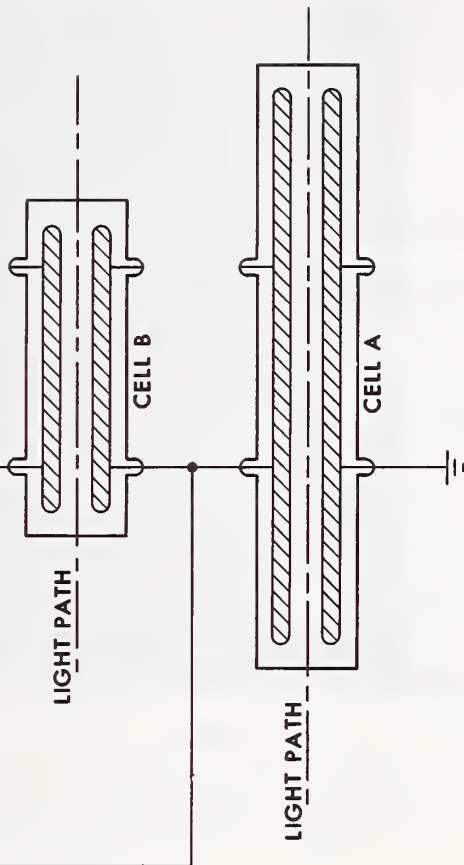


Figure 18. Schematic diagram of the apparatus used for Kerr coefficient measurements. The system is designed so that a measurement of the voltage pulse using the divider and either of the Kerr cell techniques could be made simultaneously.

taken until the bubbles produced from the mixing of the oil settle out, allowing an undispersed laser beam to be transmitted through the Kerr cell. As the nitrobenzene cools data are taken after every 1 K drop in temperature. The cooling rate is approximately linear with a slope of 2 K/h.

Typical oscillograms used to make Kerr electro-optic coefficient determinations from the two cell technique are shown in Fig. 19. Included are the voltage divider "slideback" measurements showing the peak of the applied voltage pulse and photomultiplier response to the light transmitted through cells A and B. Each Kerr cell is situated between a polarizer and an analyzer oriented at plus and minus 45° with respect to the applied electric field. The light path through each cell is aligned with a photomultiplier which provides an output voltage approximately proportional to the irradiance of the transmitted light.

The relative irradiance transmitted through a Kerr system is given in Eq. 5,

$$(I/I_m)_{x,t} = \sin^2 \left[\frac{1}{2} \pi (\bar{E}/\bar{E}_m)_{x,t}^2 \right] .$$

It is shown in Fig. 19 that as the voltage decreases the transmitted light intensity varies through a series of maximum and minimum values producing a series of light pulses. The maximum and minima defining each light pulse are assigned odd and even integers respectively for counting the first maximum before the voltage pulse falls to zero as 1, the first minimum before the voltage falls to zero as 2, the second maximum as 3, second

VOLTAGE DIVIDER SLIDEBACK MEASUREMENT

$V_{\text{peak}} = 34,000$ volts

KERR CELL B

$n = 30 \quad I/I_m = 0.78$

KERR CELL A

$n = 64 \quad I/I_m = 0.04$

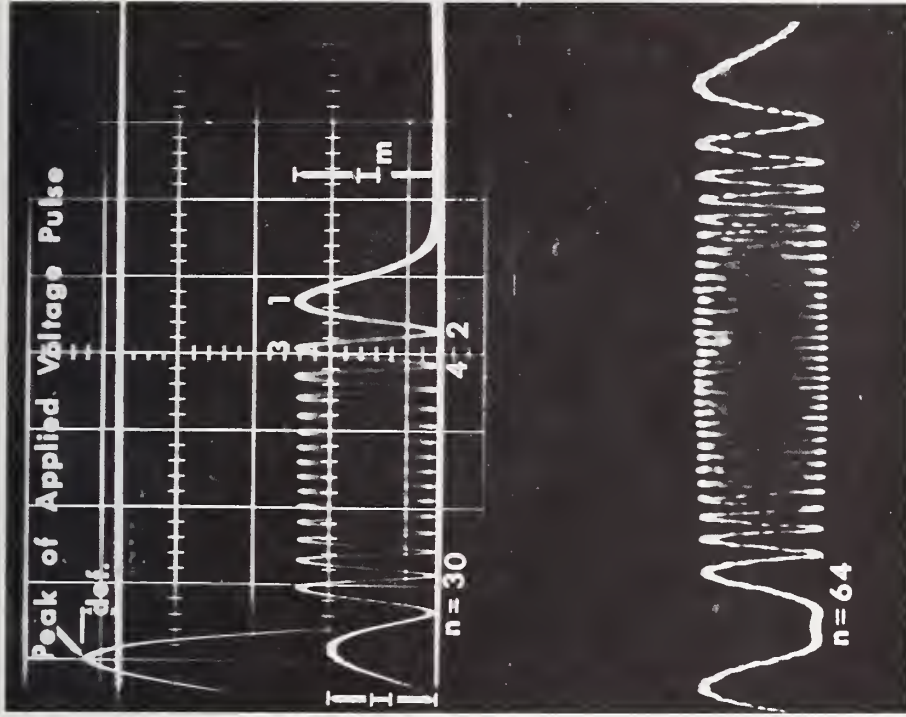


Figure 19. Typical oscillograms used in the determination of the Kerr electro-optic coefficient by the two cell technique.

minimum as 4, etc. The count is continued to the peak of the voltage pulse, thus defining the largest integer n. The values of I/I_m and n determined from an oscillographic record of the photomultiplier response are used to compute ϕ for a given Kerr system at the peak applied voltage.

The peak value of the applied voltage pulse is determined using a "slideback" technique for measurement of voltage across the low side of a 500 Ω pulse divider connected in parallel with the appropriate Kerr cell(s). This pulse measurement procedure yields a value of the peak magnitude of the voltage pulse which is estimated to be within $\pm 1\%$ of its true value.

C. Results

A comparison was made between the Kerr electro-optic coefficient of nitrobenzene, at 632.8 nm determined by the "end field free" cell technique and the two cell technique. Values of the electro-optic coefficient B of nitrobenzene were determined from a series of at least ten experiments performed using each technique at each specified temperature. The mean values of B are compared in Table [5].

Table [5] Comparison of Kerr Coefficient Determinations

	$B[m/(V)^2]$	Temperature (K)
End Field Free Cell Technique (1cmx4cm)	3.21×10^{-12}	295.8
	3.17×10^{-12}	296.1
Two Cell Technique	3.24×10^{-12}	296.0

The values quoted in this table are estimated to be accurate to within $\pm 5\%$. This estimate is obtained by assuming that there is a cumulative error of not more than $\pm 4\%$ in the measurement of ϕ and geometrical parameters involved as there is an uncertainty of $\pm 1\%$ in the voltage measurement. Within each set of at least ten measurements, no determination of B differed from the average by more than 1.6%.

The Kerr electro-optic coefficient of nitrobenzene was measured at different wavelengths using the "end field free" cell. As previously explained, it is necessary to perform experiments at two different voltage levels to correct for the birefringence due to residual strain in the glass windows of the cell.

In Table [6], the Kerr electro-optic coefficient of nitrobenzene is categorized according to wavelength and according to nominal values of the peak voltages used. The Kerr coefficient is computed from Eq. 26. More than one Kerr coefficient value entered into a given category signifies that a set of experiments were taken several days apart to verify the consistency of the measurements.

At a given wavelength, calculations (Eq. 19) indicated that the mechanical phase retardation varied according to the pair of voltages used. This situation is made explicit in Table 7, in which the Kerr coefficient and phase shift due to strain birefringence in the glass window of the cell are tabulated with wavelength and temperature as parameters. As stated previously, at least ten observations were made at each value of temperature and wavelength. The average and minimum and maximum value for ϕ_{mech} are listed. Two possible causes of the wide variation in ϕ_{mech} have been identified:

Wavelength (nm)	Kerr electro-optic coefficient of Nitrobenzene $B(m/V^2)$		
	a	b	c
632.8	3.20×10^{-12} 3.12×10^{-12}	3.19×10^{-12}	3.16×10^{-12}
514.5	4.20×10^{-12}	--	4.24×10^{-12}
496.5	4.43×10^{-12}	4.42×10^{-12}	4.42×10^{-12}
488.0	4.58×10^{-12} 4.54×10^{-12}	4.66×10^{-12}	4.58×10^{-12}
476.5	4.68×10^{-12}	4.72×10^{-12}	4.71×10^{-12}

Table [6] The Kerr electro-optic coefficient of nitrobenzene B is given for various wavelengths at a temperature of 296 K. Values of B were computed from experimental data as prescribed for the end-field free cell technique. Columns a, b, and c indicate pairs of nominal voltage levels (80 & 60 kV, 100 & 80 kV, and 100 & 60 kV respectively) at which experiments were performed to compute B using this technique.

Wavelength (nm)	B(m/V ²)	ϕ_{mech} (radians)			T(K)
		Average	Minimum	Maximum	
632.8	3.21×10^{-12}	-.451	-.625	-.171	295.8
632.8	3.16×10^{-12}	-.457	-.878	-.079	296.1
514.5	4.23×10^{-12}	-.565	-.740	-.322	296.1
496.5	4.44×10^{-12}	-.681	-.997	-.483	296.2
488.0	4.55×10^{-12}	-.584	-.855	-.146	296.1
476.5	4.70×10^{-12}	-.269	-.946	-.008	296.1

Table [7] Kerr electro-optic coefficient of nitrobenzene at different wavelengths. Values of the mechanical strain phase retardation ϕ_{mech} computed from experiments performed at the indicated temperatures is also listed.

- 1) Slight movement of the Kerr cell with respect to the light beam would result in a different value of ϕ_{mech} as expanded beam observations showed that ϕ_{mech} was a function of position
- 2) Stress caused by the coulombic attraction between the two plates, could produce voltage dependent strain birefringence in the glass.

Although further work is being performed to identify and eliminate the causes of the variation in ϕ_{mech} , it should be noted that the observed variations, because of the large values of $\phi_1 - \phi_2$ used in this work, contribute an uncertainty of less than $\pm 3\%$ to the value of the electro-optic Kerr coefficient. A comparison of the present results with results of previous measurements is given in Fig. 20. It can be seen from these plots that there is a wide variation in the measured values for the Kerr coefficient of nitrobenzene. In order to identify the actual magnitude of the discrepancy an accurate method must be developed to adjust all results to the same temperature. Our measured values of the Kerr coefficient as a function of temperature are given in Fig. 21. Previous theoretical discussions have indicated that the temperature dependence of the Kerr coefficient should be of the form^[45]

$$B = C_0 + (C_1/T) + (C_2/T^2). \quad (25)$$

Fitting the data in Fig. 21 (least squares) yields the following values for the constants

$$C_0 = 4.44 \times 10^{-11} \text{ mV}^{-2}$$

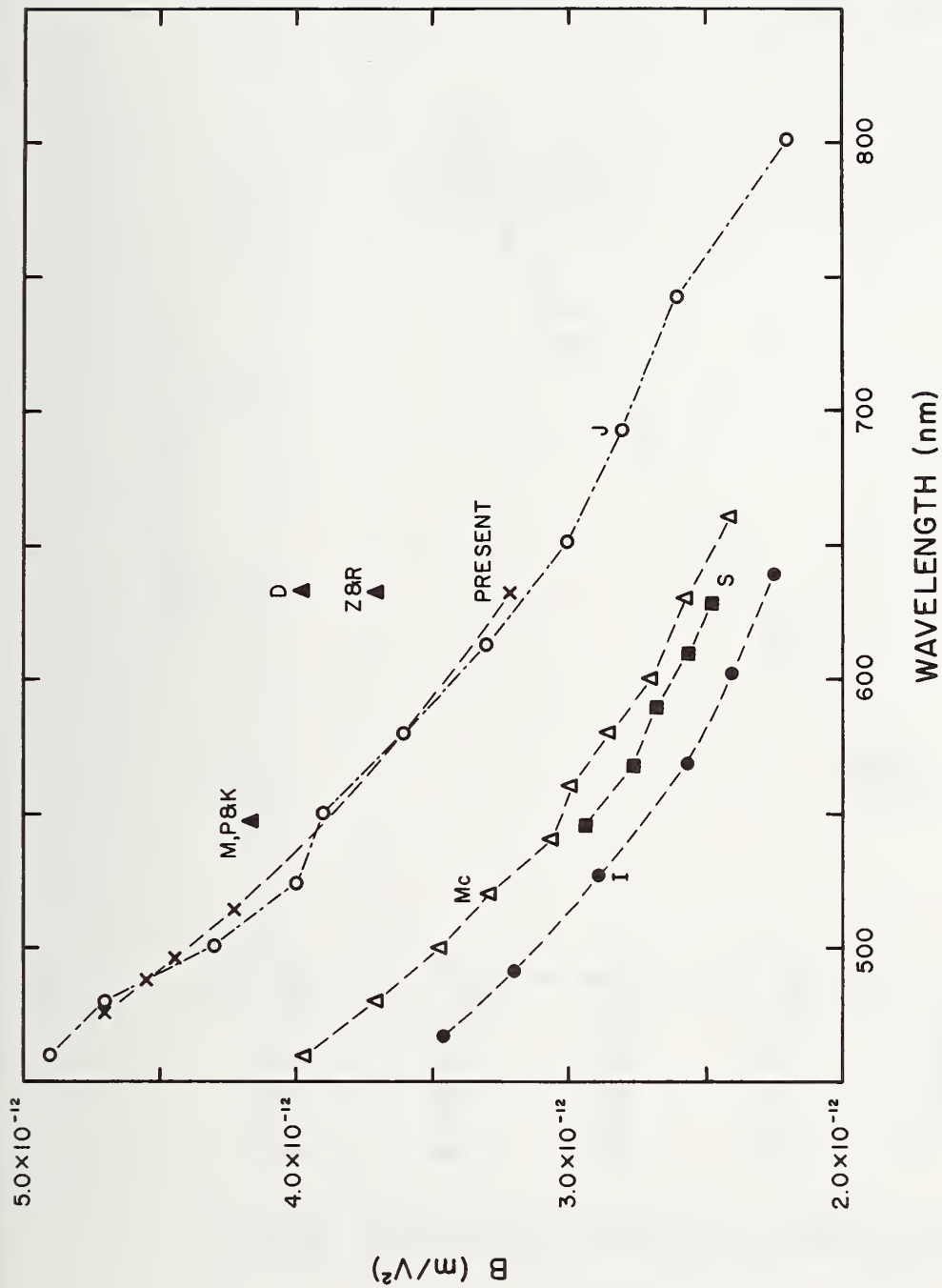


Figure 20. Comparison of measured values of the Kerr electro-optic coefficient of nitrobenzene as a function of wavelength. The data taken by Moller (M)^[46] and by Piekara and Konopka (P&K)^[47] was taken with the nitrobenzene at 20 °C, that by Ilberg (I)^[48] and by Zamkov and Radkevich (Z&R)^[49] at 21 °C, that by McComb (Mc)^[50] at 22.5 °C, that by DeIfino (D)^[51] and the present data were at 23 °C, that by Szivessy (S)^[52] at 24°, and that by Jeppesen (J)^[53] at 25 °C.

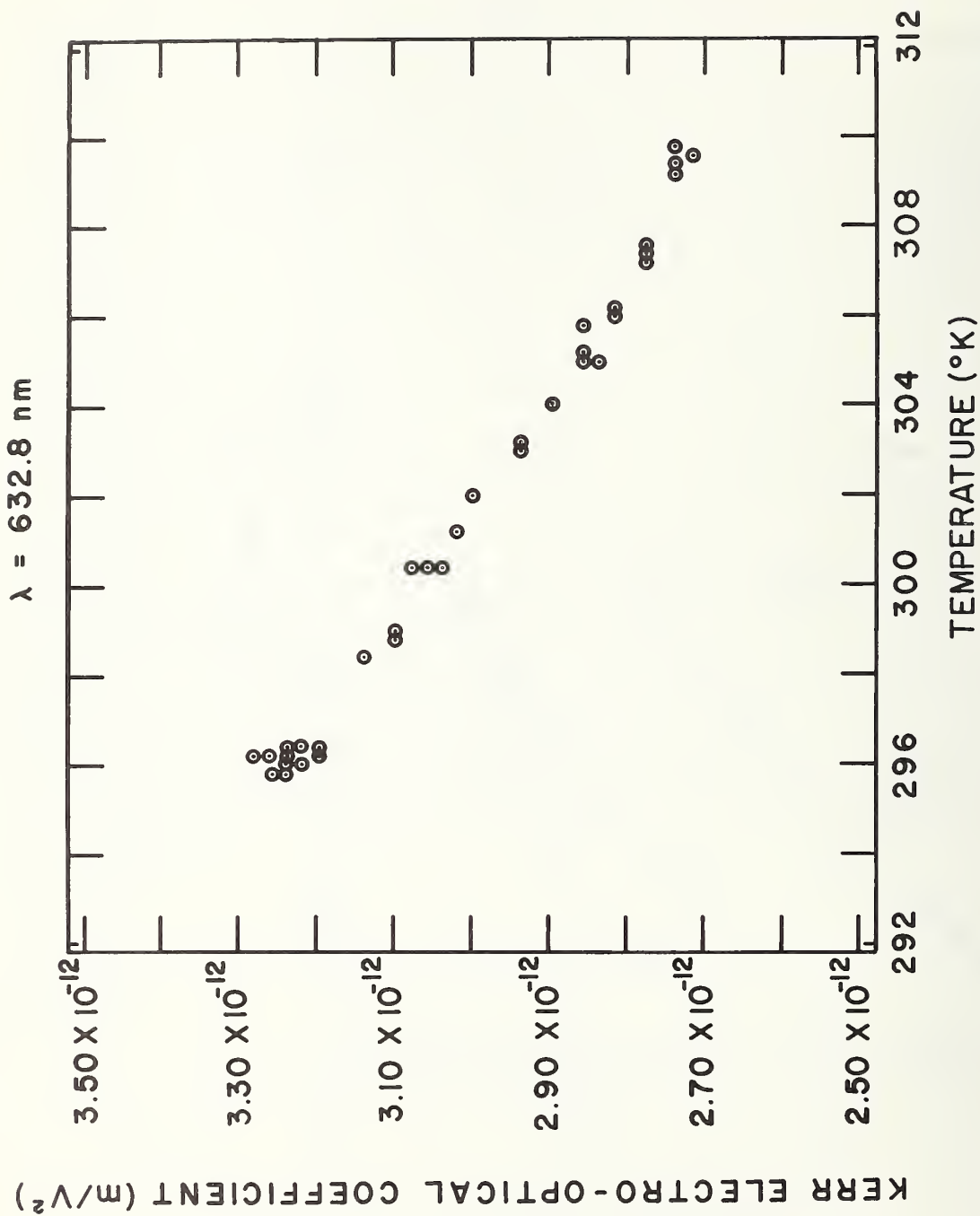


Figure 21. Measured values of the electro-optic Kerr coefficient plotted as a function of the temperature of the nitrobenzene.

$$C_1 = -2.86 \times 10^{-8} \text{ m K V}^{-2}$$

$$C_2 = 4.85 \times 10^{-6} \text{ m (K)}^2 \text{ V}^{-2}$$

From these values, the Kerr coefficient of nitrobenzene was calculated as a function of temperature in the range between 296 K and 305 K. These results are presented in Table 8. Because of the approximations used in deriving Eq. 25 and because of the narrow range of temperatures investigated, the authors are skeptical about the validity of extrapolation to temperatures much beyond those listed in Table 8. Investigations are continuing over a wider temperature range to accurately define the temperature dependence of the Kerr coefficient.

Temperature (K)	Kerr Coefficient (m/V ²)
296.0	3.24 x 10 ⁻¹²
296.2	3.23
296.4	3.22
296.6	3.22
296.8	3.20
297.0	3.20
297.2	3.19
297.4	3.18
297.6	3.17
297.8	3.16
298.0	3.15
298.2	3.14
298.4	3.13
298.6	3.12
298.8	3.12
299.0	3.11
299.2	3.10
299.4	3.09
299.6	3.08
299.8	3.07
300.0	3.06
300.2	3.05
300.4	3.05
300.6	3.04
300.8	3.03
301.0	3.02
301.2	3.01
301.4	3.01
301.6	3.00
301.8	2.99
302.0	2.98
302.2	2.97
302.4	2.97
302.6	2.96
302.8	2.95
303.0	2.94
303.2	2.94
303.4	2.93
303.6	2.92
303.8	2.91
304.0	2.91
304.2	2.90
304.4	2.89
304.6	2.88
304.8	2.88
305.0	2.87

Table [8] The Kerr coefficient of nitrobenzene is listed as a function of temperature. As discussed earlier, the Kerr coefficient values are estimated to be accurate to within $\pm 5\%$.

IV. KERR SYSTEM PEAK-READING VOLTMETER WITH AUTOMATIC DIGITAL DISPLAY

Accurate measurement of the peak value of transient high voltages is of considerable importance to those concerned with lightning-impulse and switching-surge testing^[54,55] of high-voltage power system equipment, with design and reliability of pulse components used in high power radar systems, with high power pulsed laser, particle accelerator, and fusion research^[56,57], with nuclear-explosive testing and weapons design, etc. Conventionally, such measurements are made either by use of spark gap or voltage divider methods. The procedures used in spark gap measurements and a description of the specially constructed metal ribbon resistors used in the National Bureau of Standards' 500 Ω pulse divider have previously been published^[58]. Descriptions and discussions evaluating the performance, reliability, and errors characteristic of various types (including capacitive, mixed, liquid-resistor, opto-electronically coupled, etc.) dividers are given in references^[57,59-67]. In each of these cases the oscilloscope deflection produced by the voltage across the low voltage arm of the divider is photographed to record the magnitude and waveform of the pulse voltage to be measured. In cases requiring state-of-the-art accuracy (within 1-2%), "slideback" or "suppressed zero" techniques are employed to enable higher resolution in measurement of the pulse's peak magnitude.

In recent years, a series of ever-improving alternative approaches employing pulse-measuring Kerr systems have been developed^[7-10]. The technique described here, which was suggested by the authors in a previous publication^[15], is being developed in the National Bureau of Standards' High Voltage Measurements Section as part of its pulse measurements program.

Though measurements with state-of-the-art accuracy (within $\pm 1\%$) are easily obtained by proper design of the Kerr system, the principle advantage of the present approach is its facility. It provides immediate conversion of the pulse voltage peak from analog to digital form, with digital readout and display of the critical data required for ready calculation of the voltage magnitude either at the peak or at some other selected point of interest on the waveform. Though direct and immediate display of the pulse magnitude (in volts) has not yet been incorporated, it is evident that this feature may easily be included with addition of straightforward computational circuitry. Safe and reliable operation of the active electronic circuitry incorporating the computational facility and digital display is insured by the system's optical coupling to the main high voltage circuit. The laser beam is easily directed to carry the measurement information to a remote, electrically isolated and shielded location.

Finally, it is noted that the present system is regarded as only a prototype of the more fully automated system suggested above. However, since its fundamental operations allow significant improvement in the facility of high voltage peak measurements and since these semi-automating operations are easily implemented using general purpose laboratory equipment, the present description is provided for consideration by those who might find this approach helpful in meeting their immediate impulse measurement and testing needs.

A. Instrumentation and Procedure

A block diagram showing the essential elements of the prototype Kerr system peak-reading voltmeter and the standard voltage divider system used

in evaluating its performance is given in Fig. 22. A photograph of a portable prototype 300-500 kV system showing a Kerr cell, submerged in an oil-bath tank and equipped with appropriate adjustable polarizers and mirrors for directing of the laser beam, is shown in Figs. 23 and 24. As in conventional pulse voltage measuring Kerr systems^[7-10], the beam is directed through a polarizer oriented at $\pm 45^\circ$ to the Kerr cell interelectrode field, between and along the length of parallel plate electrodes in a nitrobenzene-filled Kerr cell, through an analyzing polarizer oriented at $\pm 90^\circ$ to the first polarizer, to a detecting photomultiplier. In the system shown schematically in Fig. 22, both the laser source (a 1.5mW He-Ne laser) and the photomultiplier are located about 10 meters away from the HV pulse generator, whereas the Kerr system and "standard" 500 Ω divider are installed in parallel within 1 meter of an unshielded Marx-type impulse generator. The photomultiplier and its associated equipment, as described in the following paragraphs, are installed inside a shielded room to reduce effects of radiated interference from the generator discharge. The laser beam is directed as required for passage through the cell and back to the photodetector by use of adjustable mirrors installed on the polarizer housings on the acrylic oil-bath tank. The Kerr cell is submerged in oil to prevent flashover on the Kerr cell surface when the HV pulses are applied.

During pulse measurement operation the instantaneous relative intensity (I/I_m) of the light transmitted by the analyzer, as modulated by the instantaneous pulse magnitude, is detected by the photomultiplier and displayed on an oscilloscope screen. A pulse and delay generator system is used to synchronize triggering of the oscilloscope sweep for viewing of

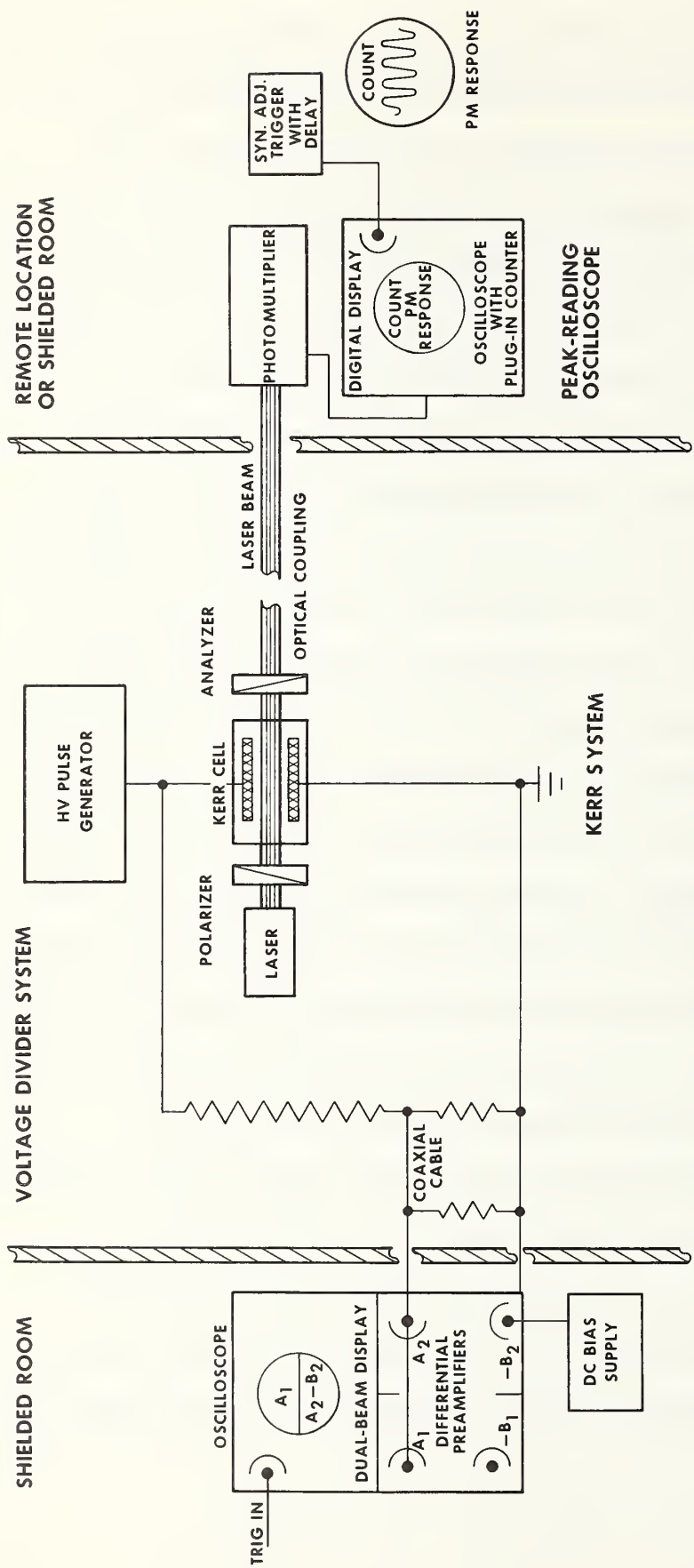


Figure 22. Schematic diagram showing the fundamentals of operation and the method of calibration of the peak-reading Kerr system voltmeter.



Figure 23. A portable prototype 300-500 kV Kerr cell. The polarizer housing is in the foreground and the screw at the upper left of the tank is the high voltage connection.

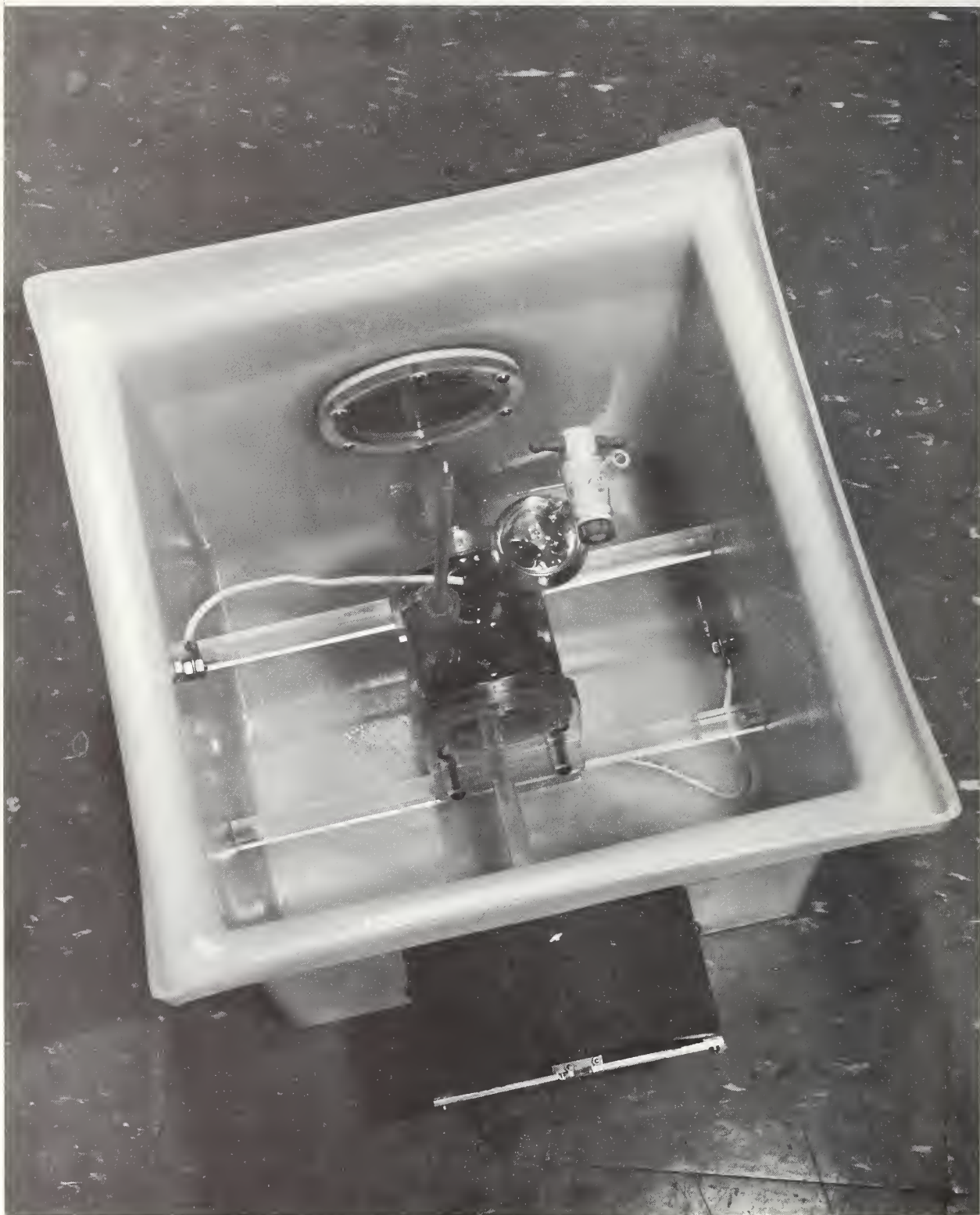


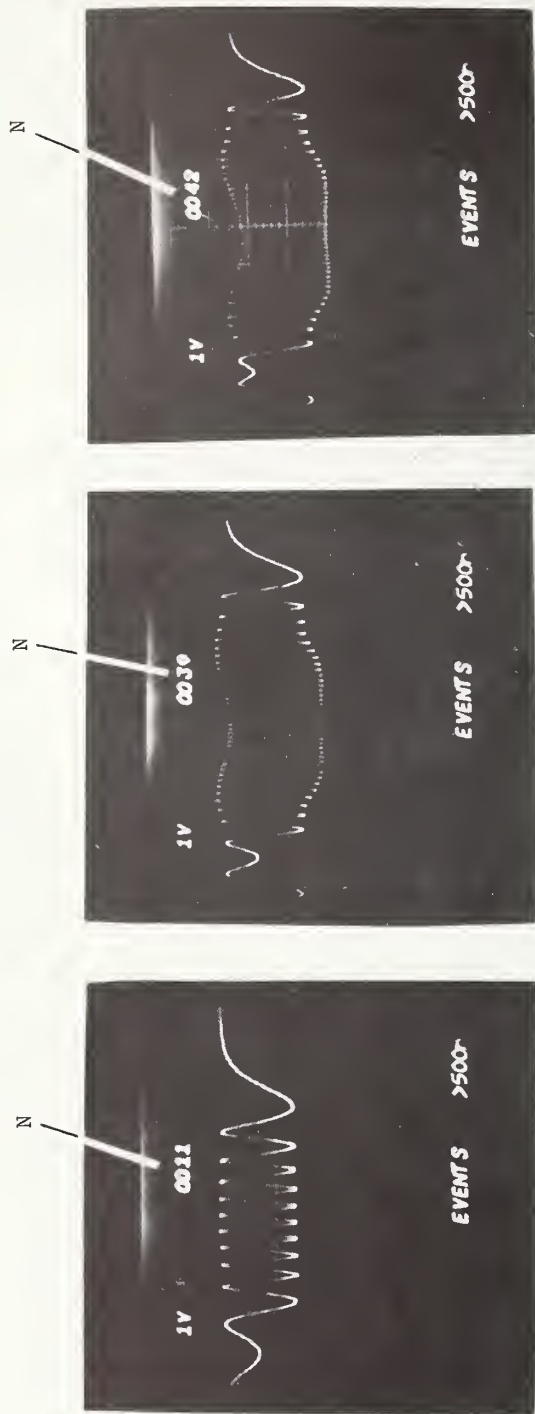
Figure 24. Top view of portable Kerr cell. During normal operation the tank is filled with oil to prevent flashover.

the Kerr system photomultiplier response during the rise (or fall) of the high voltage pulse from $V = 0$ to V_{peak} (or from V_{peak} to 0). At the same time, the number N of oscillations produced by the Kerr effect during the rise (or fall) of the HV pulse is counted by a 0 - 500 MHz universal counter/timer oscilloscope plug-in unit and displayed with the photomultiplier response directly on the oscilloscope screen. The oscilloscope's vertical (volts/div) and horizontal (ns/div) scale sensitivities are also displayed. Photographs of typical oscilloscope displays recorded during the fall (from V_{peak} to 0) of several different high voltage pulses are shown in Fig. 25. Simultaneous "standard"-voltage-divider measurements used in evaluating the Kerr-counter system performance were recorded on a dual-beam oscilloscope, the overall waveform of the nearly rectangular HV pulses (risetime: 1-2 μs , duration: 5 to 15 μs , peak magnitude: 20 to 320 kV) being displayed by the deflection of one beam and the differential measurement of the magnitude of the pulse being displayed by the other beam, as sketched schematically in Fig. 22.

To allow comparison of the Kerr-counter system result with the high resolution divider measurements triggering of the oscilloscopes and counter were adjusted for display and measurement of the same point on the pulse waveform. Typical displays photographed from the screens of the two oscilloscopes during measurements at two different voltage levels are shown in Fig. 26.

The voltage divider slideback measurement is derived by measuring from a photograph the oscilloscope deflection showing the relatively small (50-100 mV) difference V_s between the peak magnitude of the divider low-side voltage and the fixed direct voltage ($\sim 20\text{V}$ in present work) applied to

RECENT RESULTS DEMONSTRATING USE OF DIGITAL COUNTER FOR AUTOMATIC DISPLAY OF KERR-SYSTEM PEAK-READING-VOLTMETER MEASUREMENTS OF PULSED HIGH-VOLTAGES



Automated Kerr-System: $V_{\text{peak}} = 17870 \text{ volts}$ $> \Delta = 1.4\%$
 NBS Standard Divider: $V_{\text{peak}} = 17610 \text{ volts}$

34220 volts $> \Delta = 0.3\%$
 34120 volts

35530 volts $> \Delta = 0.3\%$
 35410 volts

CONVERSION OF COUNTER DISPLAYS TO PEAK VOLTAGE MEASUREMENTS

$$V_{\text{peak}} = [2N - 1]^{1/2} V_m$$

where N = Automatic Digital Display of Kerr-System Counter Readout

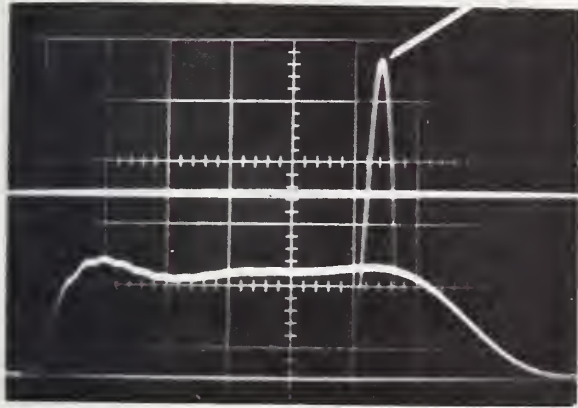
V_m = Kerr-Cell Constant = 3900 volts for this cell.

Figure 25. Typical response of the Kerr system peak-reading voltmeter at three different voltage levels. The results obtained are compared to simultaneous divider measurements.

PULSE DIVIDER

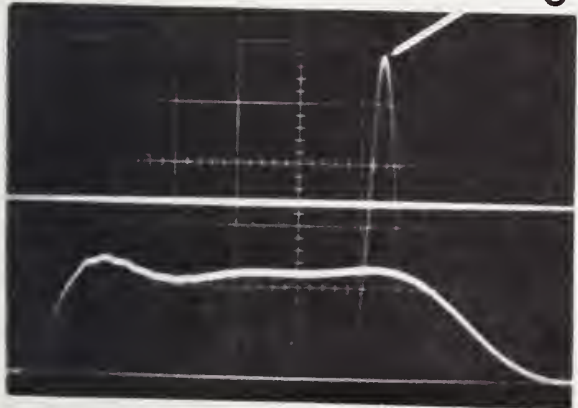
$$V_D = (\text{Bias} + V_S)DR$$

$$\text{Slideback} = V_S$$



$$V_D = 33790 \text{ volts}$$

V_S

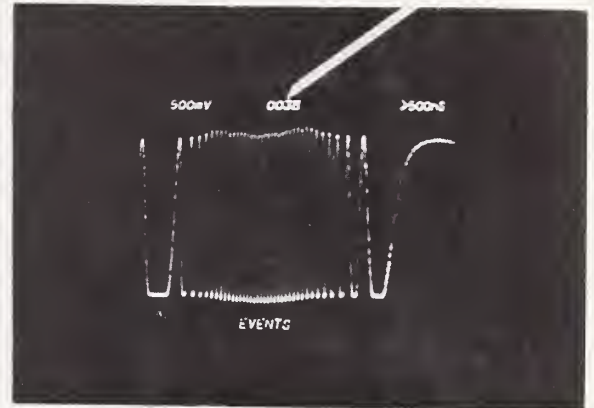


$$V_D = 50080 \text{ volts}$$

KERR CELL

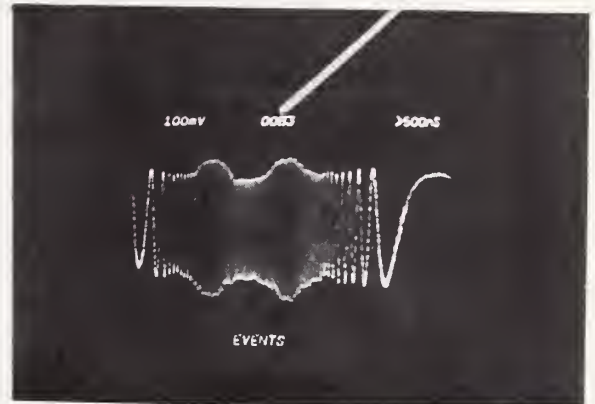
$$V_K = (2N - 1)^{1/2} V_m$$

Digital Display: $N = 38$



$$V_K = 33760 \text{ volts}$$

$N = 83$



$$V_K = 50070 \text{ volts}$$

HIGH VOLTAGE PULSE MEASUREMENTS

Figure 26. Comparison of oscilloscope records from simultaneous measurements of nearly rectangular high voltage pulses using a calibrated Kerr system and a 500Ω pulse divider. The top beams on the divider record are slideback measurements of the peak located on the tops of the pulses just prior to their trailing edges; the bottom beams display the waveform as indicated by the voltage across the divider low side. The Kerr system records show the count and the photomultiplier response during the trailing edge of the pulse.

channel B of a differential oscilloscope plug-in unit. The divider measurement V_D of the voltage peak is computed as follows:

$$V_D = (\text{Bias} + V_S) \text{DR}, \quad (28)$$

where the direct bias voltage (Bias) is readily measured using a calibrated digital voltmeter (accurate to better than 0.1%) and DR is the division ratio or attenuation factor of the calibrated standard divider.

B. Kerr System Measurement Principles

The operation of the Kerr-counter system can be understood from an analysis of Eq. 5:

$$(I/I_m)_{x,t} = \sin^2 \left[\frac{1}{2\pi} (\bar{E}/\bar{E}_m)_{x,t}^2 \right]$$

Under the same assumptions as in the previous section (Eq. 16), this expression can be rewritten^[15]

$$I/I_m = \sin^2 \left[\frac{1}{2\pi} (V/V_m)^2 \right], \quad (29)$$

where V is the instantaneous value of the applied voltage and V_m is the smallest applied voltage that yields a transmission maximum, I_m . Whenever $(V/V_m)^2$ has an integral value N , (I/I_m) is equal to either 0 or 1. If one denotes the value of $(V/V_m)^2$ at the peak of the applied voltage as $(V/V_m)_p^2$ one can, using a counter, determine the value of the integer N such that

$$N - 0.5 < (V/V_m)_p^2 < N + 0.5.$$

A simplified example of this is shown in Fig. 27. In this figure the relative transmitted irradiance is shown during one half cycle of 60 Hz alternating voltage. A simple waveform and low voltage are chosen so that the principles of the measurement technique can be more easily identified. To determine the peak voltage, it is necessary to measure the value of $(V/V_m)_p$ for a calibrated cell, i.e., a cell in which V_m is known. In section (a) of the figure $(V/V_m)_p^2 \simeq 8$ at the peak of the applied voltage signal, while in section (c), $(V/V_m)_p^2 \simeq 9$. In section (b), $(V/V_m)_p^2$ would, of course, have some intermediate value. We note that in sections (a) and (c) the number of peaks in the transmitted irradiance during the entire pulse is equal to the appropriate value of $(V/V_m)_p^2$. This is simply a consequence of the fact that the applied voltage monotonically increases to the peak then monotonically decreases back to zero. It can also be seen by inspection that if the discriminator level of an electronic counter is set at $(I/I_m) = 0.5$ a total count of 8 would insure that

$$7.5 \leq (V/V_m)_p^2 \leq 8.5 .$$

In this case then one can obtain the peak value of the voltage from the expression

$$V_p = (N_{fp})^{\frac{1}{2}} V_m , \tag{30}$$

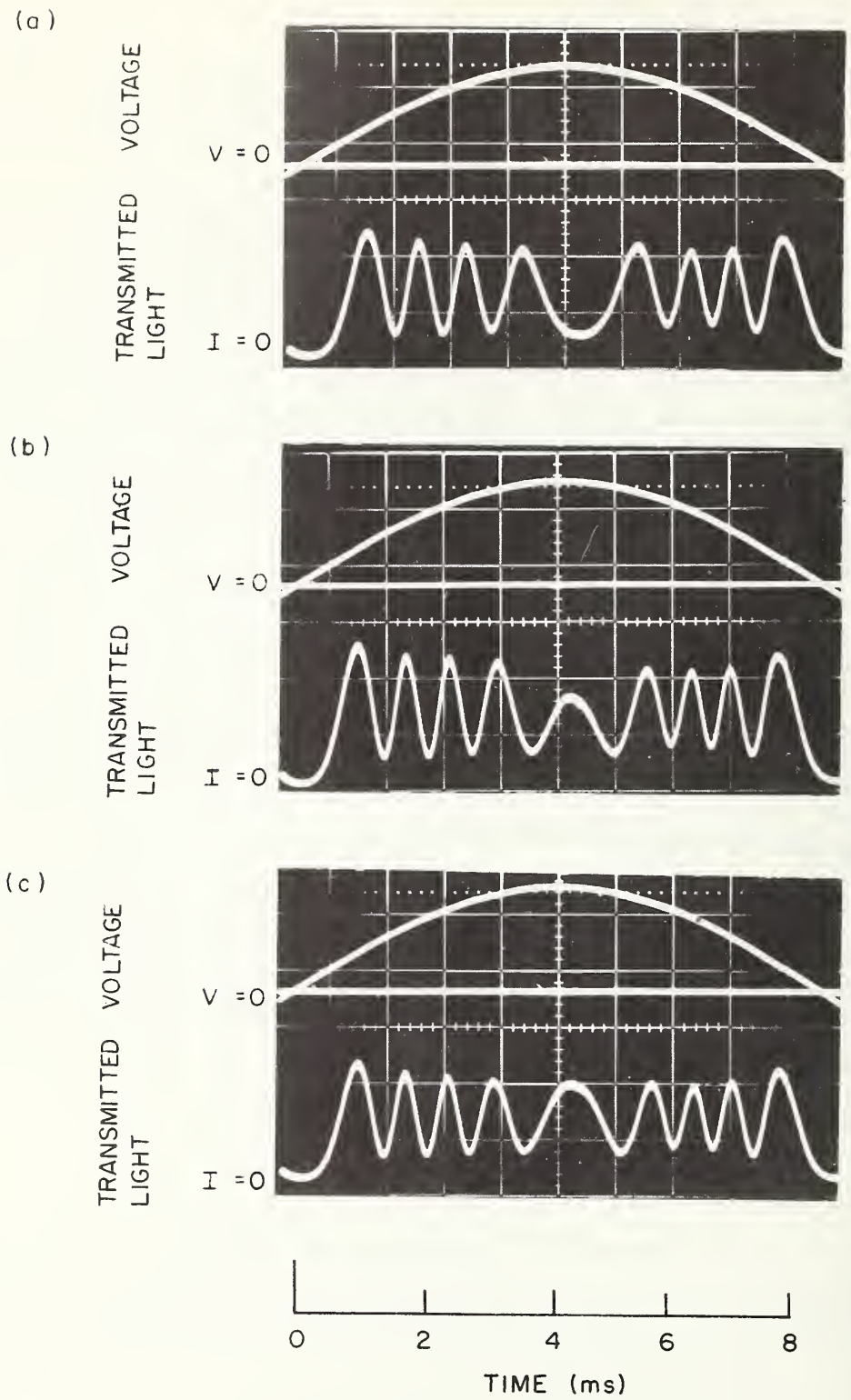


Figure 27. Transmitted irradiance during a half-cycle of a 60 Hz voltage waveform. As the peak voltage increases (from top to bottom) an additional count is added to the Kerr system response.

where the number of counts in a full pulse is denoted by N_{fp} .

The uncertainty introduced into the voltage measurement by rounding the number of counts to an integral value is shown in Fig. 28. It can be seen from this figure that the uncertainty due to rounding falls below $\pm 1\%$ when the total number of counts is greater than about twenty-five. This is a consequence, of course, of the fact that the birefringence is proportional to the square of the electric field so that the measurement sensitivity increases with increasing voltage level.

In the present work the front of the pulse waveform was distorted. It was, therefore, more convenient to detect only the trailing edge of the pulse. That being the case, the value of the peak voltage was calculated from the expression

$$V_p = (2N_{hp} - 1)^{\frac{1}{2}} V_m \quad (31)$$

where N_{hp} is the number of counts during the second half of the pulse, i.e., during the time when the applied voltage went from its peak to zero. When one records only the number of counts in half of a pulse, he must arbitrarily choose to round to either an even or an odd number for N_{fp} . This introduces a calculable, additional uncertainty beyond that graphed in Fig. 28. For large counts, this will be an insignificant error in many applications.

C. Results and Conclusions

Typical results obtained by recording the number of counts in the trailing half of the voltage pulse are presented in Table [9]. These results are compared to simultaneous divider measurements of the same pulse

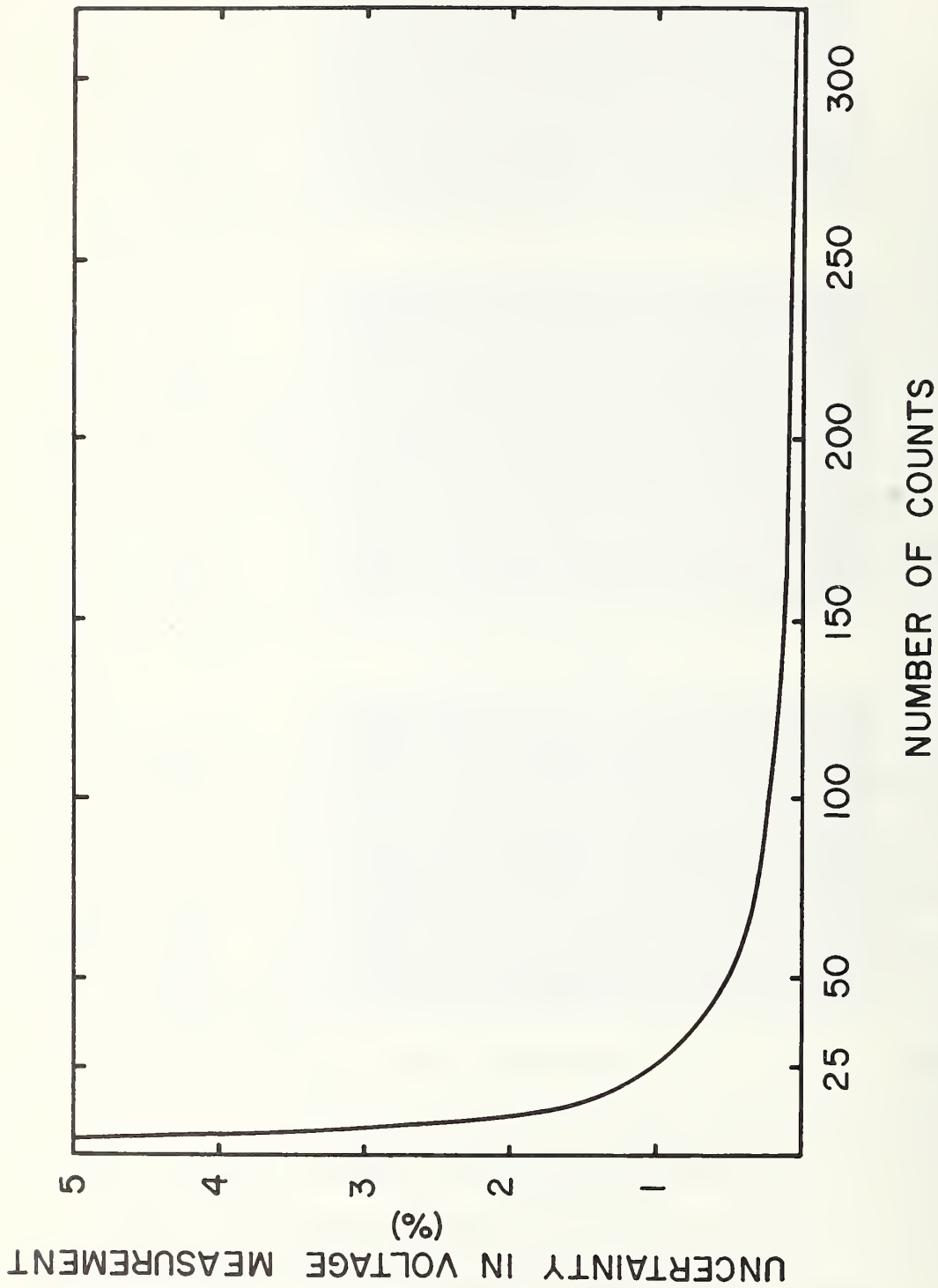


Figure 28. The uncertainty introduced into the voltage measurement by rounding to an integral number of counts plotted against the number of counts in a full pulse.

to demonstrate that the results are consistent with the predictable uncertainty limits. When the peak voltage was of order 50 kV, $N_{hp} \approx 80$, and $N_{hp} \approx 230$ when the peak voltage was of order 84 kV.

It should be mentioned that the response of the Kerr cell tracks the entire voltage pulse so, as was previously demonstrated^[4], one can reconstruct the entire pulse. The present system ignores that information so that an immediate, accurate value for the pulse peak voltage can be obtained.

In summary, a peak reading voltmeter based on the electro-optic Kerr effect has been constructed. The unique feature of the device is that it incorporates a counter which counts the number of light transmission maxima during the voltage pulse. A straightforward arithmetic computation using this count yields a value for the peak voltage. Tests of the device indicate that the system operates near the theoretical minimum in measurement uncertainty.

	V_P (kV)		% Difference
Divider		Kerr Cell	
50.10		49.97	-0.3
50.03		49.97	-0.1
50.12		49.97	-0.3
50.08		49.66	-0.8
50.08		49.97	-0.2
50.12		49.97	-0.3
50.10		49.97	-0.3
84.44		84.05	-0.5
84.37		84.23	-0.2
84.31		84.05	-0.3
84.27		83.87	-0.5
84.33		84.05	-0.3
84.24		83.87	-0.4
84.26		84.23	--
84.20		84.23	--
84.20		83.87	-0.4
84.20		83.87	-0.4

Table [9] Comparison of the results of a Kerr-counter system for the measurement of high voltage pulses with simultaneous measurement of the pulse using a conventional divider (the NBS 500 Ω "standard" pulse divider).

V. MEASUREMENT OF HIGH MEDICAL X-RAY MACHINE VOLTAGES

A. Introduction

The Bureau of Radiological Health of the HEW Public Health Service has been given the statutory responsibility for certifying that the voltage pulses in commercial X-ray machines are within their specified and approved operating ranges. Having been informed of the work performed at the National Bureau of Standards on the use of the Kerr effect for voltage measurements, they consulted the NBS High Voltage Measurements Section for advice on techniques of accurate pulse-voltage measurement. Immediate concern was with the operation and performance of medical X-ray equipment at the HEW Bureau of Radiological Health. Their current practice involves use of voltage divider techniques for measurement of these voltages. Occasional performance evaluations are also conducted by analysis of the X-ray spectrum produced. However, because this procedure is lengthy and complex, there is a need for an alternative method to check the accuracy of, or perhaps replace, divider-measurement techniques. Some doubt about the accuracy of their divider measurements was expressed. Such dividers are generally calibrated by measuring their division ratios under direct voltage conditions bearing little resemblance to those encountered in normal X-ray machine operation. Typically, medical X-ray voltages consist of a train of one or more full-wave-rectified half-cycle 60 Hz pulses, with peak magnitudes ranging from 20 to 300 kV. The likely possibility of significant error, due to voltage and/or frequency-dependent variations in the divider ratio, in divider measurements at high voltage was therefore indicated as an area of major concern. Accordingly, two field trips were made to the Bureau of Radiological Health in Rockville, Maryland. Because of their pertinence to our Kerr effect studies, the

experiments, results, and conclusions drawn from these visits are discussed in the following paragraphs.

B. Field Trip Report

The initial visit to BRH included a briefing by the chief and staff of the Radiation Measurements and Calibrations Branch on their voltage measurement problems and a tour through their laboratory. Operation of their X-ray machine and their voltage-divider measurement procedure were demonstrated. At the conclusion of this visit it was agreed that another field trip, attempting adaptation of Kerr system techniques to their X-ray machine, would be desirable. On November 15, appropriate pieces of our Kerr system apparatus, including a calibrated 1 x 10 cm pulse-measuring Kerr cell and a small He-Ne laser, were taken to the Radiation Measurements and Calibration Branch laboratory in Rockville. The cell was connected to their X-ray system, in parallel with their resistive divider, for measurement of the X-ray tube voltage. A number of exploratory experiments were conducted. Oscilloscope tracings comparing several of the simultaneous divider and Kerr cell measurements are given in Fig. 29. The higher resolution of the Kerr system measurements, which show sizable differences not distinguishable in the divider measurements of the voltage peaks, is evident.

C. Conclusions

1. The experiments conducted on November 15 demonstrated the feasibility of using Kerr-system techniques for measurement of a variety of typical X-ray machine pulse voltages. Further experiments and testing will be required to establish their accuracy. However, it should be noted that similar tests and experiments are also required for calibration and evaluation of divider performance and accuracy.

SIMULTANEOUS VOLTAGE-DIVIDER AND KERR-SYSTEM MEASUREMENTS OF MEDICAL X-RAY-MACHINE VOLTAGES

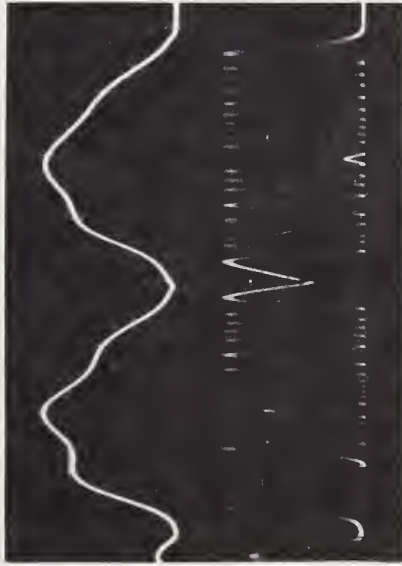
One Half-Cycle
60 Hz Pulse



Voltage Divider
Records

Kerr System
Records

Two Half-Cycles
60 Hz



Four Half-Cycles
60 Hz



Voltage Divider
Records

Kerr Systems
Records

Eight Half-Cycles
60 Hz

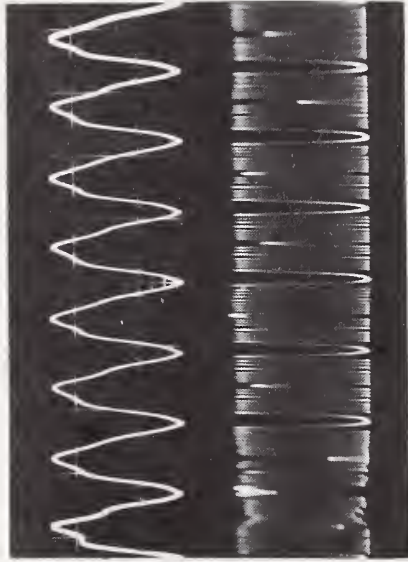


Figure 29. Simultaneous voltage divider and Kerr system measurements of typical medical X-ray machine voltage pulses.

2. Multiple voltage pulses produced by the X-ray machine (e.g., those in Fig. 29b, c and d) vary significantly in peak magnitude and in waveform. The X-ray dosage may be expected to vary accordingly.

D. Recommendations

In view of the above, recommendations for future action include the following steps:

1. Complete high voltage calibration and evaluation of a divider to be used in conjunction with the X-ray machine divider. In addition to usual calibration under high direct voltage conditions, this should include measurement of its division ratio under pulsed and steady-state 60 Hz high voltage conditions, and evaluation of its step response at intermediate voltages. The purpose of this work would be to provide reliable calibration, traceable to the NBS standard pulse divider and Kerr cell apparatus, of a BRH "standard" divider to be used by their Radiation Measurements and Calibration Branch in enforcement of regulations governing medical X-ray machine performance.

2. Simultaneous measurements of BRH X-ray machine voltages using the calibrated BRH divider, a calibrated NBS Kerr cell and X-ray spectrometer. With these three independent measurements of the voltage, the relative accuracy and precision of the devices can be defined under X-ray machine operating conditions.

3. If the results of Recommendation 2 indicate that Kerr system techniques will indeed provide relatively simple, accurate, and independent (of the divider) measurements of X-ray machine voltages, technical assistance could be provided to BRH in the establishment of their own Kerr pulse measurement system. This would include fabrication and calibration of a Kerr cell (or cells) designed to provide high measurement resolution during operation at typical medical

X-ray machine voltages. Complete automation of Kerr system measurements, to give digital display of the peak voltages applied to the X-ray tube, would be most desirable. This was attempted on the field trip, but failed due to unreliable triggering of the counting units used. Recent experiments at NBS have demonstrated the feasibility of this procedure, which is described in Section IV (see Fig. 25). Since this procedure offers promise of significant simplification in pulsed peak-voltage measurements, its development for routine X-ray voltage measurements may be particularly helpful. The higher frequency response afforded by use of Kerr system techniques is also foreseen as a significant advantage; it will allow detection of transients on the X-ray-voltage waveform. Transients, with magnitude significantly greater than the normal generator voltage, may be anticipated in X-ray machine operation particularly during switching of the high voltage. It would seem that detection and measurement of the magnitude of any such transient voltages may also be important, since they may produce potentially harmful bursts of higher energy radiation.

E. Results and Benefits

Benefits anticipated from adaption of the above recommendations include the following:

- 1) accurate calibration of a BRH divider for operation under medical X-ray-voltage conditions,
- 2) a quantitative estimate of the accuracy with which the X-ray spectrum can be predicted by voltage measurements in commercial X-ray machines,

- 3) a publication for the technical literature outlining techniques for measurement of voltage pulses in commercial X-ray machines,
- 4) increased technical expertise resulting from cooperative NBS-BRH staff effort,
- 5) if determined desirable, a calibrated Kerr cell system for BRH use in measurement of high voltages.

VI. FUTURE PLANS

During the fiscal year 1974, the following areas will be emphasized:

(1) Measurements of the Kerr electro-optical coefficient of nitrobenzene will be completed, and a paper reporting results at selected laser wavelengths and operating temperatures will be submitted for publication in the open literature. These measurements, which were begun during FY 1973 (see Section III) and which are the first to be reported for laser wavelengths, are believed to be significantly improved over previous measurements which were performed using less refined and less accurate voltage measurement techniques.

(2) The Kerr electro-optical coefficient of several other selected liquids, including water, chlorinated naphthalene, chlorinated biphenyls, etc., will be measured by reference to our improved absolute measurements for nitrobenzene. As with nitrobenzene, measurements will be made over a range of temperatures and laser wavelengths selected for their practicality in high voltage measurement applications. Results will therefore also include determination of the temperature and wavelength dependence of the Kerr coefficient and of the Kerr cell constant (for voltage measurement purposes) for each of the liquids investigated.

(3) The Kerr effect peak-reading-voltmeter concept, which allows immediate visual display of the count yielding a measure of the peak magnitude of μ s duration HV pulses, will be calibrated and evaluated to the 300 kV level by reference to calibrated standard NBS Kerr cells and pulse dividers. A paper describing the concept involved and reporting findings

from this work will be prepared and submitted for publication in the open literature.

(4) A Kerr system designed for measurement of lightning-type impulses peaking as high as 1 MV will be designed, constructed and tested to the 1 MV level. The testing will be conducted at the General Electric High Voltage Laboratory in Pittsfield, Massachusetts. In addition to NBS participation, this work will receive selected materials and some technical support from A. H. Rohlfs and F. A. Fisher of the GE High Voltage Laboratory staff.

Several other portable pulse-measuring Kerr systems, constructed during FY 1973 (see Section I) for operation to the 300 kV level, will also be calibrated and tested under both rectangular and lightning-type impulse conditions.

(5) Evaluation of results from field-mapping studies under steady-state dc and low frequency ac conditions will be continued. Included in this effort will be preparation and presentation of a paper for the 1973 Conference on Electrical Insulation and Dielectric Liquids to be held at the Institute for Electrical Research in Quebec (IREQ) in October 1973. Primary responsibility for this work will be assigned to Dr. Robert Hebner who is the principal author of an abstract already submitted and accepted by the conference. The goal of this work continues to be attainment of a thorough understanding of the basic mechanism(s) contributing to space-charge distortion of the interelectrode field in parallel plate Kerr cells during steady-state dc or ac operation, the ultimate goal being attainment of uniform field conditions which would allow higher accuracy in steady-state high voltage calibrations of voltage measuring

Kerr cells. Improvement in the accuracy of such calibrations should allow significant improvement (from $\pm 1\%$ to $\pm 0.5\%$ or better) in the state-of-the-art accuracy of transient high voltage measurements.

(6) Conference on Precision Electromagnetic Measurements, London July 1974. If time and staff permit, two papers should be planned for this conference, one being a careful evaluation of ac Kerr cell studies in insulating liquids and the other (from results obtained in cooperation with Stanley R. Booker of Sandia Corporation) reporting development and calibration of a "multiple-pass" HV pulse-measuring Kerr system.

During FY 1974, the project leader and principal investigator (Esther C. Cassidy) of the NBS Kerr Effect Studies program will be away on a U.S. Dept. of Commerce Science and Technology fellowship assignment. Accordingly, primary responsibility for this project will be assumed by Dr. Robert Hebner and Richard Sojka of the NBS High Voltage Measurements Section staff, with most of the effort carried by Richard Sojka who is planning his doctoral thesis around his work in this area. In addition to these NBS participants, significant contributions from Stanley R. Booker of the Sandia Corporation, from A. H. Rohlfs and F. A. Fisher of the General Electric Pittsfield High Voltage Laboratory, and from Esther Cassidy (in off-hours advisory capacity) are also anticipated.

APPENDIX A

MEASUREMENT OF 60 HZ VOLTAGES USING THE KERR EFFECT

This material was published in the Review of Scientific Instruments,
vol. 43, pp. 1839-1841, 1972.

Measurement of 60 Hz Voltages Using the Kerr Effect*

ROBERT E. HEBNER, JR. AND ESTHER CHRISTMAS CASSIDY

National Bureau of Standards, Washington, D. C. 20234

(Received 3 August 1972)

The Kerr effect has been used to measure 60 Hz alternating voltage up to 30 kV peak. The system behaves much as it does under the influence of a short high-voltage pulse except that in this case the frequency of the applied voltage is sufficiently low that the space charge effects in the liquid are not negligible.

For a number of years systems have been under development that use Kerr cells for the measurement of pulsed and direct voltages.¹⁻⁵ The purpose of this Note is to report the use of a Kerr cell system for measuring high alternating voltage at 60 Hz.

The Kerr cell used was conventional¹ in that it consisted of parallel plate electrodes immersed in nitrobenzene. Laser light, linearly polarized at 45° to the electric field direction, is passed between the plates and impinges on an analyzer that is orthogonal to the direction of the polarizer. The nitrobenzene becomes optically birefringent when under the influence of an electric field according to the relationship

$$\varphi = 2\pi B \int_0^L E^2 dl. \quad (1)$$

In this expression, φ is the phase difference produced between the parallel and perpendicular (to the direction of the applied electric field) components of the electric vector of the incident light beam; B is the Kerr constant of the liquid; and

$$\int_0^L E^2 dl$$

is the integral of the square of the electric field strength E along the length L of the light path in the liquid. If one makes the usual assumptions—(a) that Eq. (1) can be expressed

$$\varphi = 2\pi B E^2 l', \quad (2)$$

where E is the electric field in the medium, and l' is an effective length that includes the effects of fringing fields

at the ends of the plates; and (b) that the field between the plates is uniform—one easily obtains the following expression⁵:

$$I/I_m = \sin^2[\frac{1}{2}\pi(v/V_m)^2]. \quad (3)$$

In Eq. (3), I is the irradiance of the light transmitted through the analyzer when the applied voltage has magnitude v , V_m is the smallest applied voltage which yields a transmission maximum, I_m . If we explicitly include the time dependence of the applied voltage, we obtain

$$I/I_m = \sin^2[\frac{1}{2}\pi(V/V_m)^2 \sin^2 \omega t]. \quad (4)$$

Typical observations of the transmitted irradiance I as a function of time are shown in Fig. 1. To use this system to measure voltage, the system must be calibrated by an independent measurement of V_m . Once V_m is known for a specific cell, one needs only to record the relative irradiance as a function of time to find the peak applied voltage.⁶ It should be noted that at the peak of the voltage signal $\sin^2 \omega t = 1$. The relative irradiance, which corresponds to this peak, will be maximum or minimum for

$$(V/V_m)^2 = n, \quad (5)$$

where n is an integer.

To characterize the performance of the Kerr system, 37 values of V , corresponding to $n = 1$ to 37, were used as peak values for the applied voltage. Each value was used in Eq. (5) to find V_m . Because all 37 determinations should yield identical values, the variation in the values for V_m gives an indication of the precision of the Kerr system voltage measurements at 60 Hz. A graphical presentation of V_m vs n is shown in Fig. 2.

The scatter at low values of n is characteristic of Kerr

cells because the Kerr cell sensitivity increases with increasing field strength.^{3,5} If one then neglects the first five data points because they are inherently less accurate, one sees that there is a variation of 1%–2% in the remaining values. There also appears to be a systematic decrease in the calculated value for V_m as n increases. Preliminary observations have indicated that this may be due to a non-uniform field between the plates similar to that observed using direct voltage^{2,7,8} or long (greater than 50 μ sec) pulses.⁹

An examination of Fig. 1 shows that for the symmetrical waveform that exists for 60 Hz alternating voltage the number of maxima is equal to n , as defined in Eq. (5), when the applied voltage V is at an appropriate value so that the transmitted light is either maximum or minimum at the peak of the applied voltage. This observation is significant because when $V \lesssim 5V_m$, a 1%–2% increase in V increases $(V/V_m)^2$ from a value n to a value $n+1$.⁵ It follows, therefore, that a voltmeter could be constructed with a precision of order 2% in which data are taken by simply counting the number of peaks in the transmitted irradiance.

It was found that commercially pure nitrobenzene was

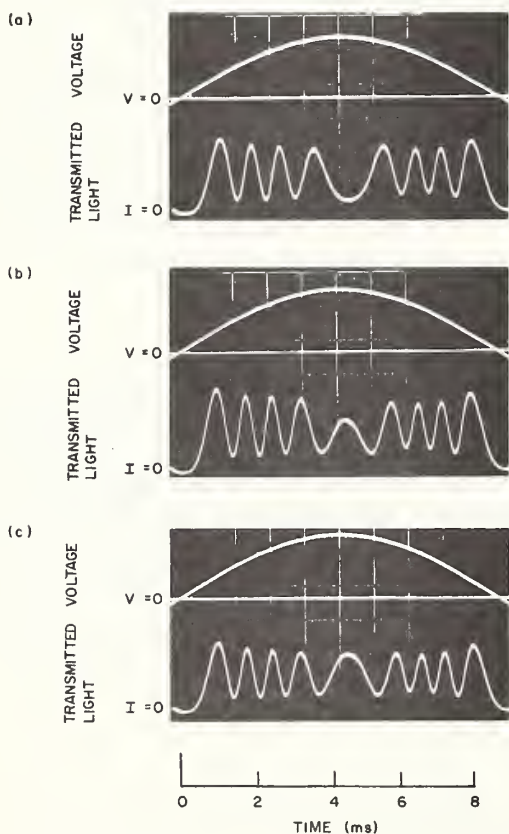


FIG. 1. Typical response of Kerr cell system to applied voltage. The top half of each oscilloscope tracing shows one half-cycle of the applied 60 Hz alternating voltage. The lower half shows the relative irradiance transmitted by the system as a function of time during the half-cycle. The applied voltage is about 6% greater in Fig. 1(c) than in Fig. 1(a). Figure 1(b) shows the response to an intermediate value.

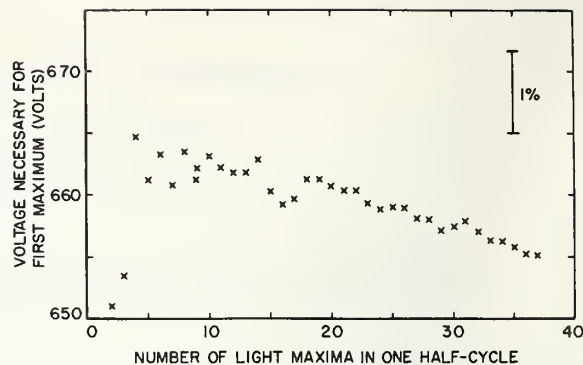


FIG. 2. Determination of the voltage necessary to obtain the first transmission maximum. This value should be independent of the applied voltage, but it does show a systematic decrease which is attributed to a nonuniform field distribution between the plates.

unsatisfactory for use in a Kerr cell to be operated at 60 Hz because the Kerr effect signal was strongly and randomly amplitude modulated. Visual observations of the light transmitted through the cell under these conditions showed a very strong "lensing" effect. That is, shadowgraph observations showed bright and dark areas in the space between the electrodes which exhibited some short term stability.¹⁰ Around the electrodes shadowgraphs of the density gradient, apparently caused by the heating of the liquid between the plates, could be observed. Upon further purification^{4,11} these effects disappeared and a stable Kerr effect pattern was obtained. The apparent resistivity of the nitrobenzene that yielded stable reproducible results was of order $10^{10} \Omega \cdot \text{cm}$ as measured with a current comparator bridge¹² operated at 60 Hz.

The Kerr cells used in this study were used to measure voltages up to 30 kV peak and maximum electric field strengths of 40 kV/cm. Caution, and not catastrophic failure, set these upper limits, so the present study offers no information on the voltage limitation of these cells.

The major conclusion of this study is that Kerr cells using purified nitrobenzene can be used to measure high voltages at 60 Hz. It is further expected that studies of this low-frequency behavior will lead to improved methods of calibration of pulse measuring systems based on the Kerr effect.

The authors would like to thank W. A. Bagley for his assistance with this work, S. R. Booker for suggestions for its extension, and O. Petersons for his support and careful reading of the manuscript.

* This work was supported in part by the U. S. Atomic Energy Commission through the Sandia Corporation, Albuquerque, N. M. 87115.

¹ E. C. Cassidy, *Rev. Sci. Instrum.* **43**, 886 (1972).

² E. C. Cassidy and H. N. Cones, *J. Res. NBS* **73C**, 5 (1969).

³ E. C. Cassidy, H. N. Cones, and S. R. Booker, *IEEE Trans Instrum. Meas.* **IM-19**, 395 (1970).

⁴ E. C. Cassidy, H. N. Cones, D. C. Wunsch, and S. R. Booker, *IEEE Trans. Instrum. Meas.* **IM-17**, 313 (1968).

⁵ D. C. Wunsch and A. Ereteza, *Rev. Sci. Instrum.* **36**, 816 (1964).

⁶ It should be noted that the Kerr effect system actually yields not just the peak voltage, but also the entire waveform. Determination of pulse shapes from Kerr effect measurements is discussed in Ref. 3.

⁷ G. Briere and J. Gosse, *J. Chim. Phys.* **65**, 1341 (1968).

⁸ G. Briere and F. Gaspard, *Chem. Phys. Lett.* **1**, 706 (1968).

⁹ Z. Croitoru, *Progress in Dielectrics* (Academic, New York, 1965), Vol. 6, p. 105.

¹⁰ J. C. Filippini, J. P. Gosse, J. C. Lacroix, and R. Tobazeon, *Conference on Dielectric Materials, Measurements and Applications*, University of Lancaster, p. 110 (1970).

¹¹ F. Gaspard, *Conference on Dielectric Materials, Measurements and Applications*, University of Lancaster, p. 134 (1970).

¹² O. Petersons, *IEEE Trans. Power App. Systems PAS-87*, 1354 (1968).

APPENDIX B

RECENT REFINEMENTS AND DEVELOPMENTS IN KERR SYSTEM ELECTRICAL MEASUREMENT TECHNIQUES

This material was presented at the 1972 Conference on Precision Electromagnetic Measurements, Boulder, Colorado, June 26-29, 1972. It was then selected for publication and published in IEEE Transactions on Instrumentation and Measurement, vol. IM-21, pp. 504-510, 1972.

Reprinted by permission from IEEE TRANSACTIONS ON INSTRUMENTATION AND MEASUREMENT
Vol. IM-21, No. 4, November 1972, pp. 504-510
Copyright 1972, by the Institute of Electrical and Electronics Engineers, Inc.
PRINTED IN THE U.S.A.

Recent Refinements and Developments in Kerr System Electrical Measurement Techniques

ESTHER CHRISTMAS CASSIDY, WILLIAM E. ANDERSON, AND STANLEY R. BOOKER

Abstract—Kerr system electrical measurement techniques are improved by progress in two important areas: 1) in the development of

methods for visualizing and measuring pulsed (microsecond) electric fields and high voltages from time-varying electrooptical fringe patterns recorded using high-speed photographic techniques, and 2) in the development of convenient experimental methods for evaluating and correcting path-dependent errors in Kerr system response. Results demonstrate use of fringe-pattern measurements in achieving accurate pulse voltage measurements and in correction of errors resulting from sizeable end-field variations in existing 300-kV Kerr cells.

Manuscript received June 21, 1972.

E. C. Cassidy and W. E. Anderson are with the High Voltage Measurements Section, National Bureau of Standards, Washington, D.C. 20234.

S. R. Booker is with the Electrical Standards Division of the Sandia Corporation, Albuquerque, N. Mex. 87115.

INTRODUCTION

THE feasibility of using the Kerr electrooptical effect for measurement of pulsed high voltages has been verified by experimental research now under way for about five years. Within the context of earlier progress, Kerr systems were used to measure pulses peaking as high as 300 kV and having rise times of 1–2 μ s with an estimated uncertainty of ± 1 percent [1], [2]. A method was developed for observation and mapping of high-intensity electric fields in Kerr cells under steady-state dc conditions [3]. Knowledge of the dc field distribution, which is often distorted due to space charge effects, permitted high direct-voltage calibrations of Kerr cells for pulse measurements. Kerr systems developed and constructed by the authors have been used to calibrate other pulse-measuring devices, such as resistive and capacitive dividers, at their rated voltages, rather than at low voltages as has been the usual practice.

This paper describes recent progress in two areas: 1) in development of methods for visualizing and measuring pulsed high voltages and electric fields from time-varying electrooptical fringe patterns, and 2) in development of convenient methods for evaluating and correcting path-dependent errors in Kerr system measurements. Unlike earlier approaches, the present methods apply high-speed photography for detection and recording of two-dimensional electrooptical fringe patterns containing the measurement data. This approach is especially useful for studies of the pulsed electric field between the Kerr cell electrodes, for evaluation and correction of path-dependent errors (due to end-field effects) in Kerr cell voltage measurements, and for voltage measurements under high noise or discharge conditions that make electrical isolation and shielding extremely difficult. Results from experiments demonstrating use of fringe-pattern measurements for each of these tasks are presented. Because of their importance in achieving accurate measurements at higher voltages (> 100 kV), procedures devised for evaluating and correcting path-dependent Kerr cell errors are emphasized.

II. APPARATUS AND METHODS

The basic HV pulse generating and measuring systems were described earlier [1], [2]. Several different nitrobenzene-filled Kerr cells with parallel-plate electrodes were used in this work as follows: a 1×10 cm (spacing \times length of electrodes) cell for operation to 100 kV, and a 2.9×6 cm cell and a 3×30 cm cell for use to 300 kV. More complete descriptions of these and other cells with a variety of electrode structures are given in [4].

The general layout of the electrooptical system with fringe recording using a rotating mirror streak camera is shown in Fig. 1. A pulsed laser serves as a light source. Suitable optical components are inserted as shown to expand the beam diameter as required for illumination of the end-view area between and around the Kerr cell electrodes. A slit aperture (width ≈ 1 mm, length 50–100 mm as required by Kerr cell dimensions) is positioned perpendicular to the direction of laser beam propagation, so that only light passing through the slit is transmitted. The inner surface of the Kerr cell electrodes are

oriented either parallel to (as in Fig. 1) or perpendicular to the long dimension of the slit. The cell, which is submerged in oil to prevent external HV flashover, is installed between "crossed" polarizers so that the analyzing polarizer passes light only during application of the HV pulses. Quarter-wave retardation plates are inserted as indicated to eliminate recording of "field-directional" fringes [4] not pertinent in these measurements. The lens directs the transmitted light to the rotating mirror where it is deflected to the film for continuous time-resolved recording of space variations (over the length of the slit) in the transmitted light intensity. The resultant fringe-pattern photographs contain information interpreted to yield measurements of applied pulse voltage and of the electric field distribution as functions of time. The time scale on the film is deduced from measurement of the mirror speed or from measurement of the time between initiation and peaking of the reproducible pulse waveform.

When equipped for instantaneous framed recordings of the light transmitted over the entire end-view cross-sectional area, the slit aperture is removed and the streak camera is replaced with an image-converter camera. Or more simply, the requirement for use of the image converter with its high-speed shuttering action is avoided by use of a pulsed laser with very short (relative to time changes in the Kerr cell field) flash duration. In either case, the rapidly changing fringe pattern is "frozen" photographically at a selected time during the pulse. Typical exposure times in the present work were 1, 0.3, or 0.1 μ s. The recorded patterns allow probeless electrooptical mapping and measurement of the electric field distribution between and around the Kerr cell electrodes. Measurements of the pulse magnitude at the time of the exposure are also easily obtained (Section III). In this work, these photographs were particularly useful because they permit convenient experimental evaluation of voltage measurement errors resulting from Kerr cell end-field variations (Sections V and VI).

III. MEASUREMENT PROCEDURE AND TYPICAL RESULTS

Kerr system operation may be summarized as follows. Whereas essentially no light is initially transmitted because of the "crossed" polarizers, transmission increases when voltage is applied across the Kerr cell electrodes. At any instant the relative intensity $(I/I_m)_x$ of the beam emergent from a given path x through the Kerr cell liquid is [1]:

$$\left(\frac{I}{I_m}\right)_x = \sin^2 \left[\frac{\pi}{2} \left(\frac{\bar{E}}{\bar{E}_m} \right)^2 \right], \quad (1)$$

where the overbar (e.g., over A) denotes the following:

$$\bar{A}_x = \left[\frac{1}{L} \int_0^L A^2 dl \right]^{1/2}. \quad (2)$$

The integral is evaluated over the length L of the given light path x through the Kerr cell. \bar{E}_m is the effective field strength that produces the first transmission maximum I_m with a given cell. The electric field E is understood to be the component perpendicular to the direction of light propagation. Thus, (I/I_m) varies as a function of time and space (around the elec-

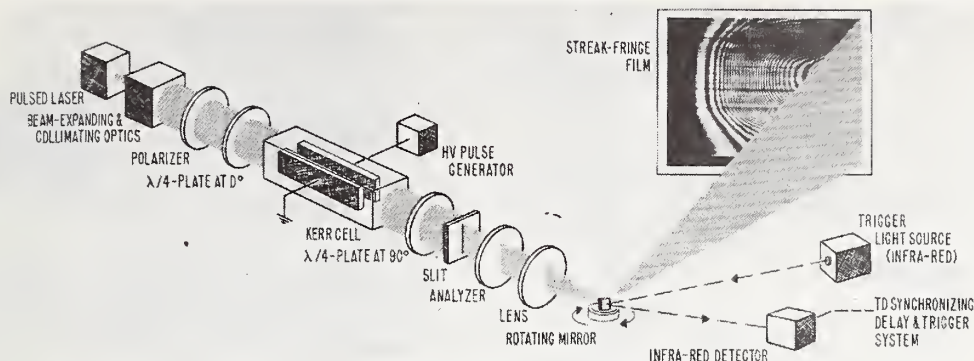


Fig. 1. Kerr electrooptical system used for streak fringe-pattern measurements of high-voltage pulses.

trodes) in accordance with the effective instantaneous electric field distribution. Transmission minima occur when (and where) $\bar{E} = 0, \sqrt{2} \bar{E}_m, 2 \bar{E}_m, \sqrt{6} \bar{E}_m, \dots$. Transmission maxima occur when (and where) $\bar{E} = \bar{E}_m, \sqrt{3} \bar{E}_m, \sqrt{5} \bar{E}_m, \dots$. When sufficiently high voltage is applied, spatial variations in the transmitted light, caused by field nonuniformities, produce fringe patterns made up of alternate bright and dark bands (see Figs. 2 and 3). The brightest or darkest points of each band delineate "equifield" lines (i.e., the effective components of the electric fields perpendicular to the light path are identical) of effective relative electric field strength

$$(\bar{E}/\bar{E}_m) = \sqrt{n}. \quad (3)$$

As in earlier work [1], [3], n is the numerical value assigned to each successive dark (even integer) and bright (odd integer) fringe by counting ($n = 0, 1, 2, 3, \dots$) from the outermost dark region where $n = 0$ inward to the desired point in space on the image-converter photograph (see Fig. 2). When end-field variations are controlled, the photograph therefore allows visualization of the pulsed electric field distribution. With a calibrated Kerr cell operating in its range of high measurement resolution, peak voltage measurements v_K are quickly obtained, with accuracy comparable to that achieved using conventional divider and oscilloscope methods, from the following equation:

$$v_K = \left(\frac{\bar{E}}{\bar{E}_m} \right)_c (V_m)_c \approx \sqrt{n_c} (V_m)_c \quad (4)$$

where $(V_m)_c = (E'_m d)_c$, the voltage that produces the first transmission maximum for the calibrated light path c , and n_c is the numerical value assigned to the fringe most proximate to this calibrated path. The prime over a quantity (e.g., over E) represents the average of that quantity, taken over a centrally located perpendicular path of length d between the electrodes; e.g.,

$$E' = \frac{1}{d} \int_0^d E_x dx.$$

Equation (4) is only valid if (E'/E'_m) equals $(\bar{E}/\bar{E}_m)_c$. It is not valid under dc or long pulse conditions because of field nonuniformities caused by space charge effects. This will be discussed in Section VI. However, for short (microsecond) pulsed voltages where path-to-path variations in (\bar{E}/\bar{E}_m) depend only



Fig. 2. 0.3- μ s image-converter exposures of high-speed fringe patterns produced at the peaks of 135- and 166-kV pulses using the 3×30 -cm Kerr cell.

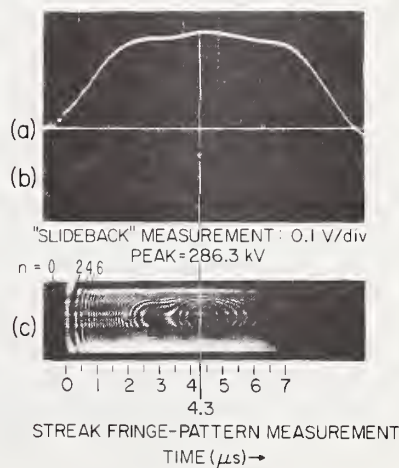


Fig. 3. Simultaneous time-resolved measurements of an HV pulse. (a) With resistive divider (ratio 5140). (b) Resistive divider with "slide back." (c) With 2.9×6 -cm Kerr cell. Pulse divider measurement scales: 20 V/div, 1 μ s/div.

on the electrode geometry, (4) is valid. More accurate measurements are obtained with $(\bar{E}/\bar{E}_m)_c$ determined from relative measurements of the calibrated-path interference intensity $(I/I_m)_c$ as follows.

If n_c is an even integer (dark fringe),

$$\left(\frac{\bar{E}}{\bar{E}_m}\right)_c = \left[n_c + \frac{2}{\pi} \arcsin \left(\frac{I}{I_m} \right)^{1/2} \right]^{1/2}. \quad (5)$$

If n_c is odd (bright fringe),

$$\left(\frac{\bar{E}}{\bar{E}_m}\right)_c = \left[(n_c + 1) - \frac{2}{\pi} \arcsin \left(\frac{I}{I_m} \right)^{1/2} \right]^{1/2}. \quad (6)$$

Though any path through the cell may be calibrated (Section VI), the central path is used in most voltage measurement applications.

Fig. 2 shows typical image converter exposures of fringe patterns recorded using a 3×30 -cm 300-kV Kerr cell. With the side-field fringes counted inward to $n_c \approx 50$ and 75, and with $(V_m)_c$ known equal to $19\,140 \pm 150$ V, $v_K = \sqrt{50}$ ($19\,140$) = $135\,340$ V and $v_K = \sqrt{75}$ ($19\,140$) = $165\,750$ V. Calibrated resistive divider measurements yielded 135 130 and 165 200 V, respectively. Repeated comparisons of similar Kerr cell and divider measurements showed agreement within ± 1 percent when end-field variation errors were corrected and "slide-back" or "suppressed zero" techniques [1] were employed to enhance divider measurement resolution. Measurements were made at the peaks of pulses ranging between 80 and 300 kV.

A typical streak camera record from an experiment with a 2.9×6 -cm Kerr cell [$(V_m)_c = 39\,500 \pm 250$ V] is shown with oscilloscope traces from simultaneous pulse divider measurements in Fig. 3. In this experiment, the cell was oriented with electrodes parallel to the slit aperture. Only the rising portion of the pulse was recorded. As with the image-converter results, peak voltage may be determined by counting the dark fringes inward to the central ("bull's eye") region, e.g., to $n_c \approx 53$ in Fig. 3. Continuous, time-resolved measurements of v_K may be derived from (4) by counting and measuring the fringe positions along a centrally located (calibrated path position) line parallel to the time scale (Section IV).

Typical streak patterns obtained with the inner electrode surfaces of a 1×10 -cm cell perpendicular to the slit aperture are given in Fig. 4. In this case the pattern consists of a series of light and dark fringes that show the relative strength of the electric field over the central interelectrode (perpendicular to electrode surfaces) path. Under short pulse conditions, where time is too short for space-charge distortion of the interelectrode field, the fringes should remain perpendicular to the time scale. However, the fringing fields at the ends of the electrodes cause the effective fields along paths near the electrodes to differ from the effective fields along paths nearly midway between the electrodes. This effect produces "bending" in the fringes, which becomes more evident as the magnitude of the voltage (and thus the measurement resolution [1]-[3]) increases. The "bent" fringes in Fig. 4 indicate that the effective field along paths near the electrodes is 1 to 2 percent higher than along the central path. Finally, it was also of interest to

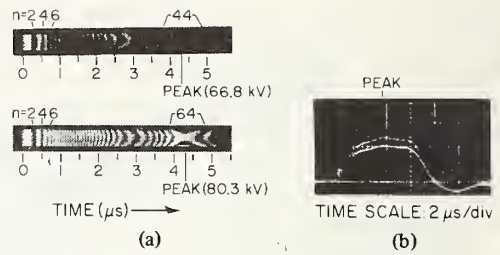


Fig. 4. Comparison of noisy pulse-divider measurements with electrically isolated streak fringe-pattern measurements using 1×10 -cm Kerr cell with slit perpendicular to electrode surfaces. (a) Streak records of fringe-pattern high-voltage pulse measurements. (b) Conventional pulse-divider measurements with noise.

compare the divider results at the bottom of the figure with computed Kerr system measurements of the waveform (Section IV). The latter showed smooth wavefronts as in Figs. 3 and 5, thereby tracing the distortion on the divider records of Fig. 4 to the divider-measurement circuit rather than to erratic behavior in the HV generator. This practical demonstration of the Kerr system's freedom from electrical interference and ground-loop currents was verified when an extraneous ground loop inadvertently included between the main HV and divider circuits was located and removed.

IV. ANALYSIS OF KERR SYSTEM MEASUREMENTS OF VOLTAGE PULSES

The modulated light output from a Kerr pulse-measuring system may be detected and recorded continuously directly on photographic film by use of a streak camera as described above, or it may be detected and recorded indirectly by photographing oscilloscope tracings of the output signal from an electronic photodetector. As reported earlier [2], the latter records are analyzed by use of a film reader, with computer processing of the measured x - y coordinate data pairs. This technique, which is still in use, has shown consistent agreement to better than ± 1 percent between computed divider and Kerr cell measurements of both the peak magnitude and the time integral of the voltage pulse waveform.

The streak fringe-pattern records of the present work are analyzed in a similar manner. Relative exposure density on the streak photograph is scanned and measured along a path parallel to the "writing" direction (the time scale) on the film. This is easily accomplished through use of a recording densitometer or film reader. Since the relative film exposure density is not directly related to the relative intensity of the light transmitted by the Kerr system, results are more readily obtained when data pairs are recorded only at the maxima and minima exposure points. Because of the high measurement resolution achieved with production of a multiplicity of fringes ($n > 25$), this procedure proved very effective in the present work.

Pulse waveforms derived from automatic scanning and computer analyses of the typical streak camera and divider-oscilloscope records in Fig. 3 are compared in Fig. 5. The peak values differ by less than 0.5 percent at 286 kV. The time integrals of the pulse waveform computed over the period of streak camera recording (over approximately $\frac{3}{4}$ of the

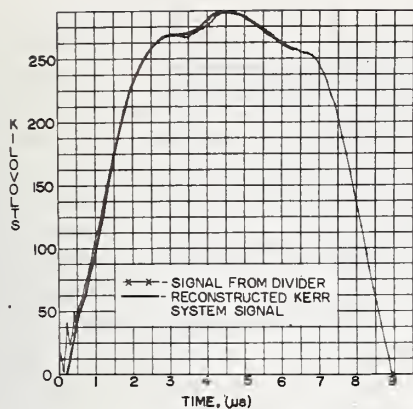


Fig. 5. 300-kV pulse waveforms derived from automatic scanning and computer analyses of typical streak camera and divider oscilloscope records.

pulse duration) were 1421 and 1433 kV- μ s. Repeated comparisons over the range from 80 to 300, with cells selected for high measurement resolution, showed similar agreement.

V. CORRECTIONS FOR EFFECTS OF END-FIELD VARIATIONS

The foregoing pulse measurements are estimated to be accurate within ± 1 percent. However, it is important to note that such accuracy requires careful consideration of the effects of the fringing fields at the ends of the Kerr cell's electrodes. These effects and methods devised for correction of resulting path-dependent errors in pulse measurements and in direct-voltage calibrations of pulse-measuring Kerr cells are discussed in Sections V and VI.

Kerr system response depends upon \bar{E}^2 , the square of the electric field strength averaged over the length of the light path in the birefringent liquid [see (2)]. If the same effective field were imposed along all paths between the electrodes, Kerr system measurements of voltage pulses would be independent of path position. With cells of our present design, having electrodes immersed in the Kerr cell liquid, results have shown that the fringing end fields may produce very significant (to 10 percent with existing 300-kV cells having $d = 3$ cm) path-dependent variations in the effective field strength imposed by an applied voltage pulse. Accordingly, the pulse voltage required to produce the first transmission maximum, which was defined simply as the cell constant, $V_m = (E_m d)$, in earlier work with smaller cells, is path dependent. This troublesome effect has been a major source of difficulty in development of a Kerr system for measurement of pulses peaking in excess of 100 kV.

Several alternative solutions to this problem have been considered, including the following: 1) correction by design; 2) confinement of the light path by affixing entrance and exit apertures to the Kerr cell windows; 3) multiple calibrations with determination of V_m for all likely measurement paths; or 4) development of reliable procedures for correcting path-dependent errors in existing Kerr cell response. Though effective and rather simply accomplished, the second and third

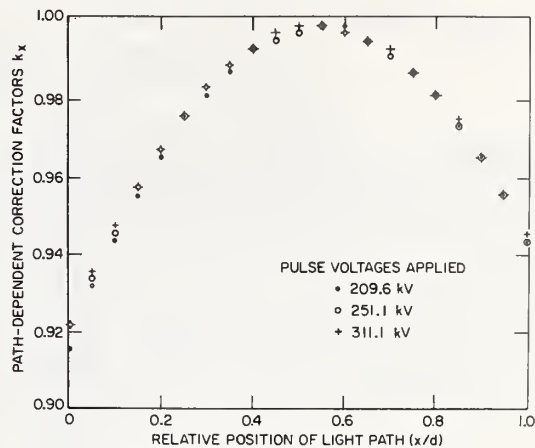


Fig. 6. Factors computed (at several different voltages) for path-to-path corrections of Kerr system measurements using the 2.9×6 -cm cell.

alternatives are not preferred because they require that calibration of the cell be referred to pulse divider measurements. This is not desirable, since calibrations referred to dc or low frequency ac voltage measurements offer promise of considerable improvement in the state-of-the-art accuracy of pulse voltage measurements—from 1 to perhaps 0.1 percent or better. Correction by design is perhaps the most attractive solution, because it would not only eliminate path-dependent errors in pulse voltage measurements, but because it would also facilitate accurate Kerr constant measurements. Accordingly, a variety of techniques for constructing cells with guarded electrodes or with the birefringent liquid confined to a central interelectrode region well removed from the electrode ends are under investigation.

In the meantime, a convenient experimental procedure for measuring and correcting errors resulting from the effects of end-field variations was developed. This approach employs high-speed fringe-pattern photographs, such as those in Fig. 2, taken near the peak of a short ($< 15 \mu$ s) voltage pulse. Except for end-field effects, parallel-plate Kerr system response should, in this case, be independent of path position because time is too short for development of space-charge distortion in the interelectrode field. Accordingly, the interelectrode fringes recorded in Fig. 2 are produced by path-to-path variations in the effective field along the length of the light path in the liquid. The relative positions (x/d) and n values assigned to these fringes, therefore, yield immediate visualization of the effects of path variations on the Kerr system's response. The effective relative field intensity (\bar{E}_x/\bar{E}_m) as a function of path position is easily determined from measurements of (x/d) versus n by scanning the distance between the electrodes along a centrally located line perpendicular to the inner electrode surfaces. A path-dependent correction factor k_x is derived from these measurements as follows:

$$k_x = \left(\frac{\bar{E}_c}{\bar{E}_m} \right) / \left(\frac{\bar{E}_x}{\bar{E}_m} \right) = \frac{\bar{E}_c}{\bar{E}_x} \quad (7)$$

This factor adjusts the cell constant (V_m)_c, known for a single

TABLE I
COMPARISON OF CENTRAL LIGHT PATH CALIBRATION RESULTS

Cell (cm)	λ (nm)	Direct Voltage			Pulse Voltage		
		Calibration Voltage	V_m (V)	$(V_m)_c$ (V)	Calibration Voltage	$(V_m)_c$ (V)	Δ (%)
1 × 10	514.5	27570	9970	10010	86160	10100	-0.9
		30430	10030	10100			-0.1
		33380	10010	10090			-0.1
1 × 10	632.8	37430	11660	11730	88970	11790	-0.5
		41100	11680	11740			-0.4
		44520	11700	11780			-0.1
3 × 30	514.5	70660	18230	18750	150200	18690	+0.3
		71260	18230	18800			+0.6
		72560	18280	18860			+0.9
		72560	18310	18870			+0.9
		72560	18290	18870			+0.9
3 × 30	632.8	75730	20960	21640	153900	21590	+0.2
		75730	20990	21670			+0.4
		77400	20980	21440			-0.7
		78420	20960	21640			+0.2
2.9 × 6	632.8	77280	45330	46300	101300	46170	+0.3

Direct voltage calibration before correction V_m , direct voltage calibration after correction $(V_m)_c$ using k_x factors, pulse-divider calibration $(V_m)_c$. Temperature: 25°C. Δ : percentage by which corrected direct voltage calibration differs from pulse-divider calibration.

calibrated light path c , for accurate voltage measurements along any other light path x as follows

$$v_K = \left(\frac{\bar{E}_x}{\bar{E}_m}\right) k_x (V_m)_c = \left(\frac{\bar{E}_c}{\bar{E}_m}\right) (V_m)_c. \quad (8)$$

Values of k_x , derived from least-square fitting of such measurements, were computed at path intervals of $(x/d) = 0.05$ over the entire interelectrode distance from 0 to 1.0 for several different cells with different pulse levels applied. Typical results from measurements with the 2.9 × 6-cm cell at three different voltages are plotted by the computer in Fig. 6. It is interesting to note that the curves show essentially no change in the pulsed effective field distribution to the 300-kV level, thereby verifying our assumption that space charge effects are not significant with operation under short ($\sim 10 \mu s$) pulse conditions. After corrections using the appropriate values of k_x , measurements along various paths of the 2.9 × 6 cm and the 3 × 30 cm cells agreed with calibrated divider measurements to better than ± 1 percent.

VI. CORRECTION OF END-FIELD-VARIATION ERRORS IN HIGH DIRECT-VOLTAGE CALIBRATIONS

In earlier work [3], Kerr cells were calibrated for measurement of pulse voltages from steady-state fringe patterns produced by application of a high direct voltage V_{dc} . In this case, where space-charge effects produce unpredictable distortion in the interelectrode field distribution, the pulse voltage V_m that produces the first transmission maximum was derived by use of the following [3]:

$$V_m = \frac{V_{dc}}{\left(\frac{\bar{E}}{\bar{E}_m}\right)'}, \quad (9)$$

where V_{dc} was measured, with accuracy to better than 0.1 percent using a precision resistive divider, and $(\bar{E}/\bar{E}_m)'$ was deter-

mined from fringe measurements along a centrally located line perpendicular to the inner electrode surfaces as follows:

$$\left(\frac{\bar{E}}{\bar{E}_m}\right)' = \int_0^1 \frac{\bar{E}_x}{\bar{E}_m} d\left(\frac{x}{d}\right). \quad (10)$$

This straightforward procedure proved effective in achieving acceptable calibrations of cells with electrode spacing $d < 1$ cm. However, in larger cells where end-field effects produce significant (> 1 percent) path-dependent variations in Kerr system response (\bar{E}/\bar{E}_m) , the steady-state fringe pattern also includes distortion due to end-field variations. This additional distortion produces errors in (9) and (10). Accordingly, accurate determinations of V_m , which is path dependent in the larger cells, require corrections for the effects of path-dependent end-field variations. Since the end-field contributions to each cell's response may be assumed fixed by its geometry, this is easily accomplished by using the appropriate k_x factor, as defined in (7), for correction of the n values assigned to each interelectrode fringe measurement, as described in Section IV. Equation (9) is thus modified:

$$(V_m)_c = \frac{V_{dc}}{\int_0^1 k_x \left(\frac{\bar{E}_x}{\bar{E}_m}\right) d\left(\frac{x}{d}\right)}, \quad (11)$$

to yield a valid calibration $(V_m)_c$ for any selected light path c .

As indicated in Section V, the required measurements of k_x versus (x/d) , such as those plotted in Fig. 6, are obtained from a single high-speed fringe-pattern photograph taken with a convenient pulse voltage. The applied pulse voltage need not be measured. Prior to development of this approach, five or more pulse-measurement experiments with the unexpanded laser beam passed along carefully measured paths between the electrodes were required for correction of these end-field-variation errors [2].

To check the validity of this procedure, repeated experi-

ments were performed using several cells at different voltage levels. Typical results, showing direct-voltage calibrations before V_m and after $(V_m)_c$ correction, and comparing $(V_m)_c$ with pulse-divider calibrations, are included in Table I. After corrections, all tests showed acceptable agreement ($\Delta < 1$ percent) between direct- and pulse-voltage calibrations.

In conclusion, it is noted that this approach is very useful in adapting Kerr system response for accurate voltage measurements, especially since it also assures normalization of errors resulting from construction faults, e.g., from strain in the cell's windows, from imperfections in electrode surfaces and their alignment, etc. However, development of a correction-free design allowing direct measurement of the uniform (along path

length) electric field between the electrodes remains a task considered worthy of future work.

REFERENCES

- [1] E. C. Cassidy, H. N. Cones, D. C. Wunsch, and S. R. Booker, "Calibration of a Kerr cell system for high-voltage pulse measurements," *IEEE Trans. Instrum. Meas.*, vol. IM-17, pp. 313-320, Dec. 1968.
- [2] E. C. Cassidy, H. N. Cones, and S. R. Booker, "Development and evaluation of electrooptical high-voltage pulse measurement techniques," *IEEE Trans. Instrum. Meas.*, vol. IM-19, pp. 395-402, Nov. 1970.
- [3] E. C. Cassidy and H. N. Cones, "A Kerr electro-optical technique for observation and analysis of high-intensity electric fields," *J. Res. Nat. Bur. Stand., Sect. C*, vol. 73, pp. 5-13, 1969.
- [4] E. C. Cassidy, "Pulsed laser Kerr system polarimeter for electro-optical fringe-pattern measurement of transient electrical parameters," *Rev. Sci. Instrum.*, vol. 42, pp. 886-893, June 1972.

APPENDIX C

EXPERIMENTAL STUDY OF THE BEHAVIOR OF NITROBENZENE UNDER VARIED HIGH VOLTAGE CONDITIONS

This material was presented at the 41st Annual Meeting of the Conference on Electrical Insulation and Dielectric Phenomena, Buck Hill Falls, Pennsylvania, October 23-25, 1972. It was subsequently published in the 1972 Annual Report, Conference on Electrical Insulation and Dielectric Phenomena, National Academy of Sciences, Washington, D.C., 20418, pp. 37-44, 1973.

Experimental Study of the Behavior of Nitrobenzene under Varied High Voltage Conditions

ESTHER C. CASSIDY AND R. E. HEBNER
National Bureau of Standards
Washington, D. C.

INTRODUCTION

The present work continues the investigation of electric field behavior between parallel-plate electrodes immersed in nitrobenzene and strives toward the realization of a Kerr cell which insures uniformity of the interelectrode field under various HV pulse, dc, and ac operating conditions. Our earlier direct voltage studies^{1, 2} are extended to include Kerr effect investigations of field distributions resulting from high pulsed (μs) and 60 Hz alternating voltages. Recently developed methods,³ employing high-speed photography for recording of transient fringe-pattern data, are utilized for visualizing time and space variations in the pulsed and ac fields. Minimization of the effects from the fringing fields at the electrode ends permits both the observation of space-charge behavior under direct and alternating voltages and measurement of the Kerr constant of nitrobenzene. Voltages are measured simultaneously using calibrated (with state-of-the-art accuracy) devices. Brief descriptions of the techniques employed and some typical results are given in the following paragraphs.

APPARATUS AND TECHNIQUES

A schematic diagram of the experimental apparatus is given in Figure 1. Basically, the system¹⁻³ consists of a calibrated⁴ Kerr cell, a triggerable pulsed Argon laser, and appropriate photoelectric or photographic detecting and recording equipment. The laser is equipped with a wavelength selector enabling operation at selected wavelengths between 514.5 and 476.5 nm. Data are also taken at $\lambda = 632.8$ nm using a continuous wave He-Ne laser.

The Kerr cells are filled with nitrobenzene with purity ranging from that of commercially available reagent grades, having apparent resistivities of 10^5 to 10^6 ohm-cm, to that of relatively pure liquid (10^{10} to 10^{11} ohm-cm) processed by chromatographic adsorption and sealed into the cell under vacuum.⁴ Whereas the purer liquid may be used for prolonged steady-state dc and ac operation without significant effects from turbulence or heating, the less pure liquid is suitable only for short (μ s) pulse operation. Cells having a variety of electrode materials and designs,³ including one designed to be virtually free of end-field effects for Kerr constant measurements, are being used. Effects of varied electrode surface conditions are also being investigated, since recent results indicate that the measured value of the resistivity depends both on the intrinsic purity of the liquid and on the composition and surface preparation of the electrodes.^{5, 6}

MEASUREMENTS DURING DC AND AC OPERATION

Figures 2 and 3 show typical results from dc and 60 Hz ac experiments with a sealed 0.5 x 12 cm (spacing x length of electrodes) cell. The field distribution curves of Figure 3 were computed by fitting a second degree polynomial to fringe measurements obtained by scanning the fringe patterns of Figure 2 along centrally located lines perpendicular to the inner electrode surfaces. A quadratic fit was used because it predicted all of the data points to well within the limits of our experimental uncertainty. With knowledge of the half-wave retardation field strength E_m for the calibrated cell⁷ and with minimization of end-field effects, the curves showing the interelectrode space-charge distributions were computed from the electric field measurements using Poisson's equation. The dc

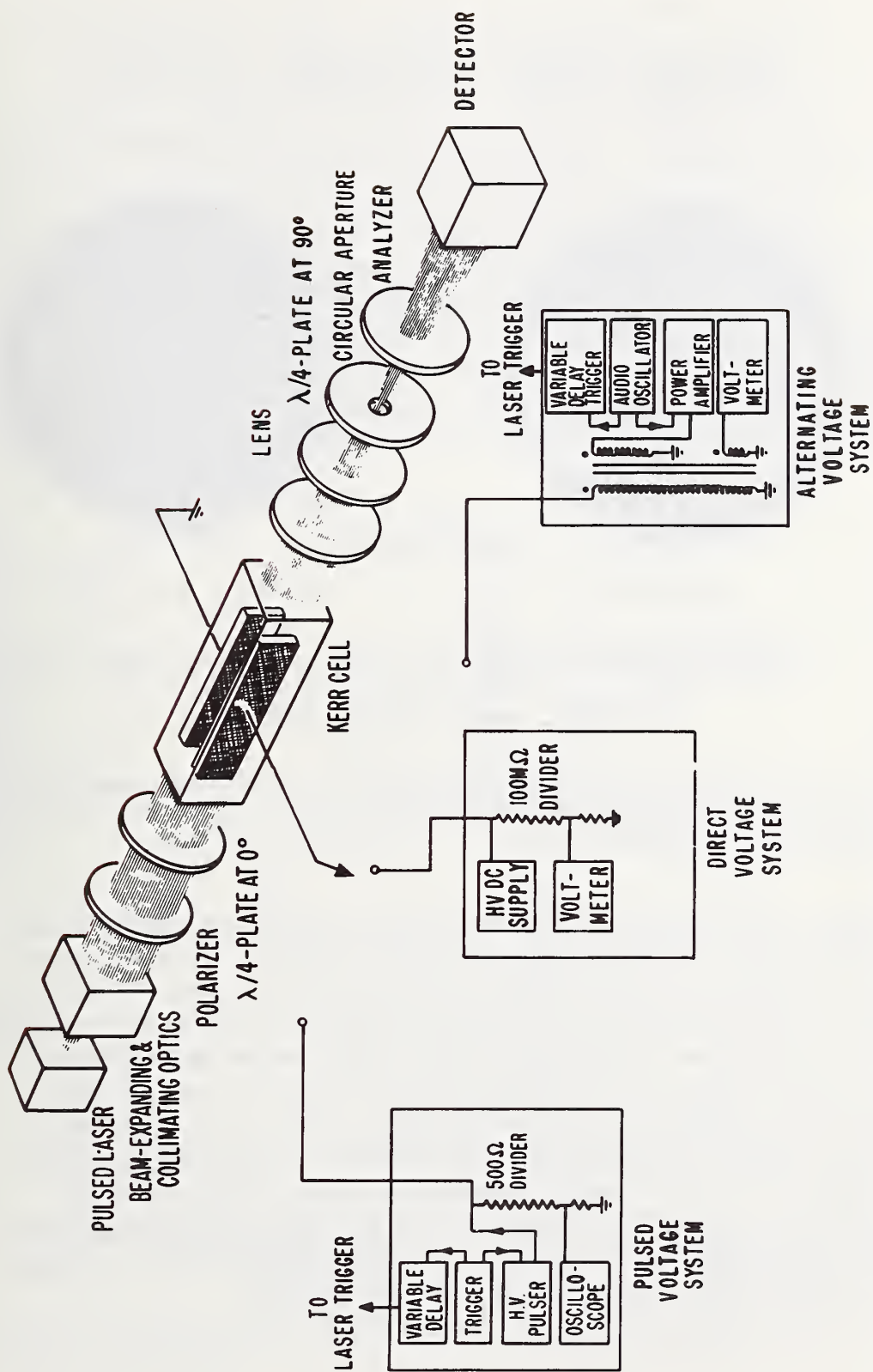
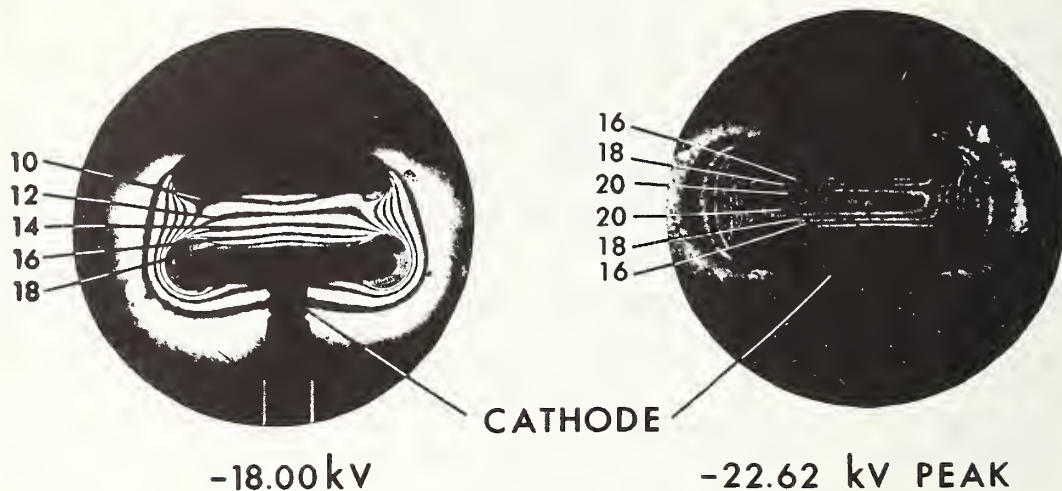


FIGURE 1 Systems for pulsed, direct, and alternating high voltage studies of nitrobenzene-filled Kerr cells.

STEADY-STATE VOLTAGES APPLIED

dc

60 Hz ac



KERR-EFFECT FRINGE-PATTERN "MAPPINGS" OF ELECTRIC FIELD DISTRIBUTIONS

FIGURE 2 Fringe patterns mapping dc and 60 Hz ac field distributions in a 0.5 x 12 cm cell. Photographs taken at peak of negative half-cycle using a pulsed laser (pulse width: 6 μ s).

results show that the field distribution is essentially linear⁶ with a uniformly distributed net positive space charge; whereas ac results with the same cell and liquid indicate the presence of nearly equal amounts of positive charge near the anode and negative charge near the cathode, thereby suggesting nearly equivalent charge formation or injection at both electrodes. However, conflicting results from experiments with apparently similar cells emphasize the fact that steady-state Kerr cell behavior is dependent upon the voltage, upon the material, design and surface condition of the electrodes, upon the relative purity of the liquid and sealing of the cell, etc. More comprehensive studies required for distinguishing the effects of these parameters are in progress.

MEASUREMENTS DURING PULSED VOLTAGE OPERATION

In contrast to steady-state behavior, electric fields produced by applying pulses as high as 300 kV with durations of 5 to 20 μs showed no evidence of space-charge distortion. Figure 4 shows a typical fringe pattern recording of the irradiance transmitted through a Kerr system at the peak of a 65.4 kV, 5-10 μs pulse. The absence of space charge is indicated by the absence of fringes between the electrodes. In higher voltage experiments, where Kerr system measurement resolution is enhanced,⁴ interelectrode fringes are recorded in some cases. Analysis of results from different voltage levels indicated, however, that these path dependent irradiance variations are caused by fringing fields at the

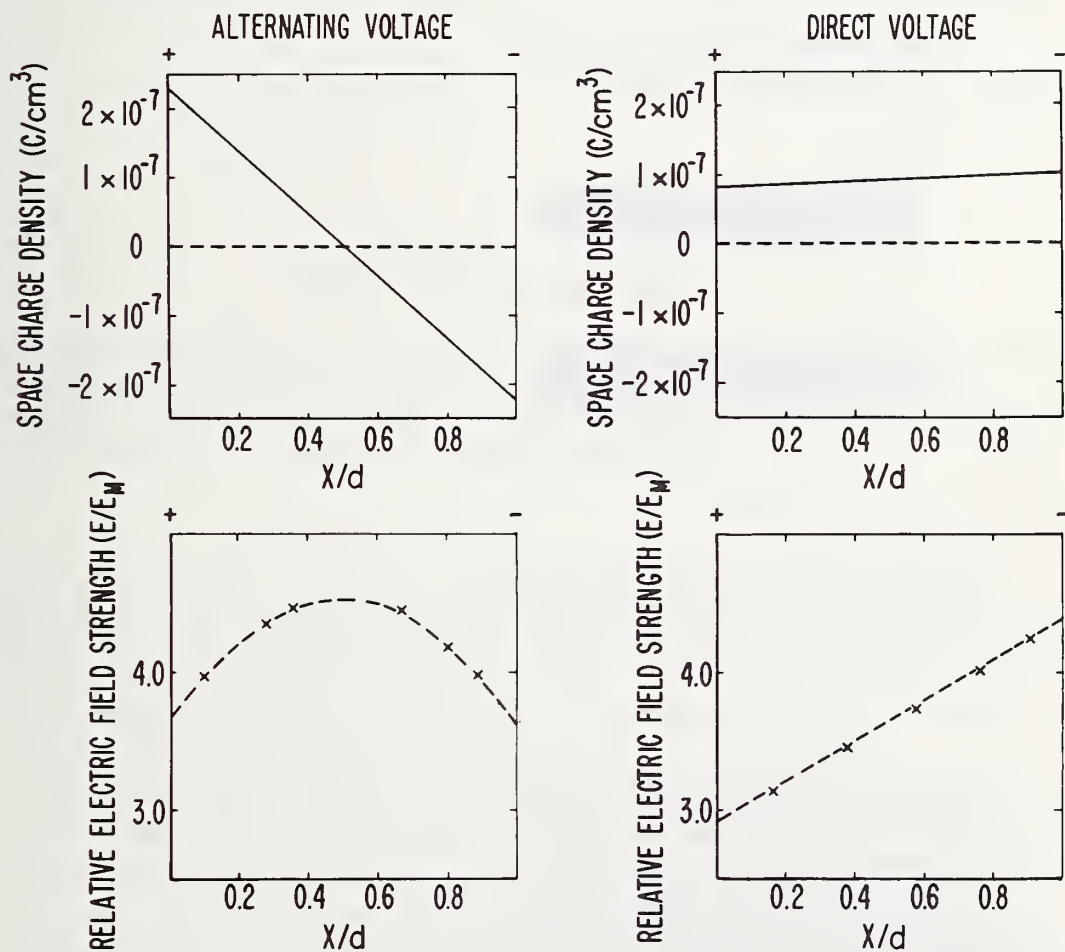
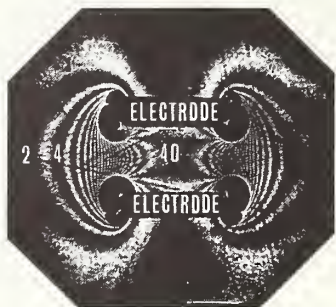


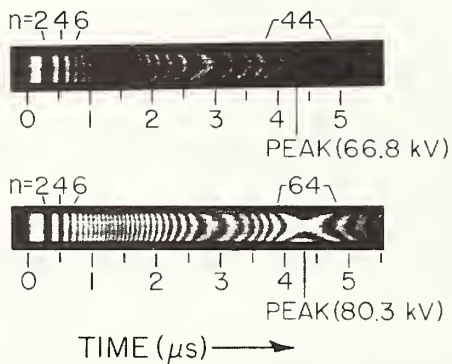
FIGURE 3 Electric field and space charge distributions computed from fringe patterns in Figure 2.

ends of the electrodes, residual strain in the cell windows, or slight lack of electrode parallelism.⁷ The effects of end-fields, which produce 1-2% variations in (\bar{E}/\bar{E}_m) in our 1 x 10 cm cell,

END-FIELD EFFECTS



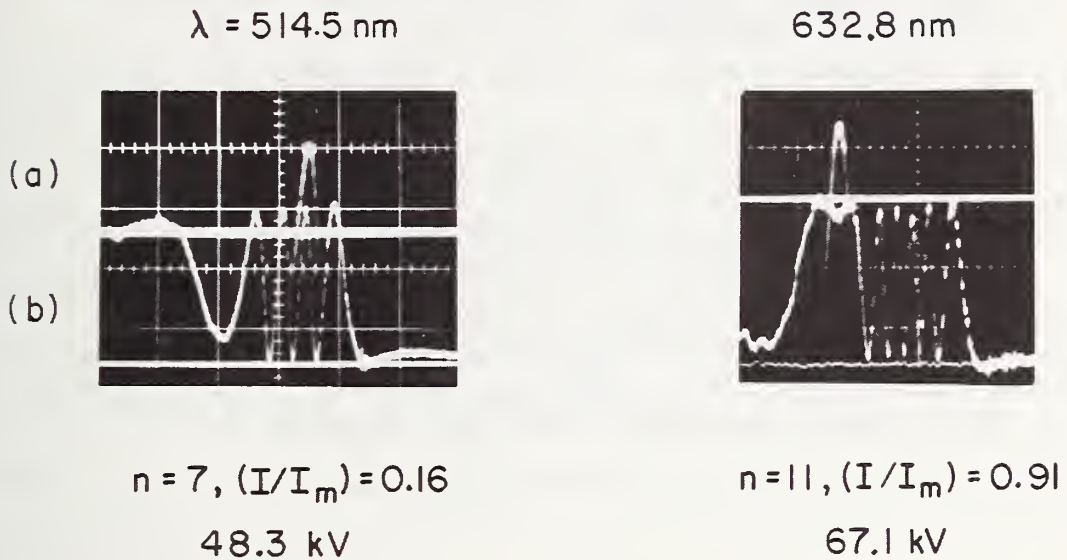
END-VIEW PHOTO AT PEAK OF 65.4 kV PULSE



STREAK CAMERA RECORDINGS OF FRONT HALF OF VOLTAGE PULSES

FIGURE 4 High-speed photographs of fringe patterns produced by applying microsecond high voltage pulses to a 1 x 10 cm cell. The streak camera records are of the light transmitted through a slit perpendicular to and extending between the central inner electrode surfaces.

PULSE VOLTAGES APPLIED



TIME SCALE: $2 \mu\text{s}/\text{div}$

FIGURE 5 Oscilloscope tracings of simultaneous a) slideback measurements of pulse divider response at peaks of applied voltage pulses and b) photo-multiplier records of the light transmitted by the Kerr system as a function of time during the trailing edges of the voltage pulses.

are, for example, evident in the streak camera photographs³ of Figure 4. The fringes would, in the absence of end-field variations, remain perpendicular to the time scale. Use of this procedure,³ for continuous recording of space-charge behavior during application of longer (into the ms range) pulses, is anticipated.

Measurements of the Kerr electrooptic coefficient B are also being made under short pulse conditions. Simultaneous Kerr system and pulse divider measurements,⁴ Figure 5, allow measurement of both the applied voltage and the resulting phase shift. Combining this with appropriate dimensional measurements indicates a value of $B \approx 3.2 \times 10^{-12} \text{ m/V}^2$ at $\lambda = 632.8 \text{ nm}$, $T = 23^\circ\text{C}$ and $B \approx 4.1 \times 10^{-12} \text{ m/V}^2$ at $\lambda = 514.5 \text{ nm}$, $T = 23^\circ\text{C}$.

REFERENCES

1. E. C. Cassidy and H. N. Cones, 1969 Annu. Rep. Conf. Elec. Insul. Dielectr. Phenom., Publ. 1764, Nat. Acad. Sci., Washington, D.C. (1970), p. 77.
2. E. C. Cassidy and H. N. Cones, J. Res. Nat. Bur. Stand. 73C, 5 (1969).
3. E. C. Cassidy, Rev. Sci. Instr. 43, 886 (1972).
4. E. C. Cassidy, H. N. Cones, D. C. Wunsch, and S. R. Booker, IEEE Trans. IM-17, 313 (1968).
5. R. Tobazeon, "Intern. sur les Phenomenes de Conduction dans les Liquides Isolants," Paris (1970), p. 407.
6. N. J. Felici, Direct Current 2, 147 (1971).
7. E. C. Cassidy, W. E. Anderson, and S. R. Booker, IEEE Trans. Instr. and Meas., Nov. 1972, in press.

REFERENCES

1. E. C. Cassidy and H. N. Cones, "Development and Analysis of Techniques for Calibration of Kerr Cell Pulse-Voltage Measuring Systems," NBS Report 9610, or Sandia Laboratories Contract Report SC-CR-67-2751, Sept. 1967.
2. E. C. Cassidy and H. N. Cones, "Calibration of a Kerr Cell System for High Voltage Pulse Measurements," Sandia Laboratories Contract Report SC-CR-68-3730, August 1968.
3. E. C. Cassidy and H. N. Cones, "Development and Analysis of Techniques for Calibration of Kerr Cell Pulse-Voltage Measuring Systems III," NBS Report 10 078, August 8, 1969, or Sandia Laboratories Contract Report SC-CR-69-3266, August 1969.
4. E. C. Cassidy and H. N. Cones, "Development and Analysis of Techniques for Calibration of Kerr Cell Pulse-Voltage Measuring Systems IV," NBS Report 10 296, August 6, 1970, or Sandia Laboratories Contract Report SC-CR-70-6153, January 1971.
5. E. C. Cassidy, "Development and Analysis of Techniques for Calibration of Kerr Cell Pulse-Voltage Measuring Systems V," NBS Report 10 493, October 1971.
6. E. C. Cassidy, et al, "Development and Analysis of Techniques for Calibration of Kerr Cell Pulse-Voltage Measuring Systems VI," NBS Report 10945, November 1972.
7. E. C. Cassidy, H. N. Cones, D. C. Wunsch and S. R. Booker, "Calibration of a Kerr Cell System for High-Voltage Pulse Measurements," IEEE Trans. on Instr. and Meas., vol. IM-17, pp. 313-320, 1968.

8. E. C. Cassidy, H. N. Cones, and S. R. Booker, "Development and Evaluation of Electro-optical High-Voltage Pulse Measurement Techniques," IEEE Trans. on Instr. and Meas., vol. IM-19, pp. 395-402, 1970.
9. E. C. Cassidy, W. E. Anderson, and S. R. Booker, "Recent Refinements and Developments in Kerr System Electrical Measurement Techniques," IEEE Trans. on Instr. and Meas., vol. IM-21, pp. 504-510, 1972.
10. D. C. Wunsch and A. Erteza, "Kerr Cell Measuring System for High Voltage Pulses," Rev. Sci. Instru., vol. 35, pp. 816-820, 1964.
11. E. C. Cassidy and H. N. Cones, "A Kerr Electro-Optical Technique for Observation and Analysis of High-Intensity Electric Fields," J. Research NBS, vol. 73C, pp. 5-13, 1969.
12. E. C. Cassidy, "Pulsed Laser Kerr System Polarimeter for Electro-Optical Fringe Pattern Measurement of Transient Electrical Parameters," Rev. Sci. Instru., vol. 43, pp. 886-893, June 1972.
13. E. C. Cassidy and H. N. Cones, "Electro-Optical Observations and Measurements of Distorted High-Intensity Electric Fields," 1969 Annual Report Conf. on Electrical Insulation and Dielectric Phenomena, Buck Hill Falls, Pa., Oct. 1969, pp. 77-86 (Nat'l. Acad. of Sci., Washington, D.C., 1970).
14. E. C. Cassidy and R. E. Hebner, "Experimental Study of the Behavior of Nitrobenzene Under Varied High Voltage Conditions" 1972 Annual Report Conf. on Electrical Insulation and Dielectric Phenomena, Buck Hill Falls, Pa., Oct. 1972, pp. 37-44 (Nat'l. Acad. of Sci., Washington, D.C., 1973).

15. R. E. Hebner and E. C. Cassidy, "Measurement of 60 Hz Voltages Using the Kerr Effect," Rev. Sci. Instru., vol. 43, pp. 1839-41, 1972.
16. S. Y. Ettinger and A. C. Venezia, "High Voltage Pulse Measuring System Based On Kerr Effect" Rev. Sci. Instru., vol. 34, pp. 221-224, 1963.
17. A. W. Bright, B. Makin and A. J. Pearmain, "Field Distribution in Nitrobenzene Using the Kerr Effect" Brit. J. Appl. Phys. (J. Phys. D) vol. 2, pp. 447-451, 1969.
18. P. Atten and J. P. Gosse, "Regime Transitoire de Conduction Lors d'une Injection Unipolaire dans les Liquids Isolants" Phenomenes de Conduction dans Liquides Isolants, Editions du Centre National de la Recherche Scientifique, Paris, pp. 325-343, 1970.
19. E. A. Cherney and J. D. Cross, "Space Charge Effects in Chlorobiphenyls" IEEE Trans. Elect. Insul., vol. EI-8, pp. 10-16, 1973.
20. J. D. Cross and R. Tobazeon, "Electric Field Distortions Produced By Solid Dielectric Spacers Separating Uniform Field Electrodes in Nitrobenzene" IEEE Trans. Elect. Insul., vol. EI-8, pp. 25-29, 1973.
21. C. E. Hill, H. House, "The Problems in Using the Kerr Electro-Optic Effect to Measure the Field Distributions in Non-Polar Liquids" Phenomenes de Conduction dans Liquides Isolants, Editions du Centre National de la Recherche Scientifique, Paris, pp. 465-481, 1970.
22. M. Zahn and J. R. Melcher, "Space Charge Dynamics of Liquids" Phys. Fluids, vol. 15, pp. 1197-1205, 1972.
23. M. Zahn, "Dynamics of Stratified Liquids in the Presence of Space Charge" Phys. Fluids, vol. 15, pp. 1408-1417, 1972.

24. W.R.L. Thomas, "The Nature of Particulate Charge Carriers in n-Hexane and Their Role in Electrohydrodynamic Phenomena" 1972 Annual Report Conference on Electrical Insulation and Dielectric Phenomena, National Academy of Sciences, Washington, D.C., pp 52-59, 1972.
25. A. W. Bright and B. Makin, "Modern Electrostatic Generators" *Contemp. Phys.*, vol. 10, No. 4, pp. 331-353, 1969.
26. A. M. Zarem, F. R. Marshall, and F. L. Poole, "An Electro-Optical Shutter for Photographic Purposes" *AIEE Proc.*, vol. 68, pp. 1-8, 1949.
27. F. J. McClung and R. W. Hellwarth, "Giant Optical Pulsations from Ruby" *J. Appl. Phys.*, vol. 33, pp. 828-829, 1962.
28. Z. Croitoru, "Space Charges in Dielectrics" in Progress in Dielectrics, vol. 6, J. B. Birks and J. Hart, editors (Academic Press, Inc., New York, 1965), pp. 103-146.
29. Ibid., W. F. Pickard, "Electrical Force Effects In Dielectric Liquids" pp. 1-39.
30. H. T. Jessop and F. C. Harris, "Photoelasticity, Principles and Methods" Dover New York pp. 68-70.
31. J. H. Park, "Special Shielded Resistor for High-Voltage DC Measurements" *J. Res. Nat. Bur. Stds.*, vol. 66C, pp. 19-24, 1962.
32. J. E. Housley, "Reconditioning of Insulating Oils By Activated Alumina" *AIEE Trans.*, vol. 58, pp. 172-178, 1939.
33. J. D. Ramshaw, D. W. Schaefer, J. S. Waugh and J. M. Deutch, "Dielectric Polarization and Alignment and the Structure of Polar Fluids" *J. Chem. Phys.*, vol. 54, pp. 1239-1251, 1971.
34. G. Nienhuis and J. M. Deutch, "Structure of Dielectric Fluids II. The Free Energy and the Kerr Effect in Polar Fluids" *J. Chem. Phys.*, vol. 56, pp. 235-247, 1972.

35. P. Mazur and B. J. Postma, "On the Molecular Theory of the Kerr Effect" *Physica*, vol. 25, pp. 251-267, 1959.
36. Details of the fitting procedure can be found in J. Hilsenrath, et.al., "Omnitab, A Computer Program for Statistical and Numerical Analysis" National Bureau of Standards Handbook 101, U.S. Government Printing Office, Washington, D.C., pp. 124-140.
37. R. Tobazeon, "Comportement du Nitrobenzene Pur Sous Champs Intenses Continus et Alternatifs" *Phenomenes de Conduction dans Liquides Isolants*, Editions du Centre National de la Recherche Scientifique, Paris, pp. 407-422, 1970.
38. N. J. Felici, "DC Conduction in Liquid Dielectrics" *Direct Current* vol. 2, pp. 90-99, 1971.
39. Z. Krasucki, "High-Field Conduction in Liquid Dielectrics" *Phenomenes de Conduction dans Liquides Isolants*, Editions du Centre National de la Recherche Scientifique, Paris, pp. 311-323, 1970.
40. A.Y.H. Cho, "Contact Charging of Micron-Sized Particles In Intense Electric Fields" *J. Appl. Phys.*, vol. 35, pp. 2561-2564, 1964.
41. For a recent discussion of these effects see A. H. Cookson and O. Farish "Particle-Initiated Breakdown Between Coaxial Electrodes in Compressed SF₆" *IEEE Trans. on Power Apparatus and Systems*, vol. PAS-92, pp. 871-876, 1973.
42. G. Briere and J. Gosse, "Electrodialyse des Solvants Polaires" *Journal de Chimie Physique*, vol. 7, pp. 1341-1348, 1968.
43. J. Lemoine, "Verification de la Loi de Kerr - Mesures Absolues," *Compte Rend.*, vol. 122, pp. 835-37, 1896.

44. L. Chaumont, "Recherches Experimentales sur le Phenomene Electro-optique de Kerr et sur les Methods Servant a l'Etude de la Lumiere Polarisee Elliptiquement" Ann. de Phys., vol. 5, pp. 17-78, 1916.
45. A. D. Buckingham and R. E. Raab, "A Molecular Theory of the Electro-optical Kerr Effect In Liquids," J. Chem. Soc., pp. 2341-51, 1957.
46. Möller, R., "Die Kerr Konstante des Nitrobenzols" Physikalische Zeitschrift, vol. 32, pp. 697-718, 1931.
47. Piekara, A. and Konopka, R., "Pulse Method for Measuring Kerr's Constant Brit. J. Appl. Phys., vol. 12, pp. 50-52, 1961.
48. Ilberg, Waldemar, "Eine Methode zur Bestimmung der Kerr-Konstante Schlecht Isolierender Stoffe mit Hilfe Elektrischer Wechselfelder" Physik. Zeitschr., vol. 29, pp. 670-78, 1928.
49. Zamkov, V. A. and Radkevich, V. A., "Polarization Interferometer for Measuring Induced Anisotropy" Opt. Spectrosc., vol. 31, pp. 437-39, 1971.
50. McComb, Harold E., "Dispersion of Electric Double Refraction and Ordinary Dispersion in Liquids" Phys. Rev., vol. 29, pp. 525-40, 1909.
51. Delfino, G., "Two Beam Method for Measurements of the Kerr Constant With Fixed Polarizers," Optics Communications, vol. 4, pp. 60-62, 1971.
52. Szivessy, G., "Über die Temperaturabhängigkeit der Dispersion des Elektrooptischen Kerreffektes" Z. Physik, vol. 2, pp. 30-49, 1920.
53. Jeppesen, Myron A., "Measurements on the Kerr Electro-Optical Effect" Am. J. Phys., vol. 24, pp. 623-25, 1956.
54. USA and IEEE Standard Techniques for Dielectric Tests, USAS C68.1, IEEE No. 4, Section 5 and 6, pp. 14-22 (Inst. of Electrical and Electronic Engineers, Inc., 345 E. 47 Street, New York, N.Y. 10017, July 1968).

55. International Electrotechnical Commission, High-Voltage Test Techniques, IEC Publication 60, pp. 51-91 (Bureau Central de la Commission Electrotechnique Internationale, 1, rue de Varembe, Genève, Suisse) 1962.
56. D. E. Skelton, "The Electrical Interference Problem In Fusion Research," in Electrical Interference in Instrumentation (IEE Conf. Publ. No. 65, Savoy Place, London WC2ROBL), pp. 1-3, 1970.
57. D. G. Pellinen and S. Heurlin, "A Nanosecond Risetime Megavolt Voltage Divider," Rev. Sci. Instr., vol. 42, pp. 824-827, 1971.
58. J. H. Park and H. N. Cones, "Spark-Gap Flashover Measurements for Steeply Rising Voltage Impulses," J. Res. Nat'l. Bur. Stds., vol. 66C, pp. 197-207, 1962.
59. A. F. Rohlf, J. S. Kresge and F. A. Fisher, "The Response of Resistance Voltage Dividers to Steep-Front Impulse Waves," AIEE Trans., vol. 76, part 1, pp. 634-646, 1957.
60. A. J. Schwab and J.H.W. Pagel, "Precision Capacitive Voltage Divider for Impulse Voltage Measurements," IEEE Trans. on PAS, vol. PAS-91, pp. 2376-2382, 1972.
61. T. Harada, et al, "A High Quality Voltage Divider Using Optoelectronics For Impulse Voltage Measurements," IEEE Trans. on PAS, vol. PAS-91, pp. 494-500, March/April 1972.
62. M. F. Simon and G. L. Leroy, "Contribution to A Better Understanding of Impulse Voltage Measuring Systems," IEEE Trans. Power Appar. Sys., vol. PAS-91, pp. 478-484, 1972.
63. F. C. Creed, M.M.C. Collins, Aa. Pedersen, and P. Lausen, "Evaluating Impulse Measurements--A New Approach," Ibid, pp. 485-494, 1972.

64. F. A. Fisher, "Transient Response of Impulse Voltage Dividers," AIEE Trans. Communication and Electronics, vol. 77, part 1, pp. 411-420, 1958.
65. W. Zaengl, "The Impulse Voltage Divider With Lead," Bull. d l'A.S.E., vol. 61, pp. 1003-1017, 1970.
66. N. R. Hylten-Cavallius and L. Vaughan, "Calibration and Checking Methods of Rapid High Voltage Impulse Measuring Circuits," IEEE Trans. PAS, vol. PAS-89, pp. 1393-1403, Sept./Oct. 1970.
67. M. M. Brady and K. G. Dedrick, "High-Voltage Pulse Measurement With A Precision Capacitive Voltage Divider," Rev. Sci. Instr., vol. 33, pp. 1421-1428, 1962.

U.S. DEPT. OF COMM. BIBLIOGRAPHIC DATA SHEET	1. PUBLICATION OR REPORT NO. NBSIR 73-403	2. Gov't Accession No.	3. Recipient's Accession No.
---	--	------------------------	------------------------------

TITLE AND SUBTITLE Development and Analysis of Techniques for Calibration of Kerr Cell Pulse-Voltage Measuring Systems VII	5. Publication Date November 1973	
		6. Performing Organization Code

AUTHOR(S) Esther C. Cassidy, Robert E. Hebner, Jr., Richard J. Sojka and Markus Zahn	8. Performing Organization NBSIR 73-403
---	--

PERFORMING ORGANIZATION NAME AND ADDRESS NATIONAL BUREAU OF STANDARDS DEPARTMENT OF COMMERCE WASHINGTON, D.C. 20234	10. Project/Task/Work Unit No. 2110426	
		11. Contract/Grant No. FAO-28-0734

Sponsoring Organization Name and Address Sandia Corporation Bldg. 894, Kirtland AFB East Albuquerque, New Mexico 87115	13. Type of Report & Period Covered July 1, 1972-July 1, 1973 Final	
		14. Sponsoring Agency Code

SUPPLEMENTARY NOTES

ABSTRACT (A 200-word or less factual summary of most significant information. If document includes a significant bibliography or literature survey, mention it here.)

To improve the accuracy of pulse voltage systems using the electro-optic Kerr effect, it is necessary to improve the accuracy of calibration of Kerr cells. In the past this has been attempted by calibrating the cell under direct voltage and relying on the frequency independence of the Kerr coefficient (below 10^8 Hz) to insure that the calibration was valid under high voltage pulses. Space charge effects, however, modify the electric field distribution in the liquid under direct high voltage. The electric field and space charge behavior in nitrobenzene have therefore been documented as functions of the level and frequency of the applied voltage. In addition, to improve the efficiency of cell design and to facilitate the investigation of other liquids for use in Kerr cells, the electro-optic Kerr coefficient of nitrobenzene has been measured as a function of temperature and wavelength. Finally a new peak reading voltmeter based on the Kerr effect is described and the results of using the electro-optic Kerr effect to measure the voltage pulses in medical X-ray machines are presented.

KEY WORDS (Alphabetical order, separated by semicolons) Electric field measurement; electro-optic Kerr effect; high voltage measurement; impulse measurement; Kerr constant; Liquid insulants; nitrobenzene; peak reading voltmeter; space charge

AVAILABILITY STATEMENT <input checked="" type="checkbox"/> UNLIMITED. <input type="checkbox"/> FOR OFFICIAL DISTRIBUTION. DO NOT RELEASE TO NTIS.	19. SECURITY CLASS (THIS REPORT) UNCLASSIFIED	21. NO. OF PAGES 128
		20. SECURITY CLASS (THIS PAGE) UNCLASSIFIED
		22. Price



